the Energy to Lead

FINAL REPORT

Real-Time Multiple Utility Detection During Pipe Installation Using Horizontal Directional Drilling (HDD) System

DOT Project # 493
DOT Agreement Number: DTPH56-13-T-000002

Reporting Period:
11th Project Quarter
September 1, 2013 through April 30, 2016

Report Issued (Period Ending):
May 5, 2016

Prepared For:
Mr. Frank Causey
PHMSA Technical Manager

Prepared By:
Gas Technology Institute
Dr. Kiran Kothari
Institute Engineer/Program Manager
kiran.kothari@gastechnology.org
847-768-0893

Technical Team:
Dr. Kiran Kothari, Gas Technology Institute
Mr. Ching-Chen Wu, SoniVerse, Inc.
Dr. David Hanson, Vermeer Corporation
Dr. Maureen Droessler, OTD

Operations Technology Development
1700 S. Mount Prospect Rd.
Des Plaines, Illinois 60018
www.gastechnology.org

Legal Notice

This information was prepared by Gas Technology Institute (GTI)/Soni-Verse Inc./Vermeer Corporation/Operations Technology Development ("OTD") for DOT/PHMSA (Agreement Number: DTPH56-13-T-000002.

Neither GTI, the members of GTI, Soni-Verse Inc. (SVI), Vermeer Corporation (VC), OTD, the members of OTD, the Sponsor(s), nor any person acting on behalf of any of them:

a. Makes any warranty or representation, express or implied with respect to the accuracy, completeness, or usefulness of the information contained in this report, or that the use of any information, apparatus, method, or process disclosed in this report may not infringe privately-owned rights. Inasmuch as this project is experimental in nature, the technical information, results, or conclusions cannot be predicted. Conclusions and analysis of results by GTI/SVI/VC/OTD represent GTI's, SVI's, VC's and OTD's opinion based on inferences from measurements and empirical relationships, which inferences and assumptions are not infallible, and with respect to which competent specialists may differ.

b. Assumes any liability with respect to the use of, or for any and all damages resulting from the use of, any information, apparatus, method, or process disclosed in this report; any other use of, or reliance on, this report by any third party is at the third party's sole risk.

c. The results within this report relate only to the items tested.

Table of Contents

List of Figures

Page

List of Tables

Project Background and Objective

Two innovative technologies, acoustic and radar, that can automatically and rapidly detect buried pipes/obstacles in front of and adjacent to the drill-head of horizontal directional drilling (HDD) machines have already been under development by Gas Technology Institute (GTI), SoniVerse Inc. (SVI), and Vermeer Corporation (VC) with the assistance of Operations Technology Development (OTD).

The acoustic technology was developed by GTI and SVI, and is based on a unique method – listening to noise made by the drill-head and reflected by the approaching pipes/objects. The highly sensitive accelerometers on the ground 'listen' to the reflected signals from objects/pipes and analyze the data to provide information on the underground infrastructure in real-time. The sensors on the ground do not require any liquid coupling to receive the signal and the data interpretation method requires no information about the soil properties surrounding the buried pipes. The system has been tested for various ground covering surfaces (e.g., grass, asphalt, concrete, dirt) in the past. The prototype system has been tested successfully in a semi-field condition to detect pipes/objects about 20 ft. in the front of drill-head in real-time. The accuracy of detecting pipes is about 2-3 ft. and appears to be somewhat coarse.

The second technology was developed by GTI and VC, is based on stepped frequency continuous wave (SFCW) modulation, and the prototype drill-head radar has been designed and built. This device is designed to fit a smaller class of HDD machines that are normally used for shorter bores in more congested 'last-mile' type applications. The drill-head with radar has been installed on a commercial HDD machine of VC and has been tested in both laboratory and in semi-field settings. A unique technique to inject and receive reflected signals from pipes/objects near the drill-head has improved the radar operation in the detection of pipes in many more types of soils than commercially available ground penetrating radars (GPRs) operated at the ground level. Also, significant improvements have been made in the software to provide information on the buried pipes near the drill-head in real-time and results are displayed as a point object and not the conventional hyperbolas to indicate pipe location. This radar technology detects pipes with high accuracy, but the detection distance of pipes has been limited to about 3-5 ft. around the drill-head.

The initial project objective was to integrate acoustic and radar technologies to detect buried pipes/objects in front of or adjacent to the drill-head during pipe installation using the HDD machine in real-time. Under the proposed development, the acoustic technology will provide an alert for pipes/objects at longer distances ahead of the drill-head and back to the HDD machine operator. The machine operator activates the radar system to accurately locate the obstacle pipes, while continuing the drilling operations to avoid hitting pipes.

The objective was revised based on the initial tests conducted in the current project. The integration of acoustic and radar system work has been deleted based on tests conducted in the project and changes have been approved by PHMSA. The revised project objective is to test acoustic-only system with improved noise generator in the local area and determine accuracy. The overall project proposed is structured to support three objectives: 1) improve noise makers and evaluate with the acoustic system in the local area, 2) update the acoustic system and test it in the semi-field environment (local area), and 3) report results. The development of the planned system will increase safety, increase use of HDD technology for pipe installations, and reduce cost. The proposed work is planned to be conducted by SVI, VC, and GTI.

This report describes work completed on the evaluation of the acoustic obstacle detection system, using a re-designed downhole source and modified sensor hardware. Three test campaigns were conducted and analyzed during May and November 2014 and December 2015. These tests produced results both in raw form in real-time and after post-acquisition processing. The first two test sets allowed evaluation of reworked noise sources and the overall functionality of the sensor. After analysis of these results, it was determined that additional work was required to improve source performance and to make incremental improvements to the sensor hardware. Specifically, the first two tests indicated that the downhole acoustic source used on an HDD produced a seismic energy level and frequency content that may have been inadequate for reliable obstacle detection. As a result, a different source was designed, built and tested. This source was then used to conduct a set of trials local to the Vermeer campus in December 2015.

The main objective of the project work was to test the performance of the acoustic obstacle detection system with a redesigned downhole energy source. This report details the results of that development and the analysis of resulting data. Recommendations are made for the future development of the system, both as an integral part of the HDD operation and as a stand-alone sensor system.

Initial Test Phase

Update Acoustic System

Based on successful demonstration of the acoustic obstacle detection technology in the previous research project, the initial test phase included a slight upgrade on the acoustic system (see Figure 1). The system electronics, sensor modules, and software development and user interface is designed, components were tested, and the complete acoustic system was built and tested.

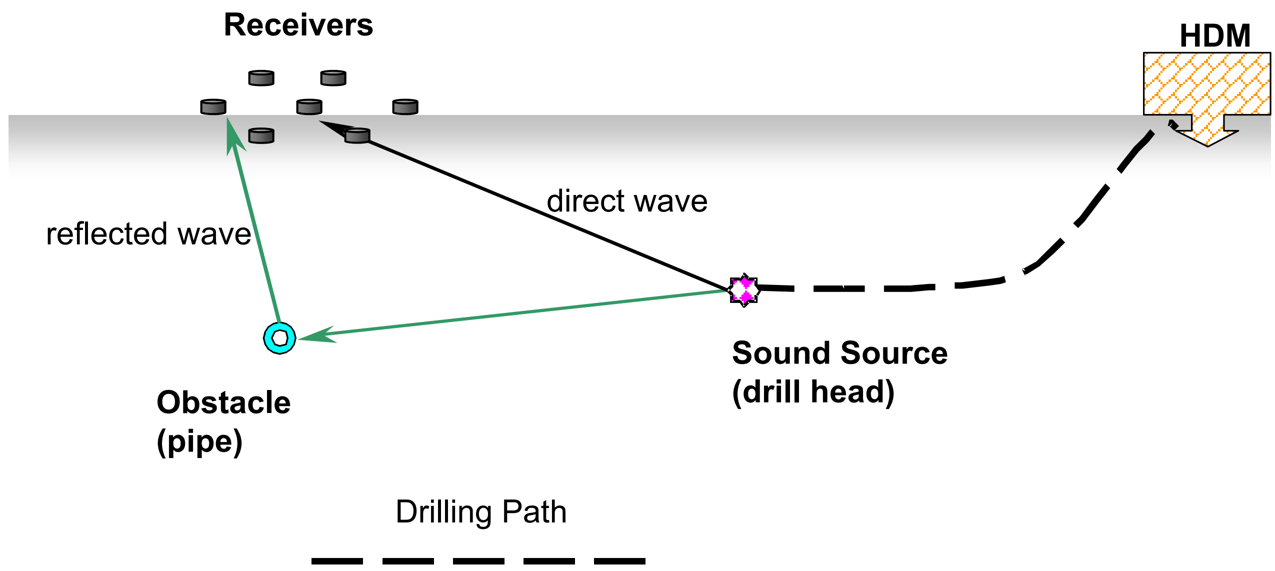

Figure 1 Conceptual Diagram for Guided Boring Operation and Passive Detection Technique.

Acoustic System – How it Works

The cross-correlation processing technology developed previously has been proved to be the most robust and effective approach in dealing with random signals and noise, such as the signals acquired from the passive imaging technique used in this project. A detail description of the correlation processes and the brief description are given below.

The cross-correlation analysis is a robust data processing technique that provides more advantages than others, as it will:

- Produce more processed data for calculating the location of the obstacle,
- Improve the signal ratio of the reflected wave to the direct signal,
- Provide better estimation of soil characteristics like speed of sound, attenuation, and
- Set-up a practical ground work for situations such as finding multiple pipes.

Figure 2 show the basic technical concept of the cross-correlation process. Cross-correlation is a mathematical process and technique that sums the multiplication results of two signals point-wise from the beginning to the end of the signals. Sensing receivers (A and B in Figure 2a) on the ground surface detect noisy signals generated from the drill-head's operation (D_{sr}, direct wave) and the potential pipe signal (R_{tr}, reflected and indirect wave). Through the cross-correlation process, the summing result of the two received signals will produce any peak signal that represents the potential target/pipe, as shown in Figure 2b. Some real-world measurements of underground pipe detection using cross-correlation processing during HDD operation are shown in the Figure 3.

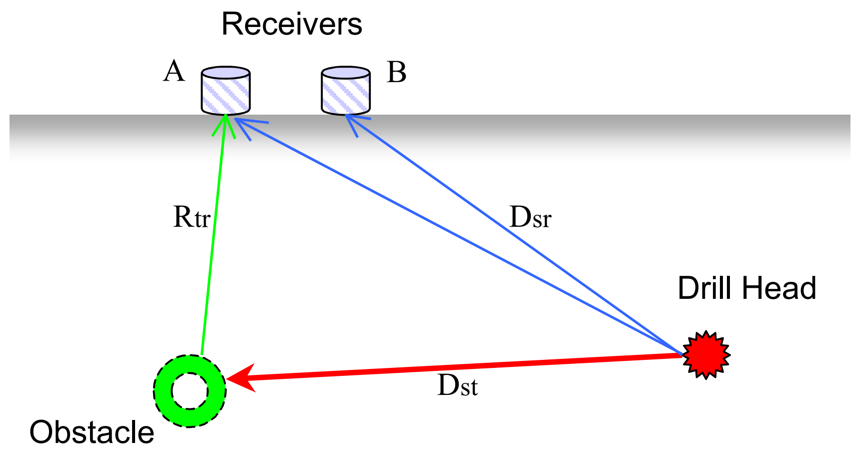

(a)

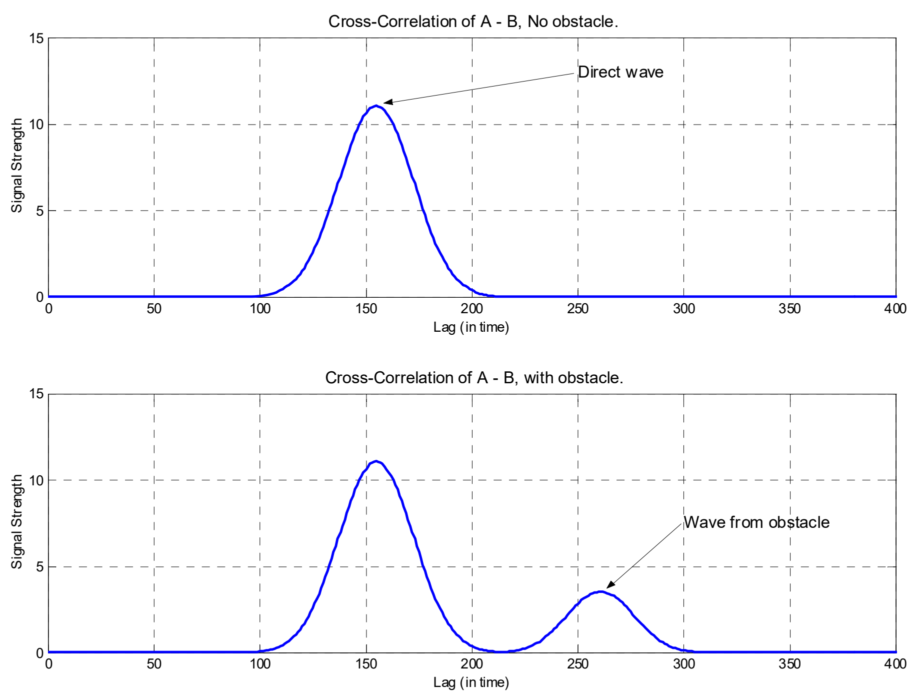

(b)

Figure 2 Cross-correlation technique and process: (a) direct waves and reflected wave to the receiving array (multiple receivers): Rtr – reflect wave, Dsr – direct waves; (b) the cross-correlation processes show pipe and no pipe situation.

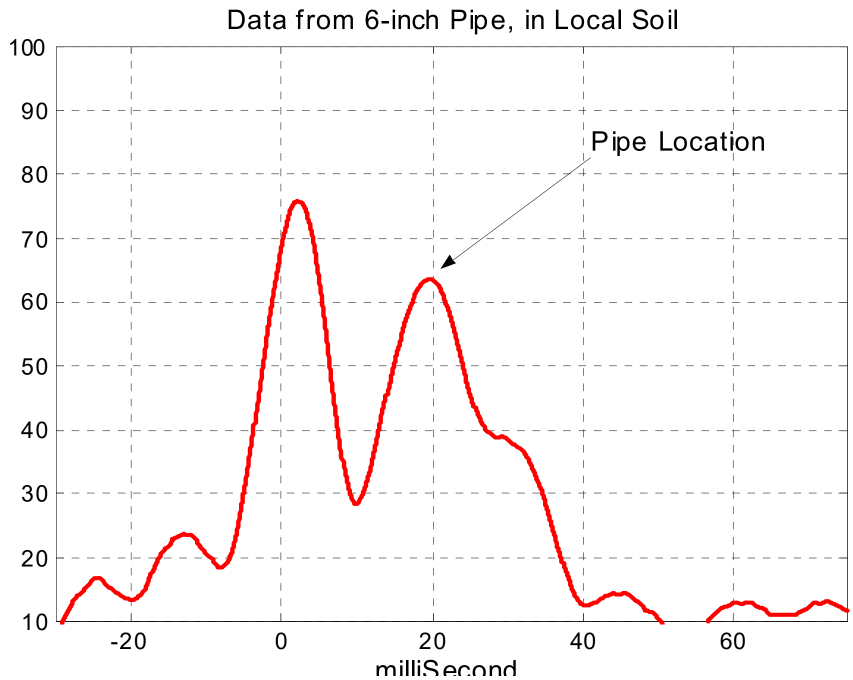

(a)

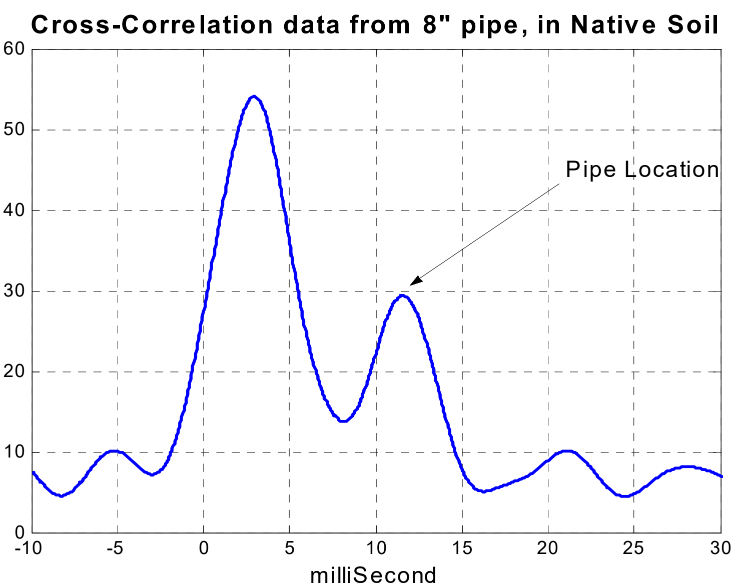

(b)

Figure 3 Real-world measurement of pipe location using cross-correlation signal processing technique: (a) 6" pipe in local soil and (b) 8" detected in native soil.

The acoustic transducer configuration is a hexagon with a central, seventh transducer. Each transducer is 18 inches from its nearest neighbors. The system software analyzes obstacle detection using a three-transducer set data. Three possible directions of the potential obstacle(s) can be analyzed and determined by three sets of transducer array orientation. The angle and distance to any obstacle is determined in this step. Any cross correlation showing a possible obstacle is considered valid. If the majority of the detections show an obstacle, it then is declared as an object; otherwise it is considered as a false alarm. The final results are then sent to a "cartoon-like" display format that, as shown in Figure 4, provides the HDD operator a visual indication of the relative position between boring head and obstacle(s). An "omnidirectional" acoustic sensor layout, as shown in Figure 5, and enhanced cross-correlation scheme was introduced for its robustness in detecting all direction and multiple pipes situation. It should be noted that pipes from all direction can be detected using the configuration within the sensible range of the system.

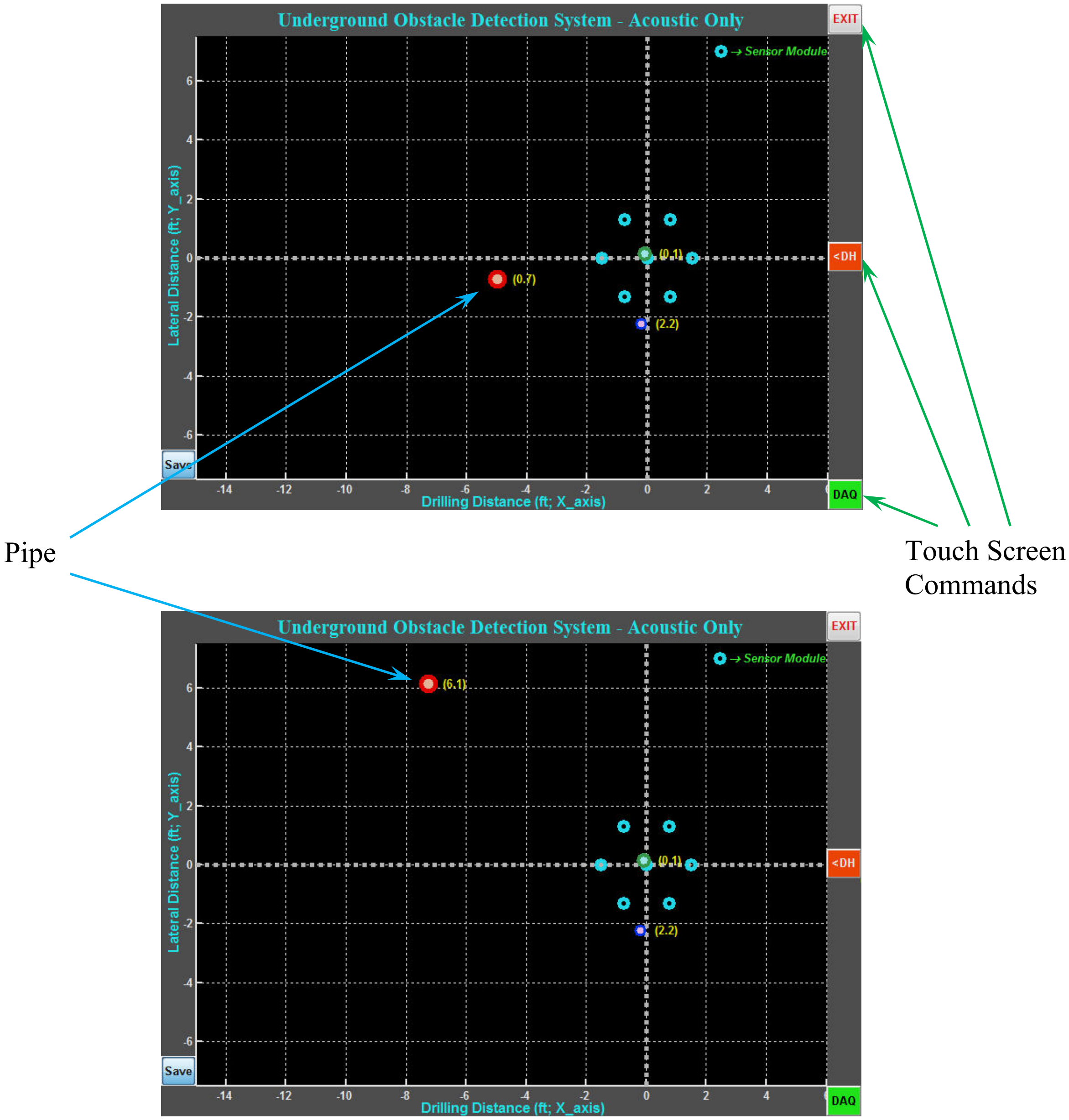

Figure 4 Display format used in the acoustic pipe detection system: top view of the test results show detected pipes near 5 feet out and about 7.5 feet away from the array center, respectively.

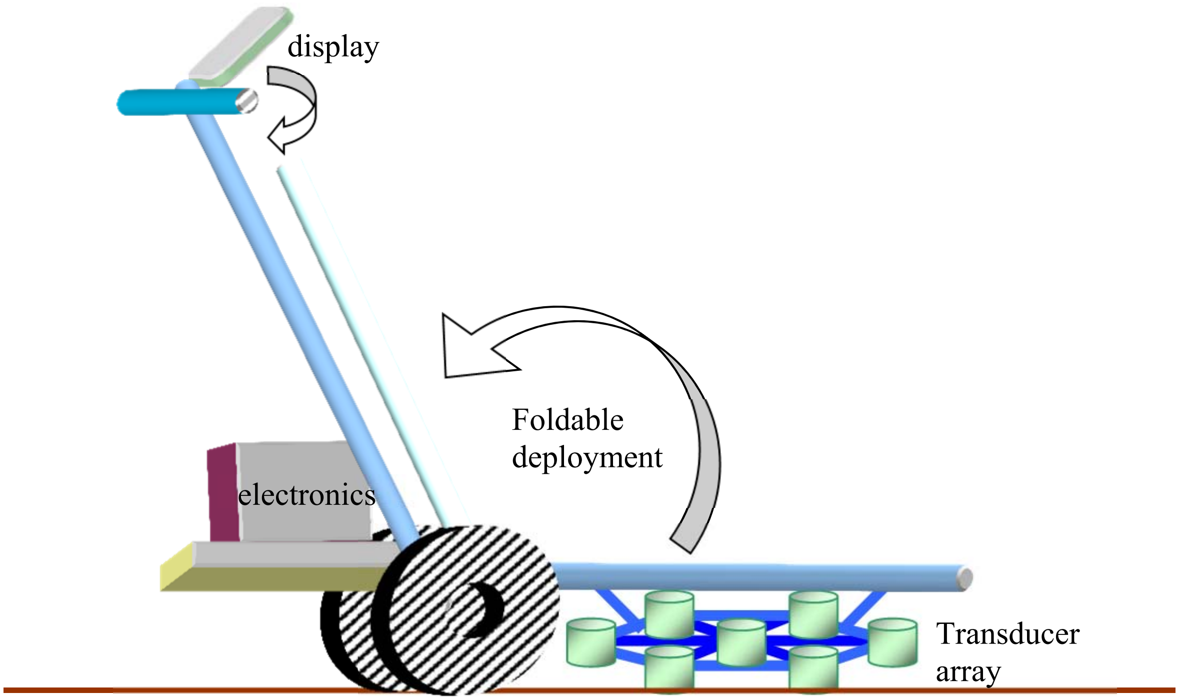

Figure 5 Conceptual drawing of the Golf-Cart style carriage for the acoustic system.

Acoustic System Upgrade

Several transducer array and a system carriage were designed, reviewed, and evaluated. Figure 6 shows the outline of the finalized sensor array and system carriage design for the upgraded acoustic system. The carriage design is similar to the previous golf-cart configuration. Figure 7 shows a couple of designs for the sensor module that replaced the old design. The design goal is to simplify the housing and packaging of the sensing transducer and to provide effective coupling suspension to the ground surface. Figure 8a shows the design for the sensor module that replaced the old design. Silicone mold fills the sensor housing for acoustic isolation and damping purposes. Figure 8b shows a detailed layout of the array structure. The overall size of the detection system allows that it is easy for functional deployment, equipment transportation, and system storage. A first article of the sensor module was built and evaluated, refer to Figure 9.

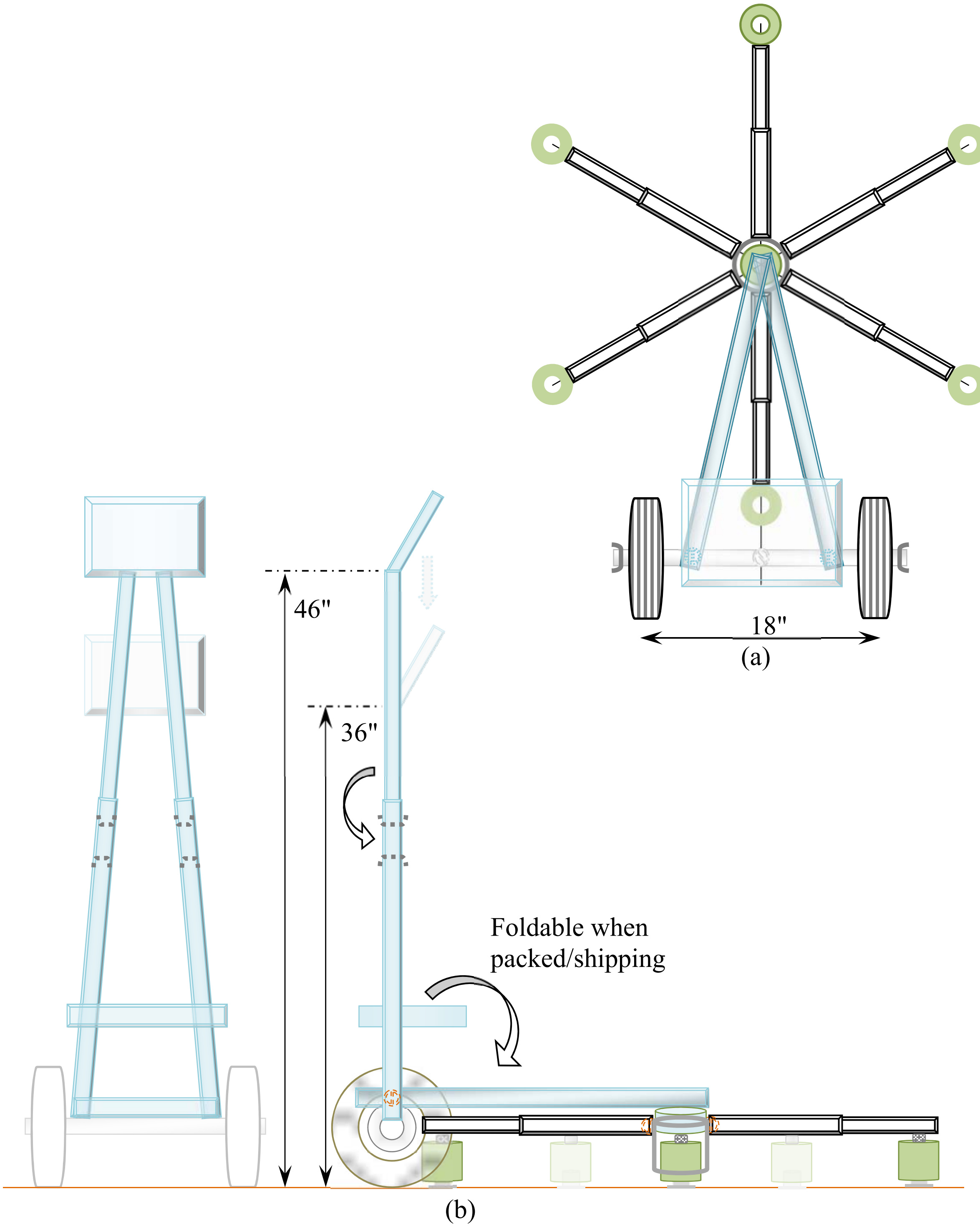

Figure 6 Sensor array and system carriage designs for the project: (a) top view and (b) side views.

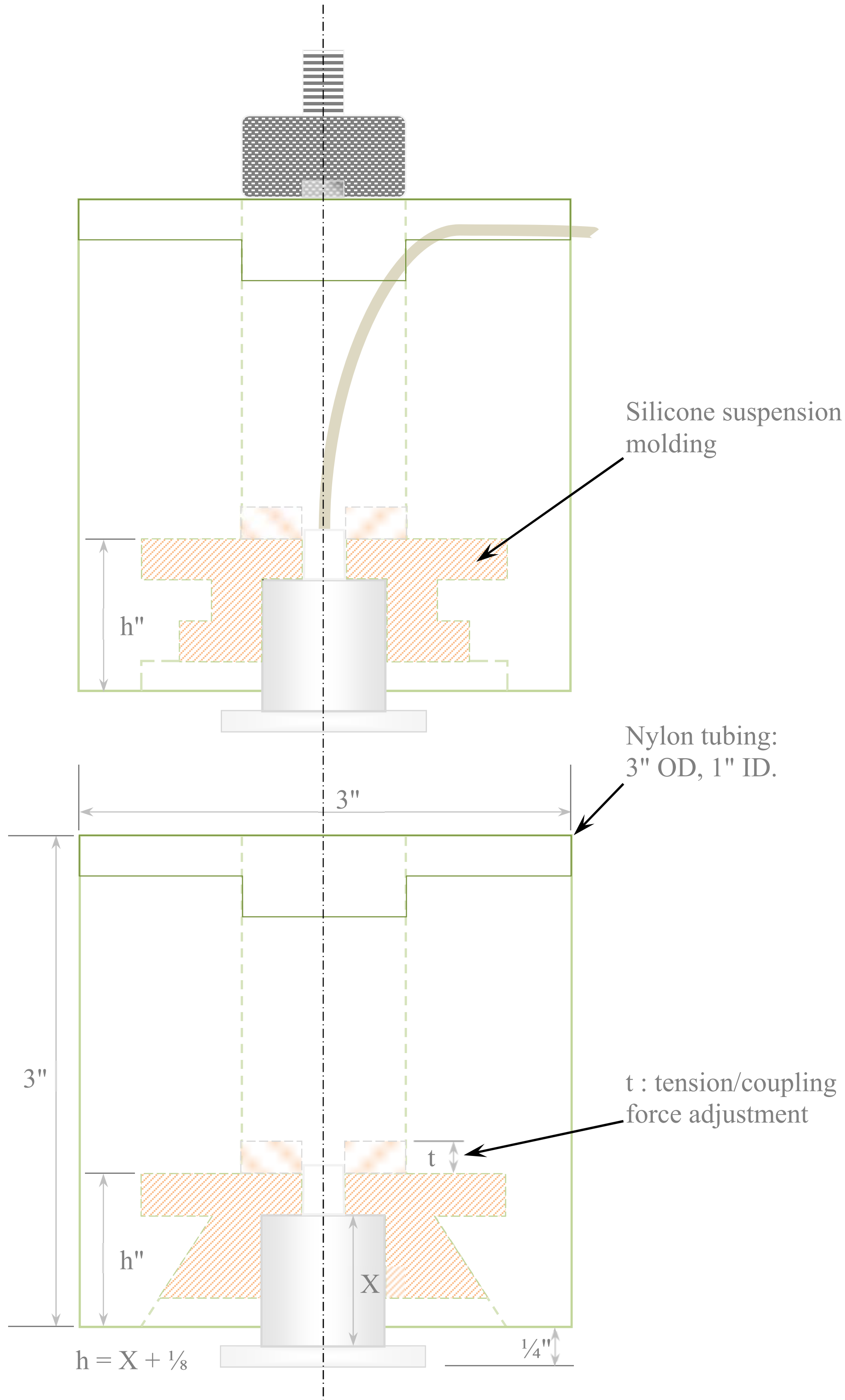

Figure 7 Suspension system designs for the sensor module used in the project.

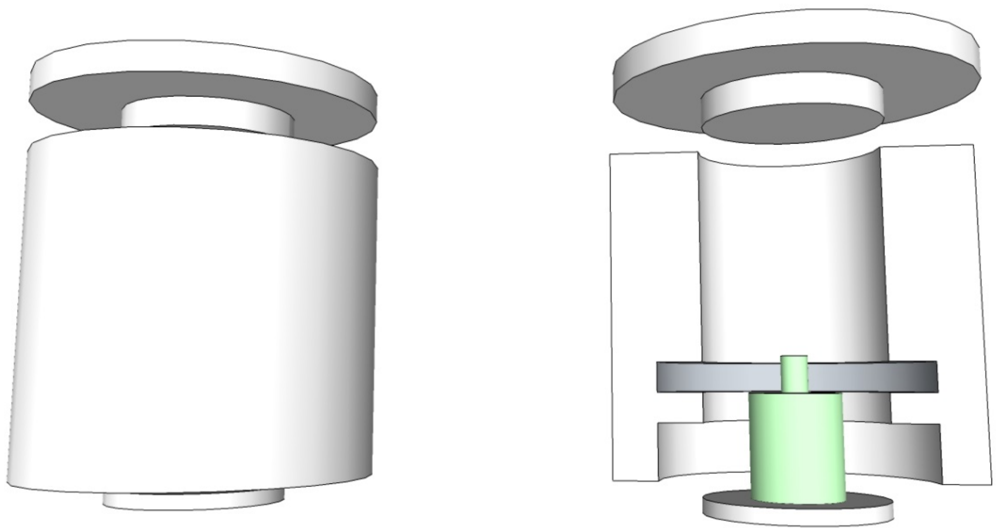

(a)

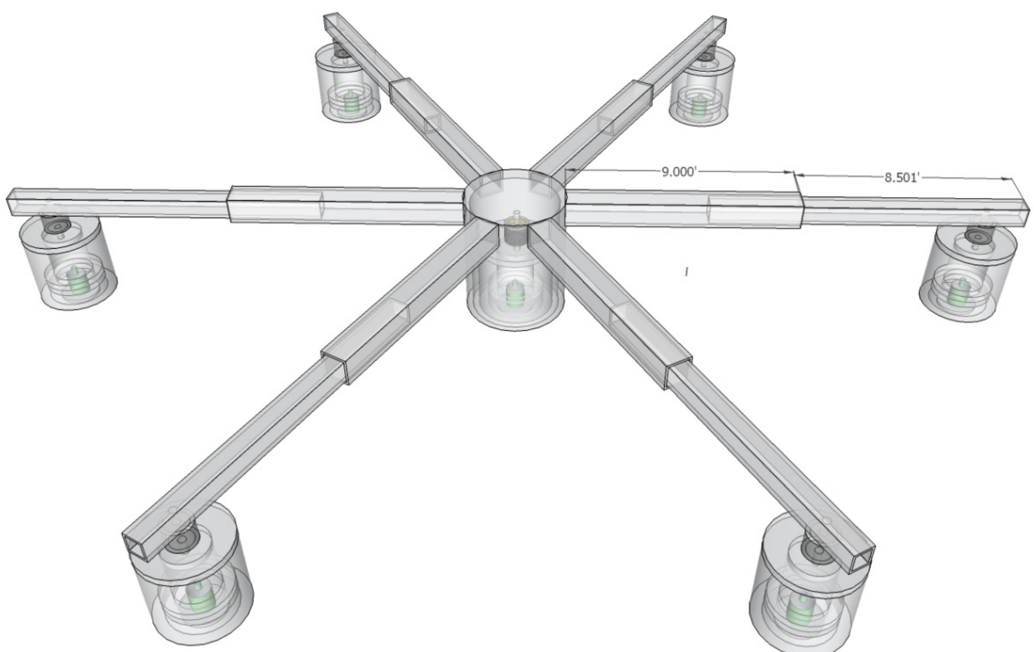

(b)

Figure 8 Three-dimensional modeling of (a) suspension and housing for the sensor module and (b) sensor array structure used in the project.

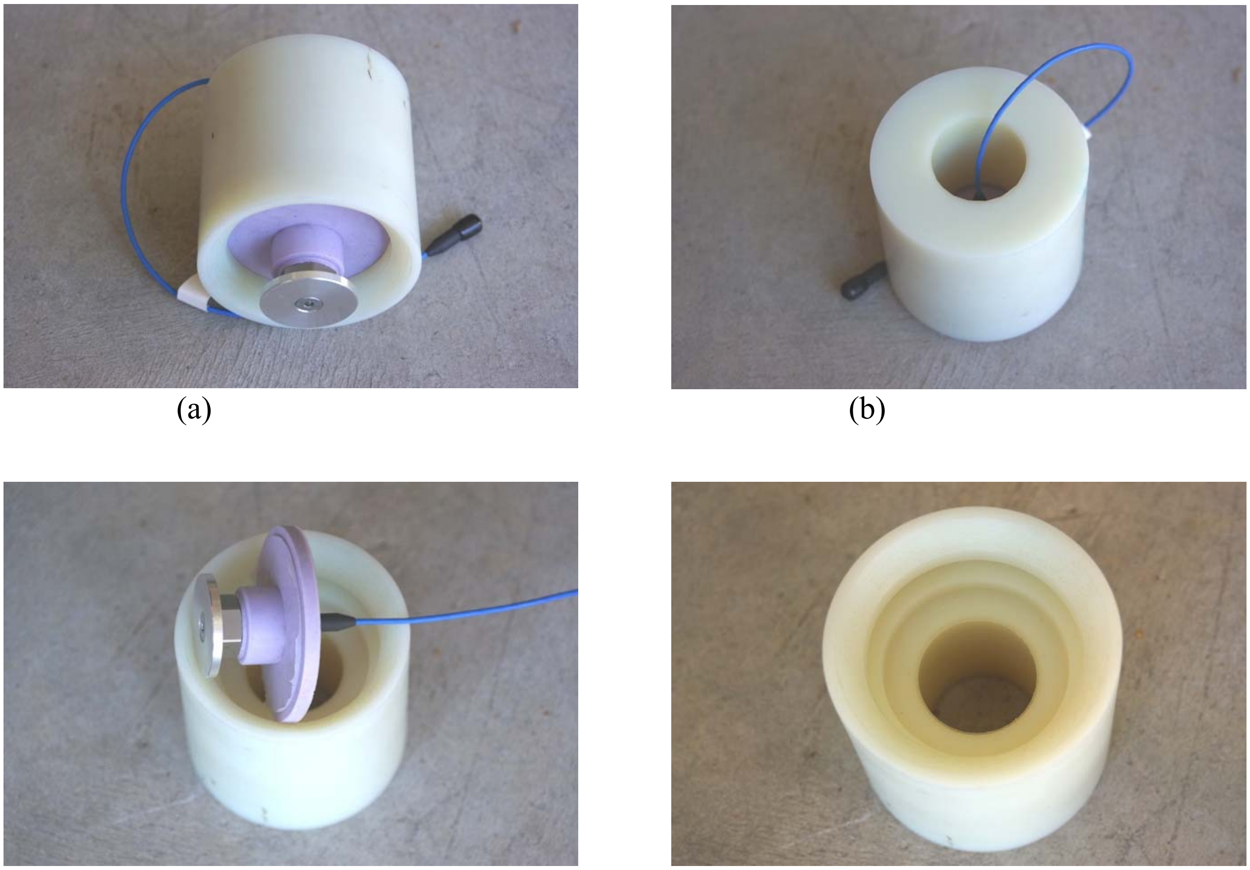

(a) (b)

(c) (d)

Figure 9 Sensor module design, first article, for the sensor array: (a - b) partially assembled sensor module and (c – d) exposed sensor module with silicone molding and housing.

Figure 10 shows the completed, fully assembled sensor module design. The silicone molding and vibration damping mount provide necessary acoustic isolation and suspension subsystem during the array deployment and system operation. The array structure uses the telescoping tubing for easy assembly, storage, and transportation, see Figure 10e-f. Figure 11 shows a partially assembled system carriage with wheels and a single sensor array arm attached.

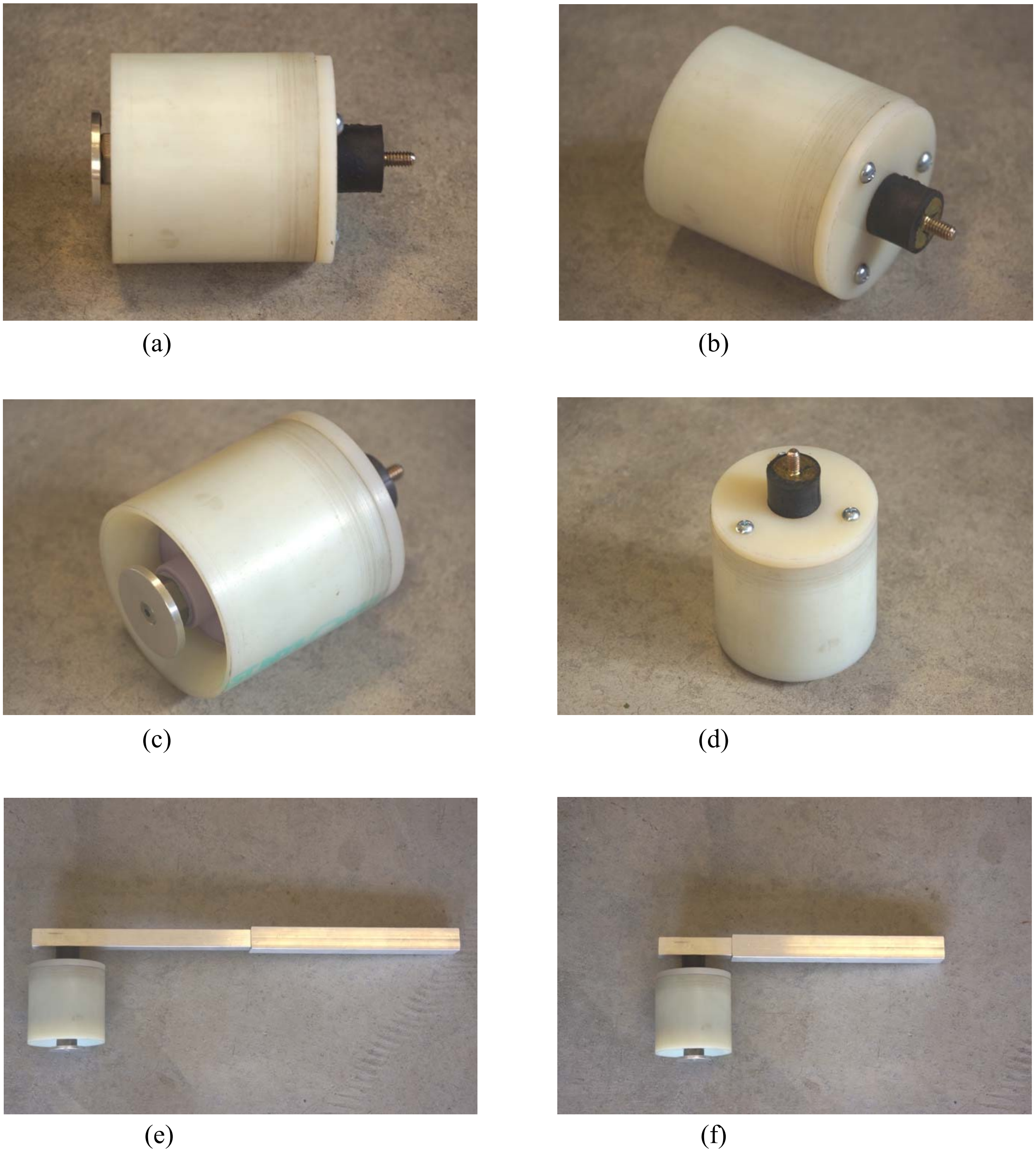

Figure 10 Final configuration of sensor module assembly: (a - d) completed module with vibration damping mount, silicone modeling, nylon housing, and transducer, and (e – f) sensor module with array arm extended and retracted.

Figure 11 Partially fabricated system carriage with wheels and array assembly.

Figure 12 shows the major components of the system electronics – CPU (single board computer), digitizers (ADCs), LCD display panel, and DC-to-DC power supply. The bench test of the system electronics was very successful and met the design requirement. The system software, under new computer operating system and device driver and the data acquisition subsystem met the operation goals for the system.

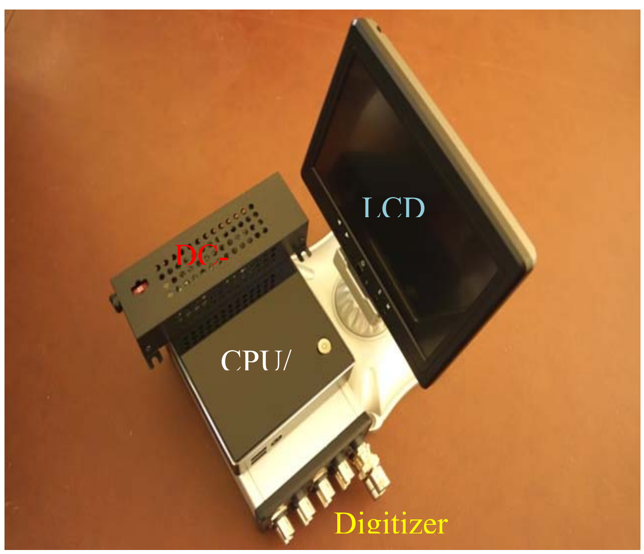

Figure 12 System electronics: CPU (single board computer), digitizer (ADCs), LCD (touch-screen) display panel, and DC-to-DC power supply.

Noise Source and Initial Test Phase

At the outset of this project, one of the first objectives was to design and build a downhole seismic energy source to replace the system used previously, and that is no longer available. In discussions between team participants the guidelines for source specifications were established. These included;

- Estimate of signal frequency content from tens of Hz to 1.5 kHz
- Measured Sound Pressure Level (SPL) of 70-80 dB measured at 1 m distance in air
- Waveform to be as close to random as possible (or coded)
- Auto-correlation function to be as sharply peaked as possible

To address these guidelines, several possible noise sources were considered, including both downhole devices attached to the drill and stand-alone surface sources. All had different mechanisms of noise generation. This was done to allow an evaluation of the different sources and to determine which was the most effective.

Source Description

During an initial demonstration, it was confirmed that the source waveform is critical to getting good results from the acoustic system. This waveform should have a sharply-peaked autocorrelation function. This can be achieved with either a completely random source function, or using a coded waveform.

Based on this observation, several vibrator designs that could use a "programmable" source capable of transmitting a well-designed waveform were created. Code was written in MATLAB that generates arbitrary waveforms, and saves them as WAV audio files for use with any programmable source. Two test waveforms were generated that have sharply-peaked autocorrelation functions: 1) a chirped sine wave in the 2 – 400 Hz frequency range with a duration of about 2 sec.; 2) a semi-square wave with randomized duty cycle in the 40 – 500 Hz range with a duration of around 4 sec.

Two different downhole source designs were selected and constructed. The first of these produces vibrations largely in the axial direction, parallel to the drill rod axis. The second is a rotary source, with the majority of the vibrations transmitted normal to the drill rod axis.

The axial downhole source was designed as a special seismic source motor with the proper form factor to fit into a sonde head. This motor has an unusual design to allow it to deliver low frequency vibrations with high power in a package that is approximately 2" in diameter, and 8" long. A cross-section view of the motor is given in Figure 13. The internal magnet assembly is driven into the end caps of the motor to produce an axial vibration. The coils can be driven with a custom designed waveform, as described above, to create a sharply peaked autocorrelation.

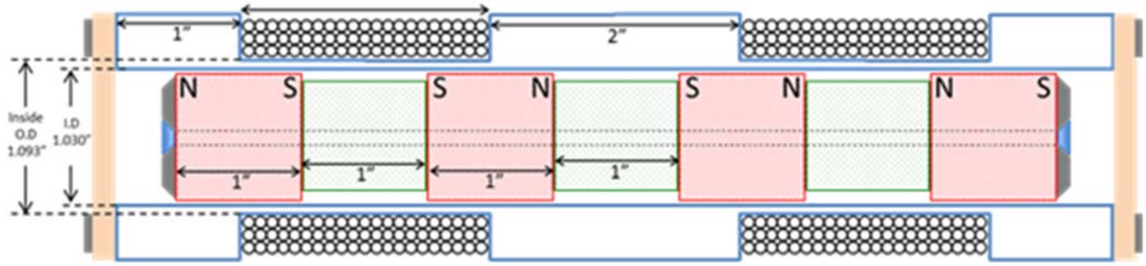

Figure 13 Cross-section of axial motion seismic motor.

The motor mandrel is machined to allow winding of two drive coils, connected with opposite polarity. Resistance of these coils is approximately 9 ohms each. Thus, they may be driven with a common high power audio amplifier. The device fits into a custom drill head. The motor is run from a 12 V DC source. Power is fed downhole by the use of a DCI CableLink® system. A higher power motor (with larger vibration potential) could be constructed by doubling the length of the mandrel and magnet shuttle.

A second downhole source was designed that produced radial or circumferential vibrations, resulting from a more standard design. In this source, a central shaft having radial hammers mounted on it is rotated. This causes the rotating hammers to strike anvils welded into the drill pipe wall. Thus, the ground motion produced by this source will be different from the axial source already described.

Figure 14 shows a three dimensional drawing of the radial source. The shaft holding the hammers is rotated by an electric motor. Placement of the anvils and variation of the driving voltage can result in quasi-random vibrations.

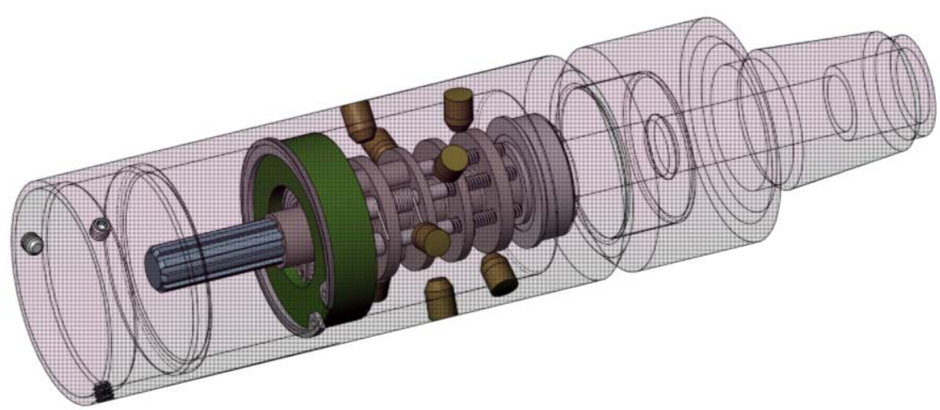

Figure 14 Three-dimensional view of the radial hammer, downhole source. Shown in solid form are the hammers and welded anvils that produce ground vibrations.

The electric drive motor is run at 24 V DC that is also supplied via a DCI CableLink® system. The power supplied by the motor is approximately 100W continuous. The amount of energy transmitted to the ground is determined by the number of hammers, their mass, and the rotation speed of the motor. The motor could be altered to include more hammers.

A third downhole source consisted of the drilling action of the HDD itself. In the test area constructed, several large concrete blocks were buried. During testing the drill head was rotated against these obstacles, creating seismic noise similar to that produced in a 'noisy' environment with rocks and cobbles in the ground.

In order to provide as wide a test base as possible, two alternative sources were prepared for testing. These include a surface seismic actuator and an underground, 2-inch diameter 'mole' or vibratory piercing tool.

The first of these is a small seismic actuator purchased commercially. This transducer uses a magnetically suspended piston to impact the ground surface or a structure, operates in the 5 to 200 Hz range, and is manufactured by Guithammer. This device can accept an audio wave file, and transmit low-frequency vibrations into the ground. Both a chirp waveform and random duty cycle square waves have been successfully applied to the source. The disadvantage of this source is that it is small and does not provide high amplitude vibrations into the ground. This is exclusively a surface source. Figure 15 illustrates the surface actuator being tested in a laboratory setting.

Figure 15 Photograph of the surface seismic actuator transducer. Fixtures have been made that allow axial or transverse motion to be applied to the ground.

For both the surface transducer and the downhole axial source, various waveform files were generated and applied to the motors. These include chirps, random square waves, and periodic square waves.

A mole is a device commonly used in the construction industry to lay pipe underground without trenching. During the mole operation, a pneumatically driven piston impacts the nose of the mole (internally), forcing the entire apparatus forward. The machine forces its way through the soil with each impact. As used in tests performed on this project, each impact produces a seismic displacement pulse that can be detected by the sensor array. One advantage of the mole is that it produces a large amplitude repeatable pulse. Disadvantages include a restricted frequency range and general limited use in utility installations. Figure 16 shows a representative picture of a mole prior to placement in the ground.

In preparation for testing, a seismic monitoring system (manufactured by Instantel) was used to measure vibrations from a 2-inch diameter mole. A vertical PPV (peak particle velocity) of 0.012 in/sec and an overpressure reading of 73 dB(A) were logged when the 2-inch diameter pneumatic piercing tool (mole) was operated at a distance of 20 feet from the sensors. The signal frequencies were typically less than 50 Hz.

Figure 16 Photograph of a utility installation pneumatic 'mole'.

Prior to obstacle detection tests undertaken with the mole, other additional measurements were made of typical SPL and ground vibration levels. With only an air compressor running, the audible noise was approximately 60 dB(A) and the vertical component of the peak particle velocity (PPV) was 1.24×10^{-3} in/sec. The compressor was positioned approximately 60 ft. from the monitoring device. A summary of background measurements and results from the mole source is provided in the table below.

Table 1. Noise Characteristics of Mole Seismic Source

	2 in. Pneumatic Piercing Tool (Mole)		
Source Distance	Vertical PPV ($x10^{-3}$ in/sec)	Vertical Frequency (Hz)	Microphone SPL [dB(A)]
Background	1.24	27.7	60
100 ft.	1.55	26.0	62
50 ft.	3.41	40.1	70
35 ft.	3.72	39.7	72
20 ft.	9.93	40.1	77

The initial data on the noise generators performance showed that they did not meet the specifications (noise intensity, frequency range, etc.) established in the past. Hence, it was expected that significant number of data generated during the local area tests may be rejected to define the acoustic system capability to detect pipes. However, the data collected with multiple noise sources will provide guidance on the next steps for future testing. All the sources described (with the exception of drilling into the concrete blocks) are envisioned for use mainly in 'quiet' areas where drilling action will not produce sufficient seismic noise for the sensor operation.

Test Procedure

A new test site in the local area was constructed for the initial testing with the acoustic system. This site contained of a number of concrete anchors buried 4 to 6 feet deep (Figure 17). Drilling into these obstacles provided a source of drill noise. In addition, about 3 feet from the anchors, two pipes were buried at 4- to 5-foot depth. In this initial testing, the total distance between the pipes is about 26', with the concrete anchors at the midpoint. There is access all around the site, so the pipes can be approached from a variety of angles and directions. The pipes are 20' long and consisted of a 10" diameter PVC pipe and a 3" diameter steel pipe. A schematic of the test site is shown in Figure 17.

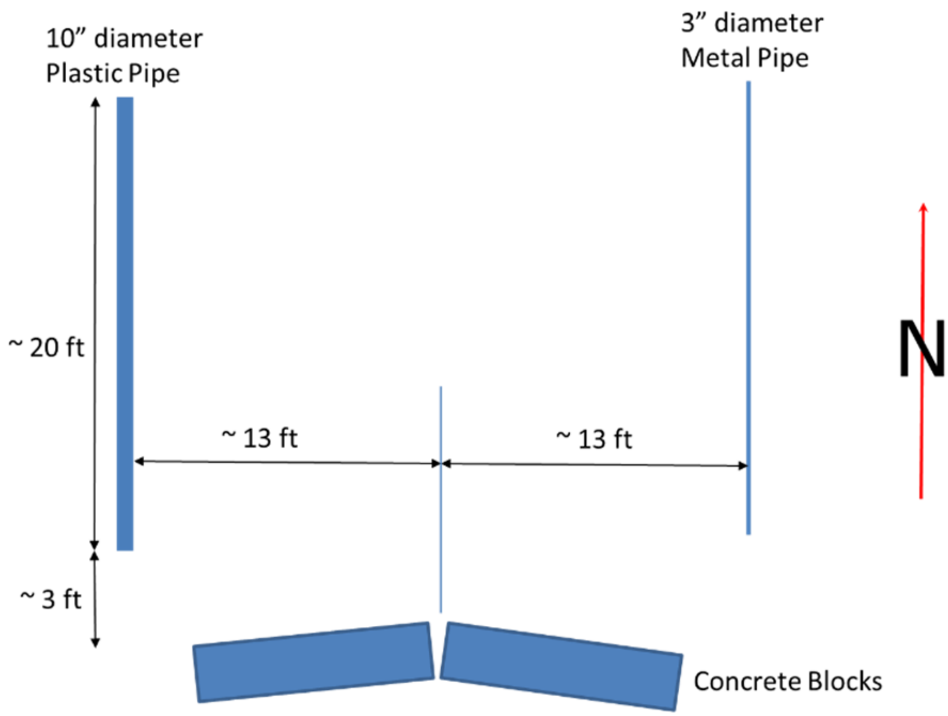

Figure 17 Schematic plan view of test site. The two target pipes were buried 4 feet deep, approximately 26 feet apart.

Soil samples acquired approximately 300 ft. north of the test site indicated the following: 1) Clay at a depth of 11 ft. below the surface, 2) Clay mixed with sand and gravel at a depth of 21 ft., and 3) Sand with some clay at a depth of 31 ft. The water table was recorded at a depth of 12 ft. The results of a nearby seismic refraction study revealed a 3-layer subsurface model. The near-surface soils have a seismic velocity of 500 ft/sec and extend to a depth of 3 ft below the surface. The second layer extends to a depth of 10 to 12 ft and has seismic velocities of 2,700 to 3,700 ft/sec. The third layer, likely the water table, extends beyond a depth of 10 to 12 ft and has seismic velocities ranging between 5,000 and 6,100 ft/sec. All velocities are for P-waves.

The acoustic system was tested with several noise generators to detect buried pipes in the local area in the last week of May 2014 and results were analyzed. Figure 18 shows the acoustic system being tested in the local area.

Figure 18 Acoustic system testing in the local area.

During the course of the four days of initial testing, over 800 trials were performed with all the different sources. Of these, about 60% generated data solutions where an obstacle detection marker was computed and placed on the system display. Often, the solution was located under the center of the array. Although this could be a valid solution, it was felt that this could be an erroneous result due to inadequate signal level or other system limitations. Because of this, results were analyzed both with and without these solutions included. Eliminating these 'zero' solutions reduces the number of 'good' solutions to about 47% of the total trials.

Data collection proceeded as follows. When the source was the drilling action into a concrete block, the source position was measured, and the receiver array was set at a fixed location. Data were collected and the locations of any data solutions for obstacle locations were logged in the field. After 10 to 25 trials were performed, the sensor was moved with the source stationary and the process repeated. When either the rotary or axial downhole source was used, the HDD was positioned and the location of the source noted by finding the drill head with a standard locator tool. The sensor was positioned and data recorded as before. Data were collected with the source stationary and with the source being drilled forward in 5 foot lifts. The sensor array was placed 5 to 10 feet in front of the source, in line with the drill rod path. When the drill reached the sensor location, the array was moved forward, toward the closest target and the process repeated. For both the mole and actuator, the source remained stationary while data were collected. The sensor was moved and the process repeated a limited number of times.

Test Results

During data collection over the four day test period, obstacle locations generated by the acoustic sensor were manually recorded, along with the sensor and source locations. Initially the obstacle locations were generated in a local reference frame, with the center of the sensor array as the origin. During processing, these locations were transformed into a global reference frame that included the target pipe positions.

Analyses of the data consisted of grouping the data into sets collected with common sources and examining the location of obstacle markers generated by the obstacle detection sensor. Data were grouped together if they were generated during the use of a common source, in roughly a common location. During these tests, the sensor may have been moved. Table 2 summarizes the results compiled. A total of 839 trial solutions were recorded. These were grouped into 11 different data sets depending on the source used, as shown in column 2 of Table 2. During the data collection, there were a large number of cases where data were collected, but no solution was developed. The number of these 'No Solutions' cases for each set are shown in column 4 of Table 2. In addition, a number of solutions were obtained where they were placed under the center of the array. These data were also compiled, and removed from the number of solutions analyzed. The final proportion of 'Good' solutions varied from a high of 70% for a concrete drilling source to 24% for the seismic actuator. In general, it is considered that the higher the number of 'Good' solutions the more appropriate the source for acoustic pipe detection.

Table 2. Compilation of Results for Initial Test Campaign

Test	Source	Total No. of Trials	No. of Trials With No Solution	Number of Trials With a Zero Solution	Total no. of 'Good' Solutions	Percent 'Good'
1	Concrete	15	4	4	7	47%
2	Concrete	22	10	3	9	41%
3	Rotary	15	8	1	6	40%
4	Rotary	85	29	10	46	54%
5	Axial	167	59	37	71	43%
6	Axial	159	113	4	42	26%
7	Rotary	113	40	1	72	64%
8	Concrete	37	9	2	26	70%
9	Concrete	156	31	37	88	56%
10	Mole	39	16	4	19	49%
11	Actuator	21	15	1	5	24%
Total		829	334	104	391	47%

After the data were compiled and pipe detection markers converted to a global reference frame, the locations of the markers were plotted along with source, array, and target positions. The first of these plots is shown in Figure 19. This figure shows the locations of all computed pipe detections in plan view, including all those that lay under the center of the array. Orange squares represent the source locations, red circles the array location, and yellow and blue lines, the two target pipes. The origin of the plot lies at the center of the two sets of concrete blocks. Distances are given in feet.

There appears to be a slight clustering of solutions over each target pipe location. However, this could be due to a clustering of solutions around the sensor locations instead. As mentioned, this plot lumps together results from all sources, and so may include data from sources that were not effective for pipe detection. Thus, a certain amount of scatter may be the result of including these data points.

To examine the idea that including weak sources might be influencing the distribution of solutions, a subset of the data from only drilling into the concrete blocks was examined. The noise generated by drilling into the concrete blocks was generally considered to be the most effective for use by the sensor array. These results are shown in Figure 20. Again, these results include solutions that fell under the center of the sensor array.

Figure 20 shows the results from drilling in the western set of blocks, closest to the 10-inch diameter plastic pipe. These data tend to cluster over the plastic pipe, but again this could be due to the concentration of sensor locations close to the pipe. The data solutions appear to be roughly uniformly distributed around the sensor locations, and do not appear to lie preferentially to one side or another.

Figure 19 Plan view of all computed pipe/obstacle locations from the initial test campaign. Also shown are the source, sensor array, and target pipe locations. The origin of the plot lies at the midpoint of the concrete blocks used as sources. Included in this plot are all the solutions that lay under the center point of the array.

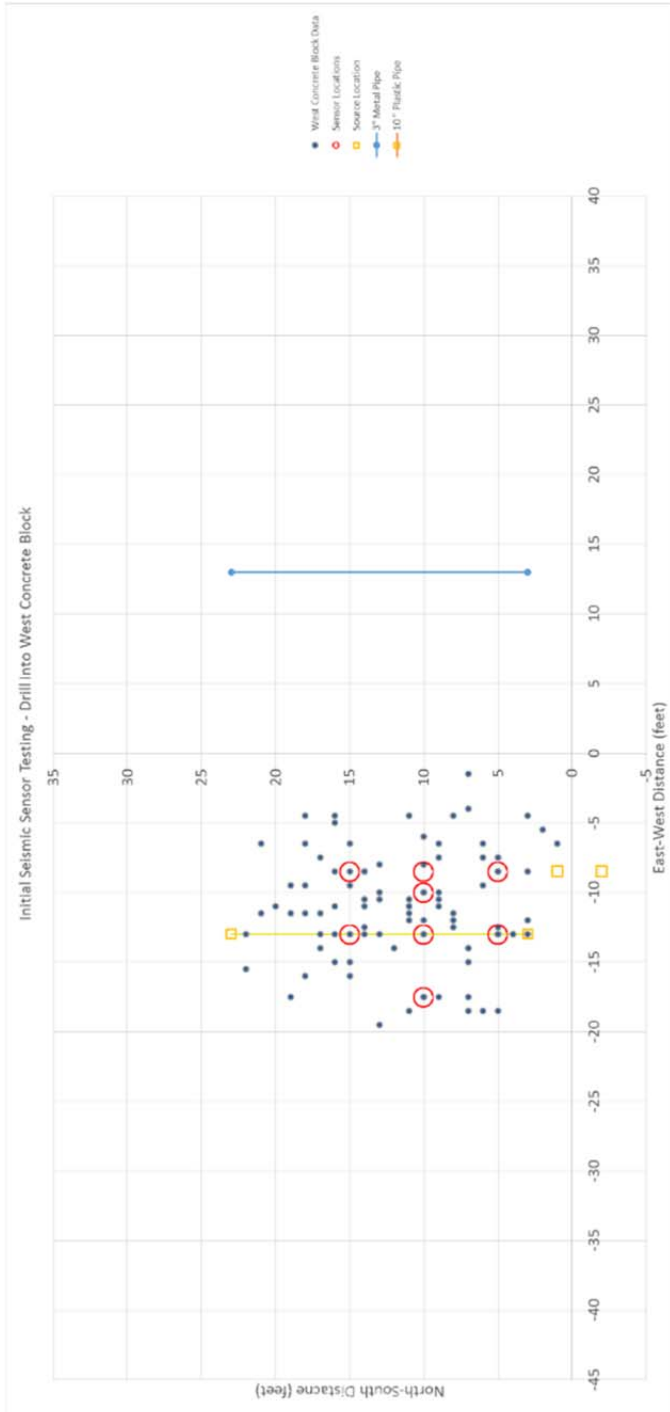

Figure 20 Plan view plot of the data solutions generated using drilling into the western concrete block as a source. Solutions lying under the array center are included in this plot. Solutions tend to cluster around the larger pipe location, but the east-west spread of solutions is relatively large.

Additional Analysis of Data Collected and Stored on the Hard Drive of System

The next step was to analyze data collected and stored in the hard drive of the acoustic system. The data included in the hard drive provides the noise source strength and frequency, and detected pipes and locations for each test. The following four aspects/criteria were used to determine adequacy of each data set:

1. Minimum noise level generated from the noise source,
2. Frequency response above detectable range for the buried pipes/obstacles,
3. Fail/pass transducers' response/activity during the tests, and
4. Verifiable and detected pipe's location (red dot on the system display).

The data analysis, with corrected drill-head position, resulted in more than 159 data sets out of 800^{+} recorded data from the local area tests that have been validated to be meaningful data sets in evaluating the performance of the HDD acoustic pipe system. These tests included data collected with noise sources from concrete blocks and electrical motors. In a few cases, the data collected with the pneumatic mole as a noise generator were reasonable and verifiable to be valid for further analysis.

The corrected system performance from these 159 data sets during the trials was separated into two categories: ***static*** and ***dynamic.*** The static data represent the stationary field test with the noise source in operation (no drilling machine movement), whereas the dynamic data refer to when the drill-head is advancing (push/rotate) with the noise source in operation. It should be noted that due to the field-of-view limitation of the acoustic test program/software, the estimated drill-head position was used and was bounded based on the recorded field test setup/situation (relative distance between the noise source and array center, and the noise source and depth of the drill-head). No compensation for the distance offset (i.e. y-axis) between drill-head and array center was applied in the corrected calculation. In the case of moving drill-head test, the correction process used the rate of drill-head advancing distance (total drill-head movement/number of test points) to estimate drill-head position during the data analysis. The advancing rate was estimated to be no more than ± (3"to 6")/test-point.

Even with the pneumatic mole which was known to generate too low frequencies, the system was able to detect pipes in a few cases after applying the corrected noise source positions. Similar situations were also observed for the tactile transducer (alternative source) which exhibited very low noise energy, but provided a few test data sets (three) to be processed with pipe detection results.

Table 3 gives the summary of acoustic system performance with various noise sources during the local area tests conducted in Pella, Iowa. The detail test log is listed in the Appendix A Overall, for both stationary and moving drill-head processes, the acoustic pipe detection system was able to achieve the average detection accuracy of ± 2.1'. The concrete blocks, although not useful as a noise source for the real-world use, showed 72 validated cases and indicated as the best effective noise making source. The data from these sets will assist in further refining required signal strength and frequency for other noise sources. The electro-mechanical noise sources, rotary (48 cases) and axial (21 cases) motors, performed well in both stationary and dynamic detection processes. The pneumatic piecing tool (15 cases) can be a good noise source if a broader spectral response was obtainable. Again it should be noted that the mole cannot be a useful device for the real-world application. The number of the effective test samples for the tactile transducer was not significant enough to be a valid noise source as tested. The test results from all noise generators will assist in redesigning and constructing the final noise source for future tests.

Table 3. Acoustic System Performance during the Local Area Tests in Pella, Iowa

Noise Source* / **Data Set**	Concrete Blocks	Rotary E. Motor	Axial E. Motor	Pneumatic Mole	Tactile Transducer
Detection† Accuracy (± ft)	**1.5'** (72)	**2.1'** (48)	**2.8'** (21)	**3.3'** (15)	**1.0'** (3)
Overall (± ft)	**2.1'**				

* Data validated from concrete blocks, electrical motors, pneumatic mole, and tactile transducer as noise generators

† Test accuracy with number of validated test cases in parenthesis

Second Testing Campaign: November 2014

Testing conducted during November 2014 constituted a second round of local area tests. The acoustic system used in this tests was identical to the one used in the first round of testing. However, the noise source used during these tests was different and improved. This section addresses work completed on development, test, and evaluation of a modified noise source with the acoustic system. The local area tests were conducted from November 11 to November 14, 2014 at the Vermeer facility.

The main objective of the work was to repeat performance testing of the acoustic obstacle detection system with a redesigned downhole energy source, in the same area as previous testing, with both a new target and one of the targets from previous testing. An additional goal was to gain insight into what parameters were critical to the system operation, what the technique operating limitations might be, and what the expected probability of detection and accuracy under the specific test conditions were.

Source Description

The test results from all noise generators used in the first local area tests assisted in redesigning and constructing the improved noise source for the second local area tests. The acoustic system was reconditioned, tested to assure that it is functioning properly, and was shipped to Pella, IA for the second local area tests to be conducted with the improved noise source. This report addresses work completed on development, testing, and evaluation of the acoustic obstacle detection system. Specifically, a set of local area tests were conducted on the Vermeer Manufacturing Company (VMC) campus.

The first local area tests identified inadequacies in the downhole energy source referred to as a noise generator. This inadequacy could have been due to a nonrandom waveform, inadequate energy coupled to the ground, or an energy spectral content not compatible with the acoustic sensor array. Hence, it was decided to re-design the downhole source for higher amplitude and wider frequency.

The analysis of the May 2014 data generated by the different noise sources showed that the best results were obtained from the rotary hammer source. This was true in terms of both energy and spectral content produced. However, the energy produced by this source was still considered low and the spectral content was marginal. In addition, the source was not as physically robust as desired. Since the waveforms produced appeared to be the best of all sources tested, a re-design effort was undertaken to improve the rotary hammer source. This revised source was based on the electric-motor driven design of the prior tests.

A new source was designed to couple more energy into the ground through a better hammer design, more hammers, and greater power. Revisions to the design included slightly altered hammer shapes and a different restoring spring assembly. Figure 21 shows the revised mechanical drawing for a single hammer assembly. In this assembly, two hammers are rotated on a central shaft striking three anvils embedded in the housing walls.

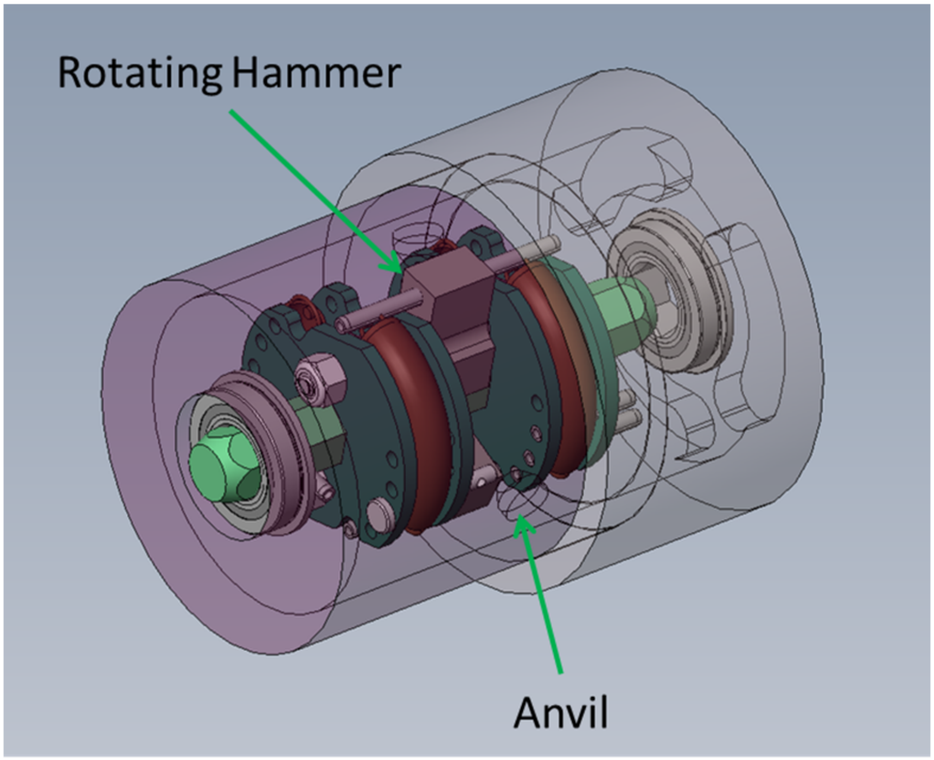

Figure 21 CAD drawing of one hammer assembly of the re-designed source. Three of these assemblies were installed in the final source used in field testing.

The overall source consisted of three hammer assemblies illustrated in Figure 21, for a total of 6 hammers. All are mounted on a central shaft which is rotated by an electric motor. The motor runs on 24 V DC, and has a nominal current draw of 4-10 A.

To confirm the source design functionality, a prototype was first constructed using parts machined from hardened steel and a high temperature 3D printed plastic. After assembly, the source was tested in the lab for around 30 minutes of continuous operation. During this time, the electric motor drove the assembly at 200 rpm, resulting in an impact frequency of 60/second. Current draw was as high as 9 A at 24 V for a draw power of 216 W. This was done with stiff restoring springs on the hammers, which resulted in mechanical failures in the springs. Softer springs were installed which lengthened the spring life but dropped the current draw to around 6 A (144 W).

Figure 22 shows the full six hammer assembly ready for installation in the downhole casing. The hammers were of hardened steel and showed minimal wear after testing was completed.

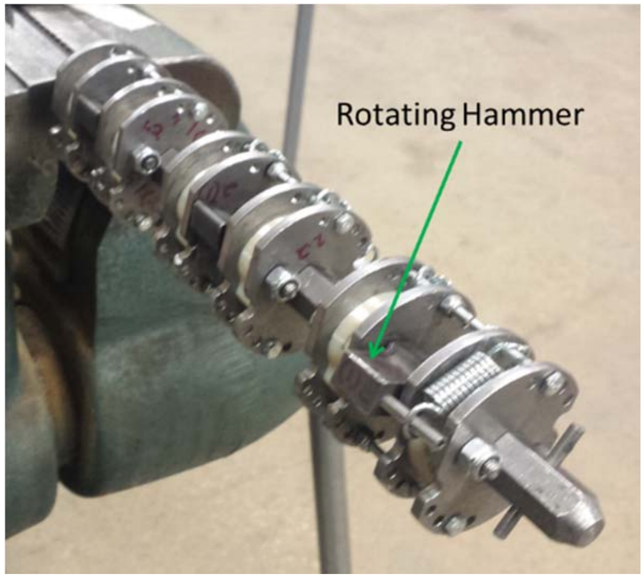

Figure 22 Photograph of the three hammer assemblies ready for installation in the downhole casing. In the final source, there were six hammers, each striking 3 anvils on each revolution. This resulted in 18 impacts per revolution.

As in the first generation source, the electric drive motor is run at 24V DC supplied via a DCI CableLink® wireline system. As mentioned, the motor current draw varies from about 4 to 10 A. Current draw is sinusoidal in nature, reflecting the power needed to rotate the hammers past the embedded anvils. Figure 23 shows a screen shot of a Volt/Ammeter during operation of the source. Both the supply voltage (24 V) and the current (average 5.92 A) are shown. During operation in the field, the springs supplying restoring force to the hammers would weaken and in some cases fail. This causes the current draw to drop along with the average power supplied by the source. Typically the source would start at 6 A (144 W), but drop to 3.5 A (84 W) at the end of a series of tests. The amount of energy transmitted to the ground is determined by the number of hammers, their mass, and the rotation speed of the motor. The motor could be altered to include more hammers.

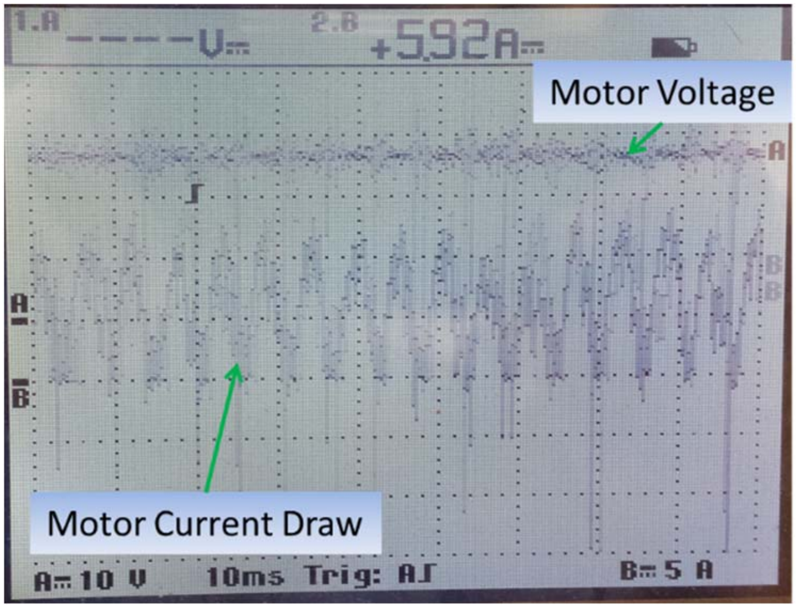

Figure 23 Screen shot of Volt/ammeter showing the supply voltage and motor current draw for the downhole rotary hammer source. Motor voltage was about 24 V, and the current draw was siinusoidal with an average value of 5.92 A.

An additional source was used during testing. This consisted of simply drilling into a buried concrete block and using the vibrational noise generated as a source. This was also used during the first set of tests, but the geometry of the blocks with respect to the target pipes was poor, resulting in a theoretically small scattering cross section from the pipes. A block was reburied for the November testing so that the pipe scattering cross section was maximized with the pipe broadside to the concrete block source.

Test Procedure

From early work on the acoustic system, it was determined that the diameter of the target obstacle should be greater than one-third (Cribbs and Wu, 2004) of the seismic wavelength for it to be detected. Using the measured soil velocity of 500 ft/sec with a frequency of 100 Hz, this means a pipe diameter greater than 20 inches. Other published works report the detection threshold as 1/10 or 1/20 wavelength. These criteria would suggest a working diameter of 6 inches or 3 inches, respectively.

Thus, for the energy sources under development, to provide a test site with the better probability of detecting an obstacle, larger diameter targets need to be installed. To accommodate this, two pieces of 18” diameter culvert were installed at the test site. Figure 24 shows the 18” culverts prior to burial. These pipes were capped and buried end-to-end to form a 20 foot long target. Hence for the November tests, there were a 10 inch diameter PVC pipe target and an 18 inch diameter metal culvert target, both 20 feet long.

Figure 24 Photograph of 18" culverts to be used as test targets prior to their burial.

Figure 25 is a plan view of the test site showing the location of the pipe targets and the source and sensor locations from the November 2014 testing. The concrete block was located at coordinate (0,0). The 18” culvert was located at x = -20 ft., and the 10” PVC pipe was at x = -40 ft.

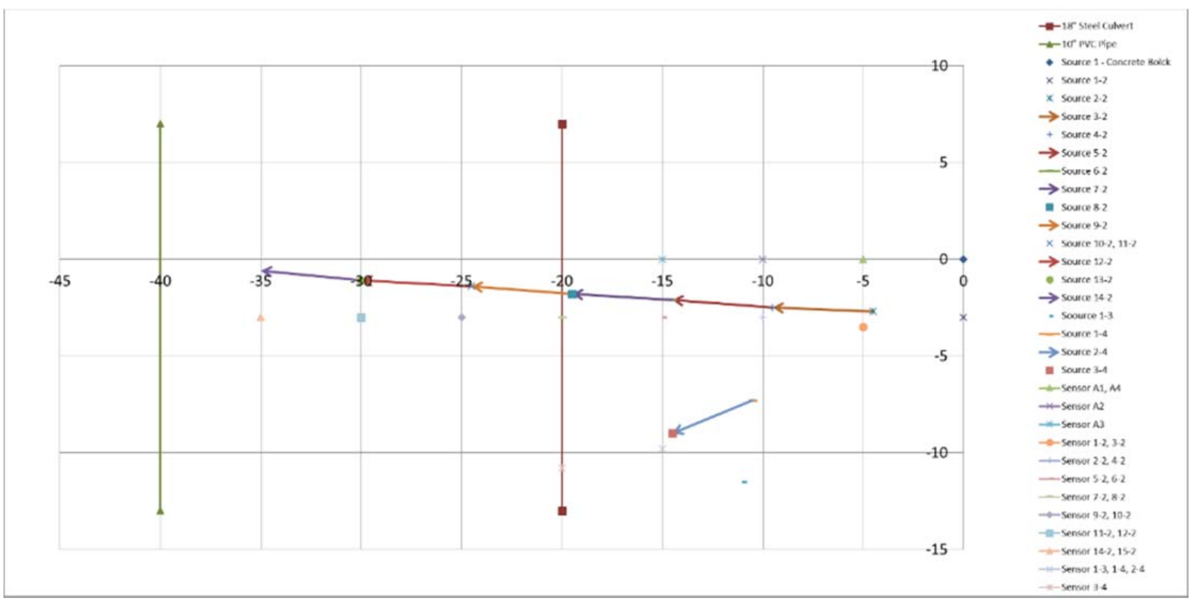

Figure 25 Target, sensor, and source locations used in the November 2014 field testing. An explanation of the symbols used is given in the text.

Source and receiver locations are noted on Figure 25, and in Table 4. Source locations indicated by a line with an arrow head represent cases where data were collected using the rotary source as the drill head was moved forward. Source locations designated as a single points are cases where data were collected using the rotary source while both source and sensor were stationary. Table 4 provides a correlation between source and sensor locations. That is, data were collected at the sensor location given in column 2 when the source was at the location given in column 1. Also shown is whether the source was moving or stationary.

Data collection proceeded largely as it did for the May 2014 tests. When the source was the drilling action into the concrete block, the source position was measured, and the receiver array was set at a fixed location. Data were collected and the locations of any data solutions for obstacle locations were logged. After completion of data collection, the sensor was moved with the source stationary and the process was repeated. When the rotary downhole source was used, the HDD was positioned and the location of the source noted by finding the drill head with a standard locator tool. The sensor was positioned and data recorded as before. Data were collected with the source stationary and with the source being drilled forward in 5 foot lifts. The sensor array was placed 5 to 10 feet in front of the source, in line with the drill rod path. When the drill reached the sensor location, the array was moved forward, toward the closest target and the process repeated.

During the course of 2 days of testing, approximately 270 trials were performed. Of these, about 75% generated data solutions where an obstacle detection marker was computed and placed on the system display.

Table 4. Correlation of Source and Sensor Locations: November 2014

Source Location	Sensor Location	Stationary or Moving (S or M)	Location
Concrete Block	A1, A2, A3, A4	S	1, 2, 3, 4
1-2	1-2	S	5
1-2	2-2	S	6
1-2	3-2	S	7
2-2	4-2	S	8
3-2	4-2	M	9
4-2	5-2	S	10
5-2	6-2	M	11
6-2	7-2	S	12
7-2	8-2	M	13
8-2	9-2	S	14
9-2	10-2	M	15
10-2	11-2	S	16
11-2	12-2	S	17
12-2	13-2	M	18
13-2	14-2	S	19
14-2	15-2	M	20
1-3	1-3	S	21
1-4	1-4	S	22
2-4	2-4	M	23
3-4	3-4	S	24

Test Results

During data collection, obstacle locations generated by the sensor were manually recorded, along with the sensor and source locations. Initially the obstacle locations were generated in a local reference frame, with the center of the sensor array as the origin. During processing, these locations were transformed into a global reference frame that included the target pipe positions. Note that the origin of the global frame is not the same between the data sets collected. This was done to allow scaling so solutions could be more easily viewed.

Two sets of analyses were performed on data collected during the November testing. The first involved examination of solutions recorded in the field, recorded to the nearest foot. The second analysis took the same data and reprocessed it post –acquisition, reporting the detection locations to the nearest 0.1 foot. In both cases the same processing steps were applied, the only difference was a numerical output for the reworked data versus reading the location off a plot in the field.

As was done for the data collected in May 2014 tests, analyses of the data consisted of grouping the data into sets collected with common sources and examining the location of obstacle markers generated. Data were grouped together if they were generated during the use of a common source, in roughly a common location. During these tests, the sensor may have been moved.

Table 4 summarizes the results compiled. A total of 199 trial solutions were recorded. These were grouped into 23 different data sets depending on the source used, as shown in column 1 of Table 5. During the data collection, there were again a number of cases where data were collected, but no solution was developed. The number of these 'No Solutions' cases for each set are shown in column 3 of Table 5. The final proportion of 'Good' solutions varied from a high of 100% for a rotary downhole source to 0% for one of the concrete drilling tests. About 75% of the tests resulted in a usable computed target solution.

Testing was started by drilling into the concrete block. This source should have resulted in large amplitude, wide bandwidth, and temporally uncorrelated vibrations. Four different tests were conducted, with the sensor placed at different distances from the concrete block. The proportion of useful solutions had a maximal spread from 0% to 100 %. At the time of data collection, the efficacy of the concrete block source was questioned. Figure 26 is a photograph of the excavated concrete block after testing was completed. There may have been one test where the block was missed, but there were at least three other cases where good drill contact with the block occurred. These are noted in Figure 26. In one case a circular hole was drilled into the block. Hence, for at least these three test cases good seismic vibrations should have been produced.

Table 5. Summary of Test Results: November 2014

Location	Source Moving or Stationary	No Solution	Good Solution	Total Tests	% Good Solutions	Drill or Rotary Source
1	S	0	7	7	100.0%	Drill
2	S	6	0	6	0.0%	Drill
3	S	9	4	13	30.8%	Drill
4	S	1	8	9	88.9%	Drill
5	S	1	7	8	87.5%	Rotary
6	S	1	1	2	50.0%	Rotary
7	S	3	7	10	70.0%	Rotary
8	S	1	8	9	88.9%	Rotary
10	S	0	12	12	100.0%	Rotary
12	S	4	11	15	73.3%	Rotary
14	S	4	10	14	71.4%	Rotary
16	S	4	11	15	73.3%	Rotary
17	S	5	12	17	70.6%	Rotary
19	S	0	13	13	100.0%	Rotary
21	S	1	10	11	90.9%	Rotary
22	S	2	7	9	77.8%	Rotary
24	S	3	8	11	72.7%	Rotary
9	M	7	13	20	65.0%	Rotary
11	M	1	9	10	90.0%	Rotary
13	M	4	9	13	69.2%	Rotary
15	M	3	9	12	75.0%	Rotary
18	M	3	8	11	72.7%	Rotary
20	M	7	7	14	50.0%	Rotary
23	M	0	8	8	100.0%	Rotary
	All Stationary	45	136	181	75.1%	
	All Moving	25	63	88	71.6%	
	Rotary Source	54	180	234	76.9%	
	Drill Source	16	19	35	54.3%	
	Total	70	199	269	74.0%	

Figure 27 shows the results for tests conducted while drilling into the concrete block. Unfortunately, no solutions computed in the field lay within a reasonable distance from the 18" diameter metal culvert. A statistical analysis showed that the solutions were much more likely to occur closer to the sensor location than the culvert location.

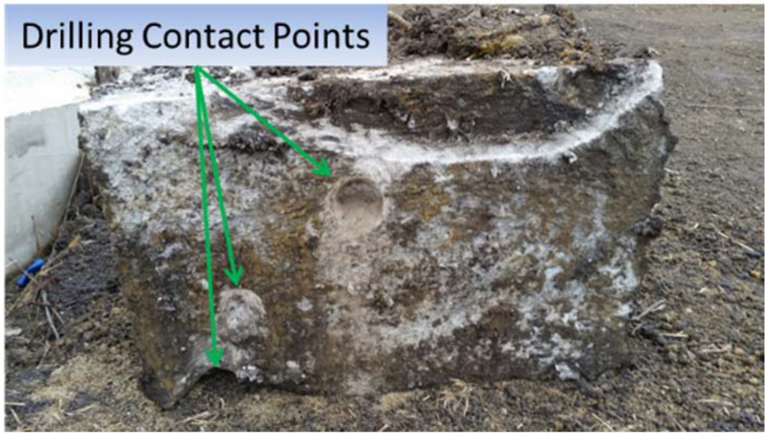

Figure 26 Photograph of the concrete block used as a seismic source. The block was excavated after the testing was completed.

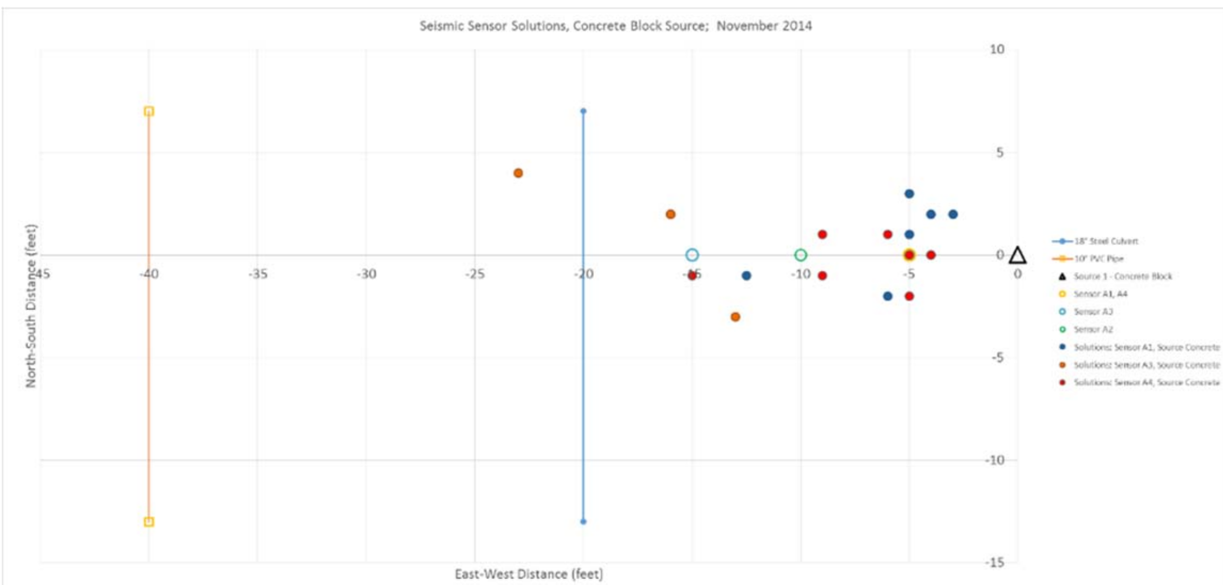

Figure 27 Plot of data solutions obtained when drilling into the concrete block was used as a source.

The remainder of the solutions were obtained using the rotary downhole hammers as the source. From Table 5 it can be seen that 77% of the tests conducted using this source resulted in a usable solution. It is unclear whether the source provided an optimal waveform, but since solutions were generated for three-fourths of the tests, it is assumed that the source was at least adequate. Figure 28 shows a summary plot of all solutions computed and logged for both the rotary hammer and concrete block sources, with the source both moving and stationary. The distribution of these solutions shows little correlation between computed target locations and the actual locations of the buried pipes. After all the target solutions were compiled, a field exercise was conducted where all the target locations were marked in the field with flags. These locations were found by locating the solution with respect to each sensor location as noted in the raw field notes. Figure 29 shows a photo of the source and sensor locations. As can be noted, the sensor and source locations were along lines indicating the linear nature of the test bores.

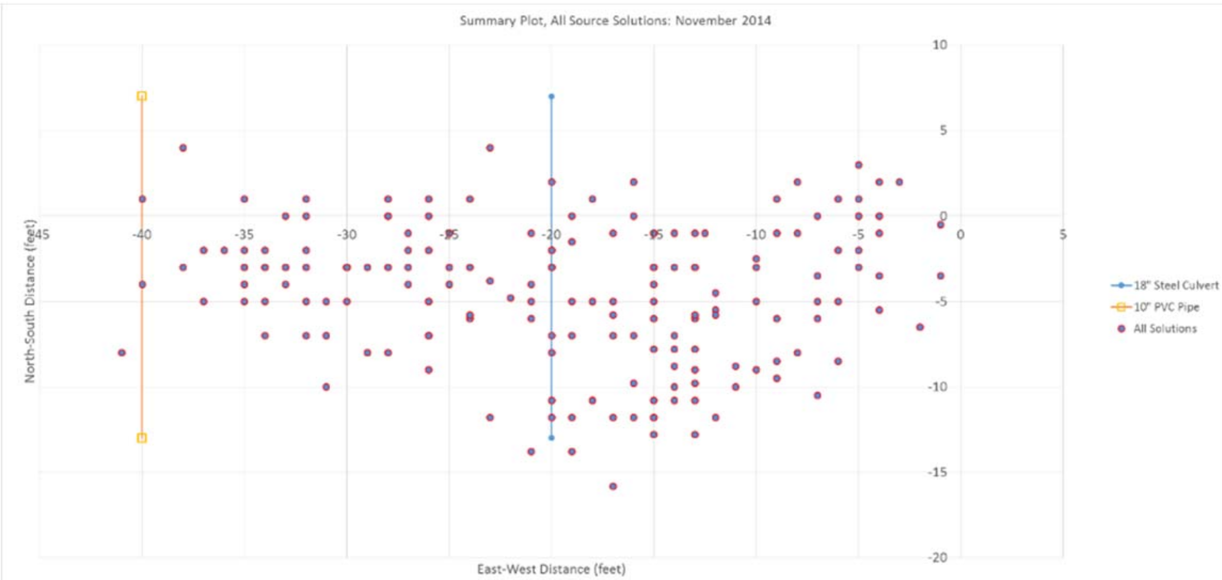

Figure 28 Summary plot of all calculated target locations from all tests conducted during the second round of field tests performed in November 2014.

Figure 30 shows that there does not appear to be any clustering of target solutions on or near the known target locations. It is possible that other seismic discontinuities exist within the survey area that could give rise to 'false positives' or clutter from unintentional targets. However, the pattern of target locations appears random enough to discount this possibility.

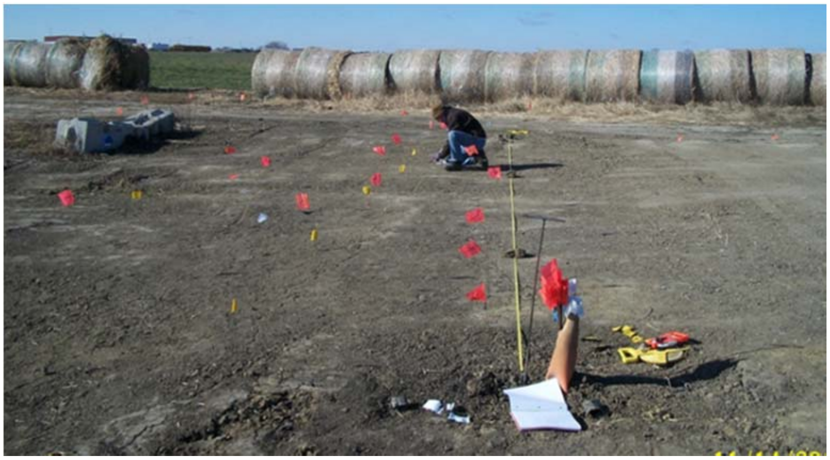

Figure 29. Photo of the sensor and source locations marked in the field. Red flags show the sensor locations and yellow the source locations. Not all source and receiver locations have been flagged in this photo.

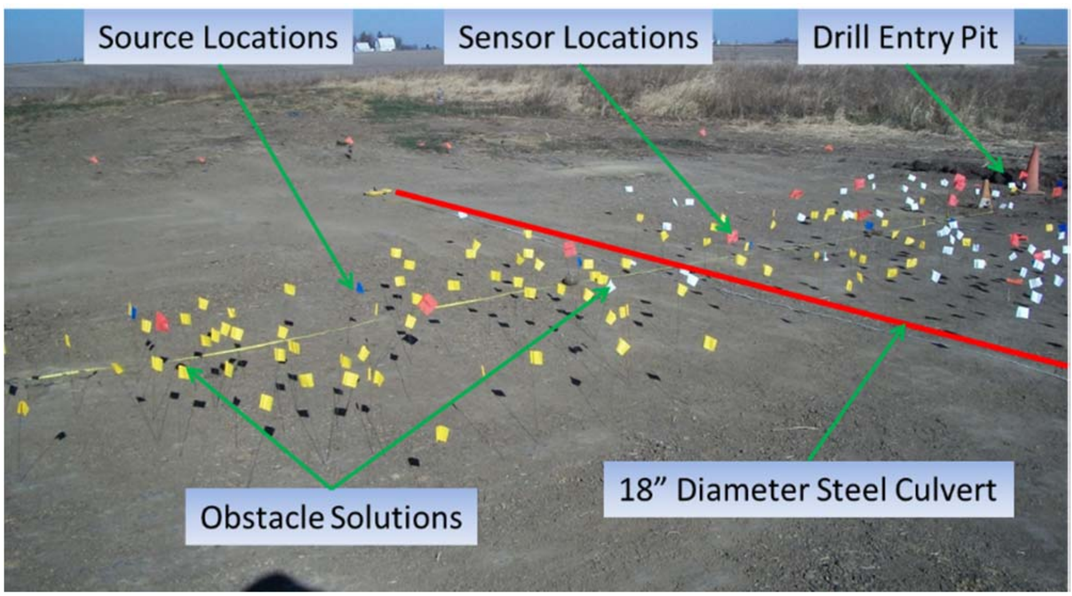

Figure 30. Target solutions marked with flags in the field relative to known source and sensor locations. Also marked on the photo is the location of the 18" diameter metal culvert. Sensor locations are shown with red flags, sources with blue flags, and solutions with yellow and white flags.

A statistical analysis was performed on the distribution of target locations with respect to both the target location and the sensor location, as was performed for the data collected in May 2014. Again, the cumulative fractions of the distance from the computed target location to both the actual target and to the sensor location were computed. The distances were computed as the minimal distance between the target and sensor or computed location. The cumulative fraction is the fraction of the distances that lie at, or closer to, that particular distance from either the pipe or sensor location. The results for the November 2014 data are shown in Figure 31. This plot shows whether the computed locations were statistically more closely associated with the sensor location or the target locations. In this plot there is a strong correlation between the sensor location and the computed target location. Thus, the computed target locations are much more strongly spatially associated with the sensor location than with the known target location.

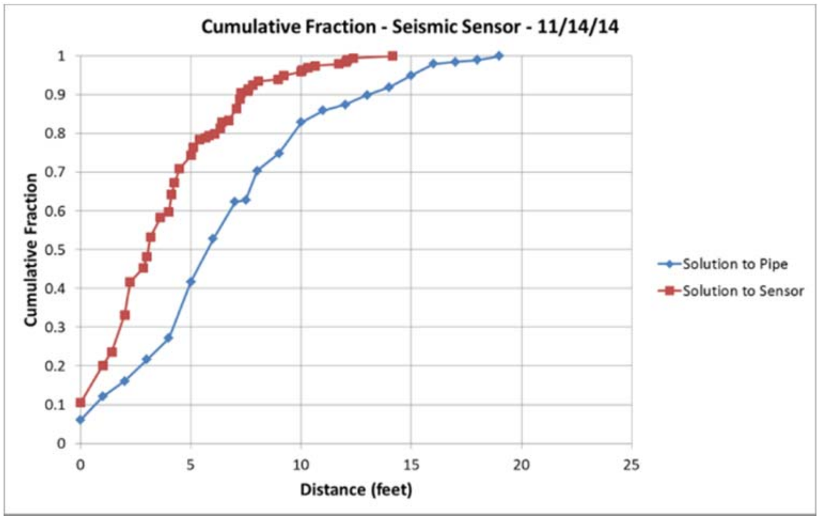

Figure 31. Plot of the cumulative distributions of the distance from solution to target and solution to sensor.

Several data acquisition issues should be noted when evaluating the results presented. First, several times during data collection, the source failed. These failures were traced to multiple root causes, including failure of the hammer restoring springs and loss of power continuity down the wireline in the drill rods. This resulted in needing to remove the head from the hole, make repairs, and reinsert the head in the drill hole. This reinsertion could have resulted in poor coupling between the source and ground, and hence lower quality data for location computation. In addition, wind chills during testing hovered around 0 to -10F, stressing electrical, mechanical, and personnel assets.

Reworked Data Results

The following discussion details analysis of data that were processed post-acquisition, using the same processing flow as was used in the first local area tests. More than 285 data sets were collected and stored during the three-day tests. It should be noted that not all these data sets resulted in locations logged in the field. The test summary was based on the validated 240 data sets (out of the 285 total) recorded from the tests. The performance evaluation of the HDD acoustic pipe system was based on the following test aspects/criteria:

1. Minimum acoustic energy level generated from the noise source,
2. Frequency response above detectable range for the buried pipes/obstacles,

3. Verifiable and detected pipe's location (red dot on data display), and
4. Activated and functioning noise maker during the tests.

The test data were collected and analyzed from the test setups using noise from the concrete block and rotary electrical motor. As reported before, the buried pipes were an 18" metal culvert and 10" PVC for these tests. The system performance during the local area tests was separated into two categories – ***static*** and ***dynamic*** – which represent the stationary field test with noise source only in operation (no drilling machine movement) and the drill-head advancing movement (push/rotate) plus activated noise source.

Due to the field of view limitation of the acoustic test program/software, the estimated drill-head position was used and bounded based on the recorded test setup/situation – relative distance between noise source and array center and the depth of the drill-head. No compensation for the distance offset ("Y-axis") between drill-head and array center was applied in the corrected calculation.

Tests were conducted under freezing temperatures and windy conditions. Based on a review of data waveforms, the new rotary noise source seemed to have broader spectral response than the previous design. However, the acoustic power is still considered somewhat weak for the soil situation at the test area – highly attenuative clay soils. The mechanical structure of the noise making device, unfortunately, was not as robust as desired. Several breakdowns were observed and required service during the local area tests. It was also observed that inconsistent acoustic energy (see Figure 32 and Figure 33) was sometimes detected among receiving sensors. In general, the high frequency acoustic signal tends to be attenuated faster than the other end of the spectrum as sound propagated - propagation distance of acoustic energy is inversely proportional to the source frequency. However, the other possible causes of such phenomena could be due to:

1. Overall weak acoustic noise generated under highly attenuative soil conditions,
2. High frequency sound energy content dissipated quickly within the array spacing during propagation,
3. Soil characteristics of the frozen ground, and
4. Inconsistent transducer coupling to the ground.

Overall, for both stationary and moving drill-head processes, the acoustic pipe detection system was able to achieve a detection accuracy of ± 2.1' on average for pipe and sensor separations of less than 10 feet. For the detection ranges greater than 10 feet, the detection accuracy goes down to 11.5', on average. These tests were the first ever test for the acoustic system conducted under freezing temperatures, very windy conditions, and frozen soil. It is unknown whether a 6 inch thick (or less) layer of frozen soil will impact system performance. The acoustic system mechanically and electrically operated well and achieved better than 84% (240/285) success rate in calculating a location solution.

Another issue to be considered in evaluating the system performance is the separation between the HDD and the sensor array. In Cribbs and Wu (2004) the minimum distance between the HDD and sensor was quoted as 50 feet, whereas the distance between the source and array was

10 to 15 feet. Distance between the HDD and array in the local area testing performed here was 35 feet or less. It is possible that surface waves from the HDD operating vibrations sometimes swamped those from the noise generator, resulting in inaccurate solutions. This behavior might be accentuated by the frozen soil layer acting as a waveguide.

Table 6 is a brief summary of the reworked acoustic system performance with the improved rotary noise generator and concrete block as the noise sources during the second local area tests conducted in Pella, Iowa. A detailed test log is given in the Appendix B.

Table 6. Acoustic System Performance during the Second Field Tests in Pella, IA.

Noise Source (Pipe-to-Array)[*]	Concrete Block (<10ft)	Rotary E. Motor (<10ft)	Concrete Block (>10ft)	Rotary E. Motor (>10ft)
Detection Accuracy (± ft)	**1.4'**	**1.8'**	**15.0'**	**10.5'**
Forward-Looking Detection[†] (± ft)	**1.8'**	**0.5'**	**12.6'**	**7.6'**
Overall (± ft)	**1.4'**		**11.4'**	

[*] test condition – Concrete Block and Rotary Electrical Motor test setups with pipe-to-array distance in parenthesis (in foot)

[†] only test results showing detected target located in front of the sensor array (along the drilling direction) were used in statistical calculation

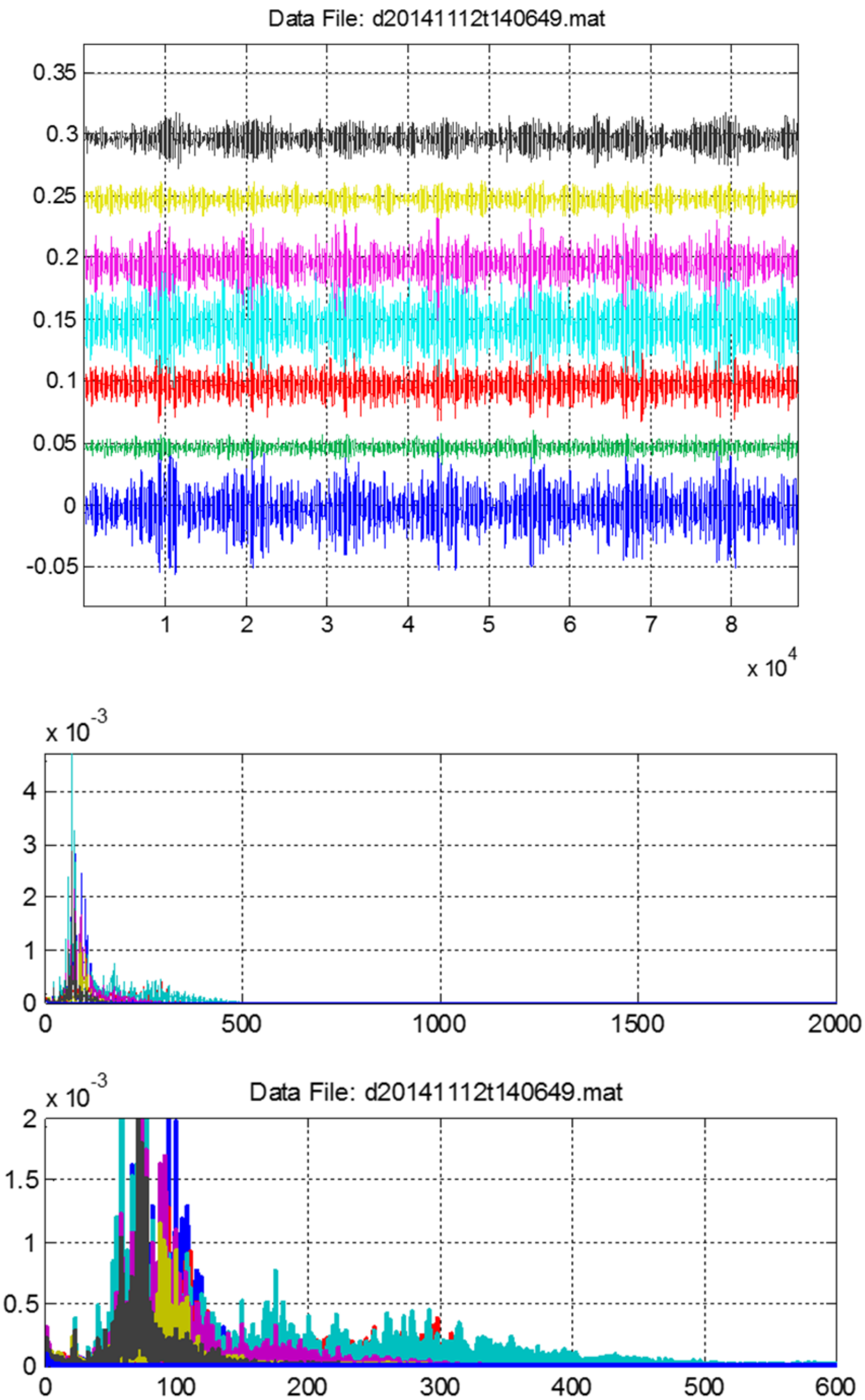

Figure 32 Noise source waveforms with consistent sensitivity readings among receiving sensors. The upper plot shows waveforms recorded at each of the array sensors and the bottom plot gives the associated spectrum of each trace.

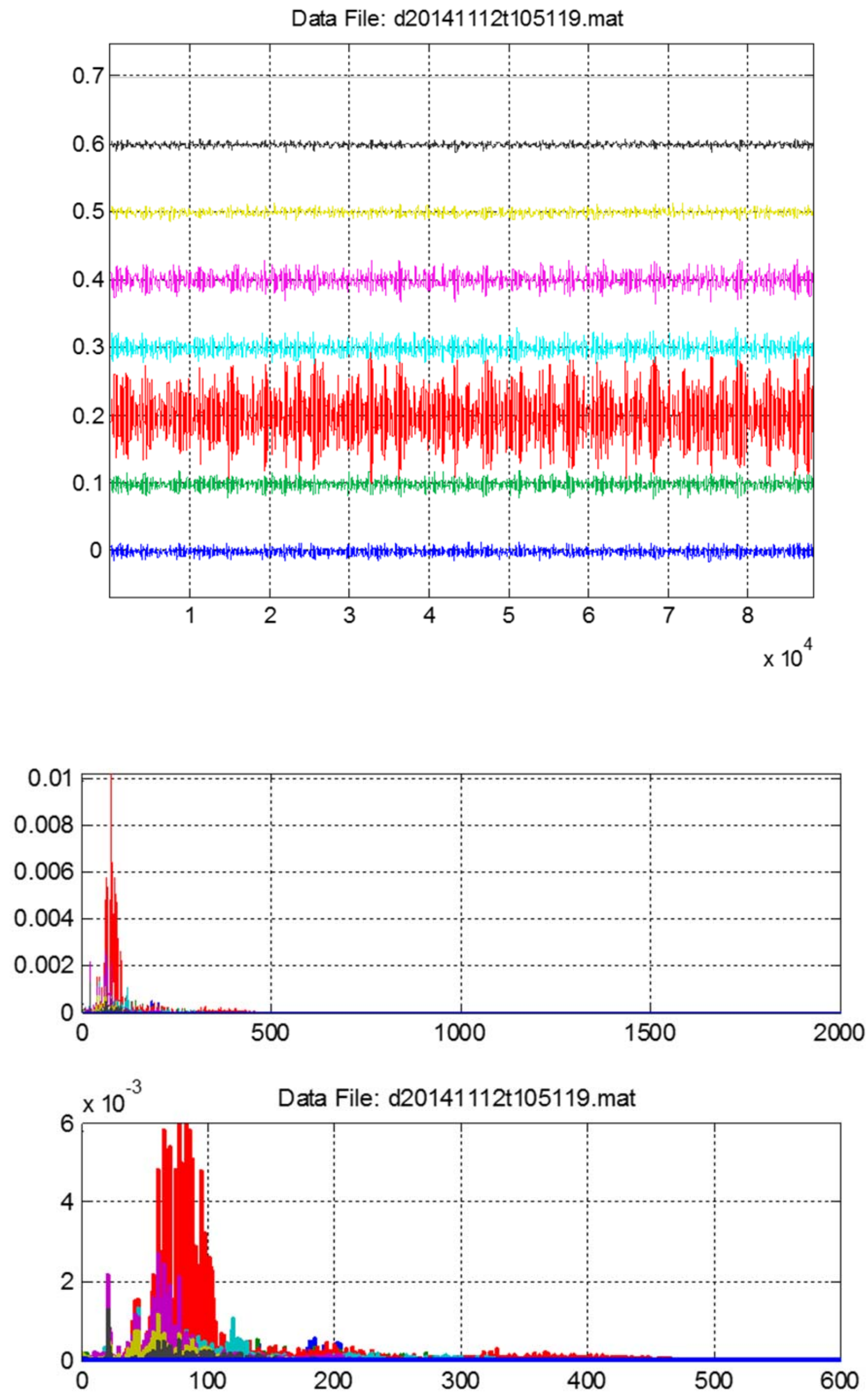

Figure 33. Noise source measurements with inconsistent waveforms (red trace vs. other traces) among receiving sensors. As in Figure 32, the lower plot shows the spectrum of each trace.

During the course of analyses, the data collected during the November 2014 field tests were run through the processing software, post-acquisition. The same processing flow and parameters were applied to recorded data. The main difference in the solutions recorded real-time in the field and those from reprocessed data was a better precision for solutions. This was possible because the reworked solutions were obtained from a numerical result rather than reading the solution location from a data display in the field. The field results were reported to ±1 foot, and those from data reprocessed off-line were reported to ±0.1 foot.

The reworked data was divided into two subsets. The first consisted of data sets where the distance from the array to the target pipe was 10 feet or greater, and the second was where this distance was less than 10 feet. Each of these sets was further divided into groups. The first consisted of the entire data set, and the second consisted of solutions where the detection was defined as 'forward-looking' or toward the target, ahead of the array in the direction of drilling. These different data sets were reported to have significantly different accuracy.

Where either the concrete block or the rotary motor were used, and the array was less than 10 feet from the target, an overall accuracy of ±2.1 feet was reported. Where the distance between the array and target was greater than or equal to 10 feet, this accuracy degraded to ±11.4 feet.

The reworked and field log data sets were processed independently, and hence, some discrepancies exist between the number of solutions per array location, the order of the data collection, and the solution locations. The difference in solution location should at most be ±1 foot, due to the different computed precision. However, the location differences tended to be much larger than this, as seen in Figure 34 to Figure 36. The source of this discrepancy is unknown.

All the data sets of the field logged and reworked solutions were correlated and plotted on corresponding graphs. As seen in Figures 34-36, there were significant differences in the absolute positions of the detections. The most striking feature of all these plots is that the detection solutions seem to follow the array location much more strongly than the target location. When the array is within 10 feet of the target, the overall accuracy of solutions does improve. However, this seems to be more a function of the array being closer to the pipe than the detections actually being more accurate.

If only forward looking solutions for data sets with the array target distance less than 10 feet are examined, the overall accuracy again appears to improve. This also seems to be more of a function of array position. If only forward solutions are used from Figure 34, for example, they necessarily must have a reduced error simply because they lie ahead of the array, toward the target, with a limited east-west distribution. This is true for all data sets with the array within 10 feet of the target. Thus, it would appear that the improved accuracy reported for forward-looking solutions with the array less than 10 feet from the pipe may not be a true measure of improved system performance.

If the data are split into subsets with greater than 10 feet, or less than 10 feet between array and target, Figure 37 and Figure 38. Even when looking at subsets of the entire data set, there does not appear to be an unambiguous indication of either target. If anything, the data appear to track the array location and not the pipes.

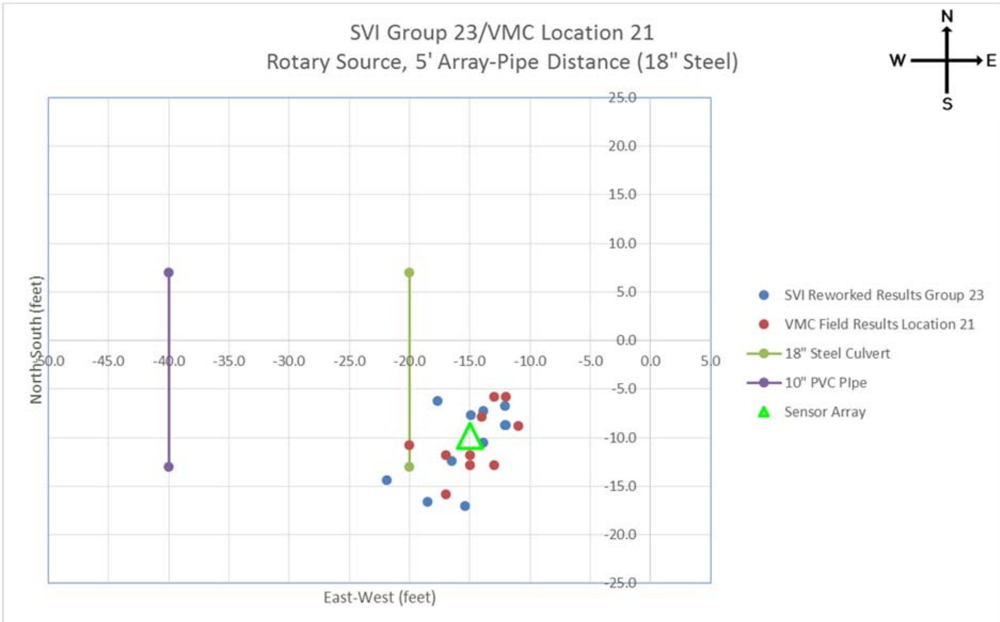

Figure 34 Plot of original field and reworked solutions. This test used the rotary hammer as a source and the sensor array was located at the green triangle on the plot, within 5 feet of the 18" steel culvert.

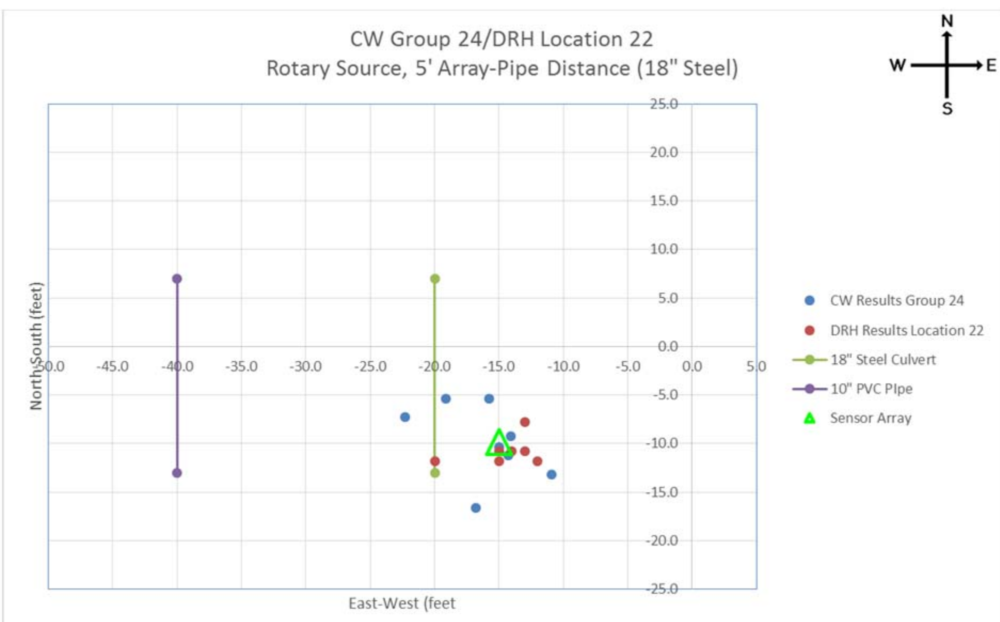

Figure 35 Analogous plot to Figure 17, but this time with the detection array located directly above the steel culvert. There again appears to be a significant difference in solutions between the field and reworked data.

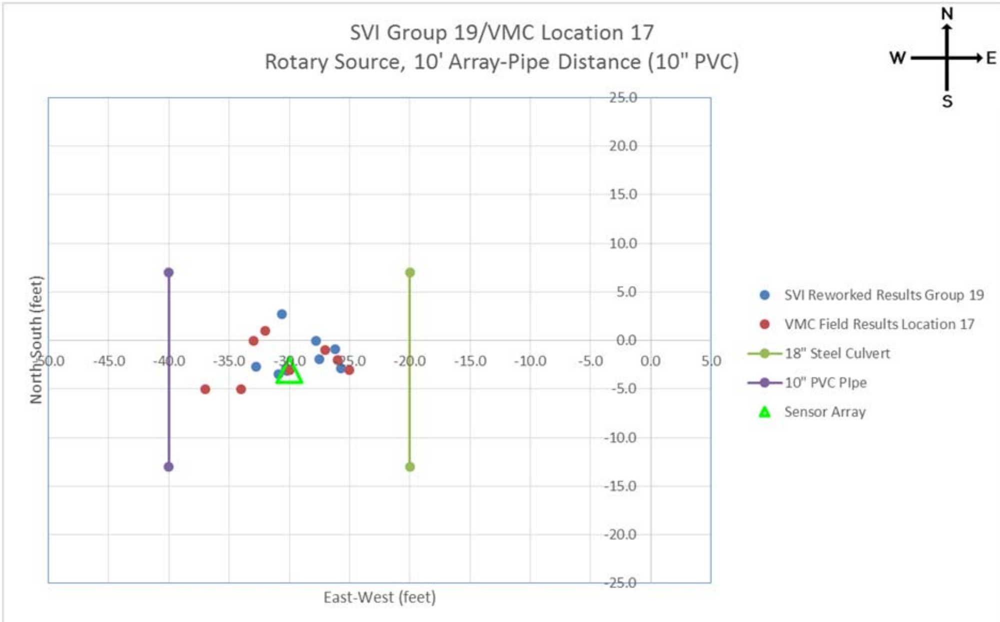

Figure 36 A third example of the field and reworked detection solutions. In this case the array is between the steel culvert and PVC pipe.

When all of the reworked solutions are plotted on a single graph, the distribution of Figure 39 results. As with the original field data of Figure 28, there does not appear to be a strong indication of either target (18" diameter steel culvert, 10" diameter PVC pipe).

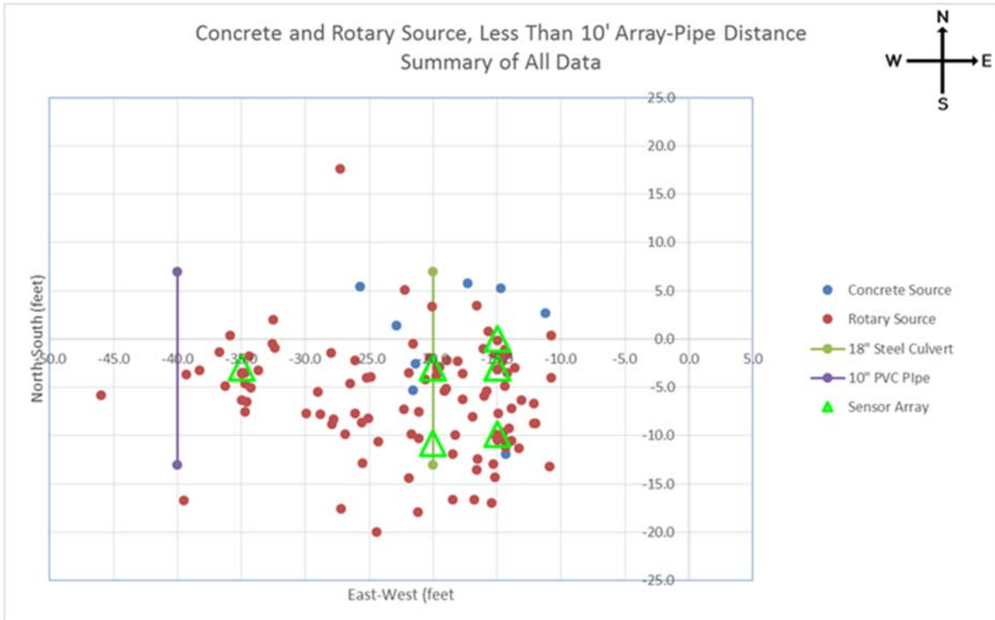

Figure 37 Plot of reworked solutions including only those where the array-target distance was less than 10 feet. Green triangles show the array locations.

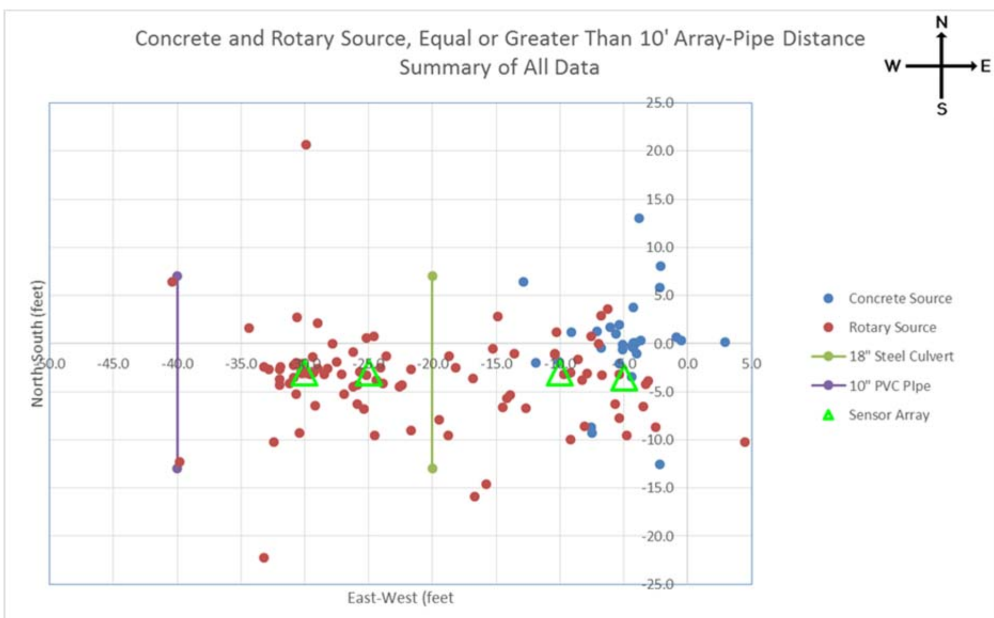

Figure 38 Plot of reworked solutions including only those where the array-target distance was 10 feet or greater. Green triangles indicate the array locations.

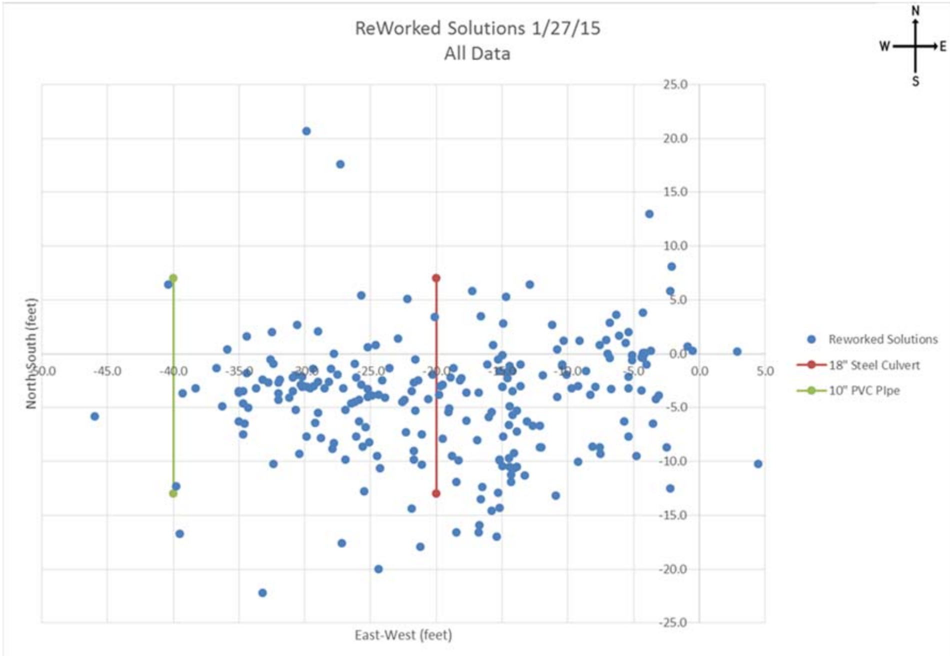

Figure 39. Summary plot of all reworked detection solutions.

<u>Recommendations Based on the Second Test Campaign, November 2014</u>

In general, the real-time solutions generated for the data set as a whole did not clearly indicate the existence of either the 18-inch or 10-inch pipe. However, the current results showed that post-processing the data can give potential accuracy required for the HDD operation to detect pipes. The past results were quite better for the real-time detection of pipes during the HDD operation. The main differences between the past and current tests were the noise generators used with the system and soil conditions. In the past, much stronger and consistent noise signals were generated with the rotary hammer source powered by the mud motor.

A further analysis identified potential issues with the integration of the acoustic and GPR systems and operation of the integrated system in the field and these concerns are given below:

- Integrated system cannot accommodate the mud motor to generate noise
- Difficult to increase noise amplitude with the use of electric motor
- Significant expertise required to operate the GPR system
- GPR system requires significant real-time data collection/analysis
- Operation and maintenance issues associated with the GPR mounted in the drill-head
- Additional costs for the integrated system equipment and up-front GPR system cost

It is believed that the accuracy of acoustic system between the pipe(s) or objects to be detected and the drill-head position within 10 ft. can be similar to the GPR system. With the system integration issues identified, the team recommended the following steps:

- Eliminate tasks associated with the integration of acoustic and GPR systems

- Revise the current tasks for proceeding with a stand-alone acoustic system with emphasize on the following:
    - Implement a rotary hammer source powered by a mud motor (similar to the one used in the past)
    - Improve the real-time processing of the acoustic system data
        - Examine solution algorithms to improve the probability of detection and reduce the false alarm rate
        - Improve sensor coupling
        - Potentially change the operating frequency of the sensor to a lower range that may be more compatible with seismic soil propagation properties
    - Demonstrate the system performance in a semi-field (local) environment.

As reported in the past, the advantages of the acoustic system are:

- Easy to operate
- Minimum calibration
- Applicable in most ground conditions
- Rapid deployment
- Limited or no maintenance, and
- Low up-front cost

These advantages will ultimately assist in commercializing the system. The proposed recommendations were approved by the project sponsor and the project continued to determine capability of the acoustic-only system with a demonstration of the system in the local area.

Third Test Campaign and Redesigned Source: December 2015

Local area testing performed at the Vermeer facility in May and November 2014 resulted in detection of pipes, but required post-processing of data. At least part of this failure to obtain repeatable results was felt to be due to an 'inadequate' downhole acoustic source. This inadequacy could have been due to a nonrandom waveform, insufficient energy coupled to the ground, or an energy spectral content incompatible with the acoustic sensor array.

The acoustic source used in November 2014 local area tests was driven by an electric motor and made use of a hammer/spring assembly as shown in Figure 40. This design functioned, but had hammers that in practice were probably too small, resulting in low energy P- and S-wave generation. In addition, the springs used to restore the hammers to their striking position tended to fatigue and fail.

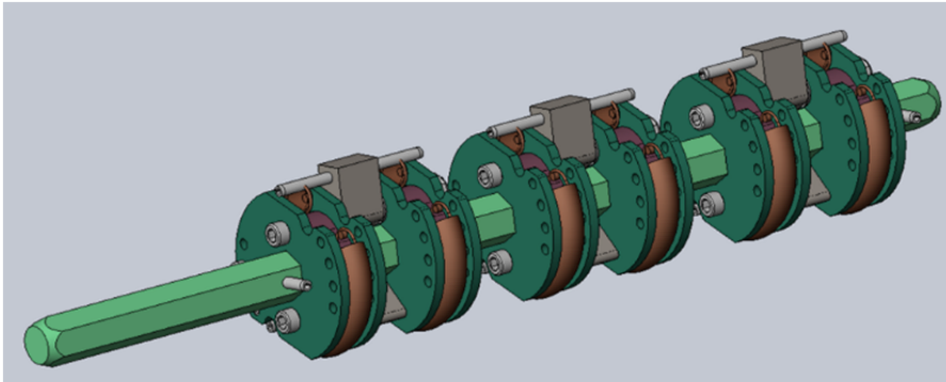

Figure 40 CAD drawing of the original hammer assembly with restoring springs.

Thus, another source design was required that had a longer operating lifetime, generated higher frequency content and coupled more vibrational energy into the surrounding soil.

Several options were explored, but all relied on a set of rotating hammers to create vibrations in the drill body that was coupled to the soil. Both a mud motor and separate rotating inner rod were considered to provide the rotation to spin the hammers. Due to ease of implementation and no need to use drilling mud, the latter option was chosen.

The redesigned acoustic source uses the Vermeer 36x50 DR drill. This machine has a dual rod-in-rod design. An inner rod is rotated independently of the outer rod, and so can be used to spin a shaft which has a hammer assembly, conceptually similar to the previous system. The inner rod can transmit up to 1500 ft-lbs of torque at 240 rpm. Thus, considerably larger hammers can be used resulting in more energy transmitted from the source into the ground.

Figure 41 shows a drawing and cross-sectional view of the source. The head is a bent sub assembly, with a 2° bend in the head between the sonde housing and the hammer section. This bend allows steering of the head in hard rock applications. A series of 10 hammer sets are shown in the figure. Each set has two hammers and three anvils. An option was included in the design to allow a second assembly of 10 hammers to be added if additional energy was needed.

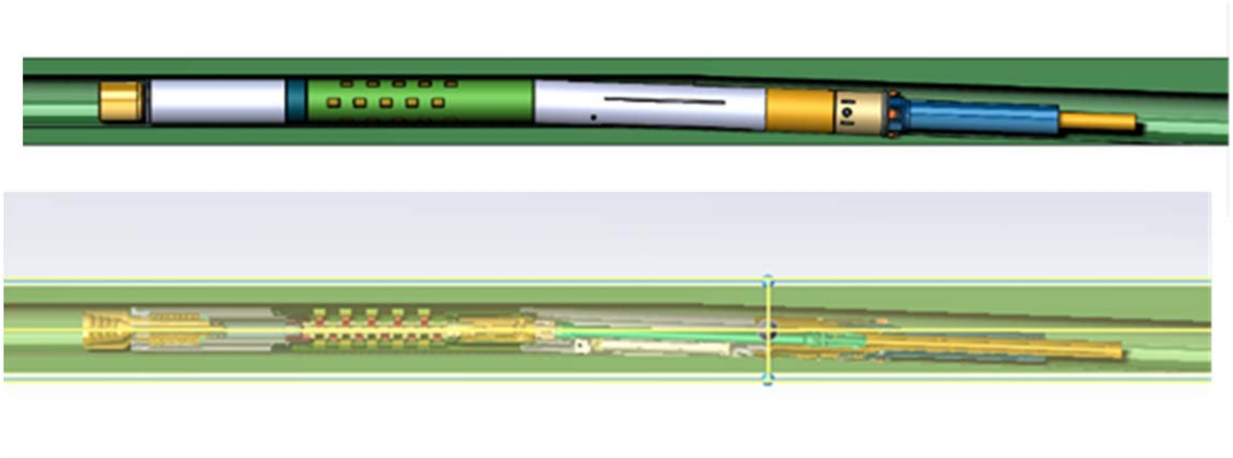

Figure 41 Views of the source as built. As shown, the source section contains 10 sets of 2 hammers each, striking three anvils per revolution. The inner drive rod spins the axis with hammers installed which rotate and strike anvils welded into the outer rod. If more energy is required, a second section of 10 hammer sets can be added for a total of 20 hammer sets.

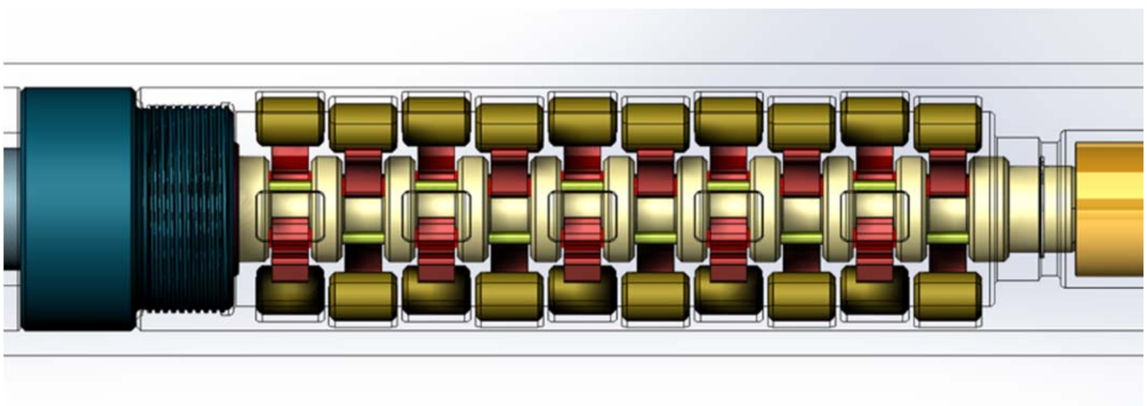

Figure 42 Detailed view of the hammer assembly. Hammers (red) are rotated by the smaller inside shaft so they strike the anvils (olive) welded into the larger outer rod.

Figure 42 shows a detailed view of the hammer assembly design. The cylinders in olive are the anvils that are struck by the hammers. These are sections of hardened steel rod that are welded into slots cut in the outer larger diameter rod. The hammers (in red) are rotated by the central inside shaft and strike the anvils.

Several changes to the electric motor design were implemented to increase the vibration amplitude and improve source longevity. First, all springs were removed and centrifugal force used to restore the hammer position for repeated striking. To simplify manufacturing, a round main shaft was used instead of a hex shaft. The hammer size and mass were increased and more hammers added, increasing the total to ten assemblies with two hammers per assembly. Figure 43 shows another schematic of the revised hammer design.

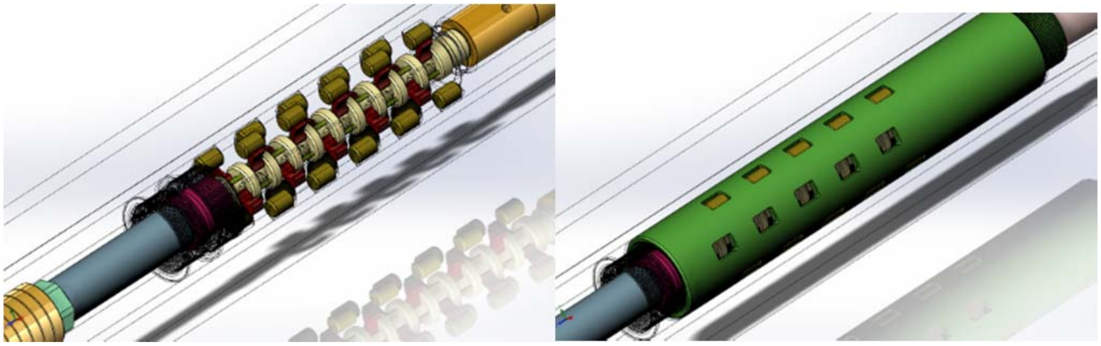

Figure 43 Revised source hammer design. The left-hand figure is the internal hammer assembly. The right-hand drawing is a schematic of the outer sub-assembly showing anvil positions.

The new source is approximately 22 inches long and 5.5 inches in diameter. The hardened rod sections welded into the sub-assembly case act as anvils. Each anvil set consists of three rows of anvils spaced at 120^{o} intervals. The hardened hammers and anvils are designed to produce an approximation to Hertzian impacts.

The rotation rate of the DR inner rod can be continuously varied up to a maximum of 240 rpm. Thus, the impact pattern can be varied to approximate a random sequence by varying the internal rod rotation rate, should this prove necessary. In the new design, five hammers are set to strike anvils at the same time, increasing the overall energy output per impact. Thus, with 10 rows of hammers (half of which strike at the same time), two hammers per row and three anvils per row, there will be 12 distinct impacts per revolution. At a rotation rate of 240 rpm, this results in 48 distinct impacts per second.

The size and shape of the hammers has also been changed. A comparison of the old and new hammer designs is shown in Figure 44. The hammer of the original source design has a mass of 0.0484 lbs. (0.0219 kg), and a radius to the center of mass of 0.1542 in. (0.0039 m). Thus, the angular kinetic energy of each of these hammers at a rotation rate of 240 rpm is 2.66 x 10^{-5} J. The new hammer design has a mass of 0.1 lbs. (0.0454 kg) and radius of 0.5 in. (0.0127 m). With these values the new hammer design results in a kinetic energy per impact of 5.78 x 10^{-4} J. The new design results in a 21.7 times increase in angular kinetic energy. If five hammers strike simultaneously and it is assumed that the energy adds linearly, the new design will result in a two order of magnitude increase in effective hammer kinetic energy. The foot present at the lower right position of the new hammer design is intended to prevent the hammer from rotating forward beyond normal to the shaft, which would cause jamming of the hammer assembly.

Figure 45 is a cross section view of the new hammer assembly, cut normal to the drill head shaft. The rows of the hammers (purple) and anvils (maroon) can be seen in this view. At a rotation rate of 240 rpm, there will be a delay of 0.042 sec between hammer impacts. For each row of hammers there will be 0.083 sec of recovery time where the hammers recover from one anvil strike to be ready for the next row of anvils.

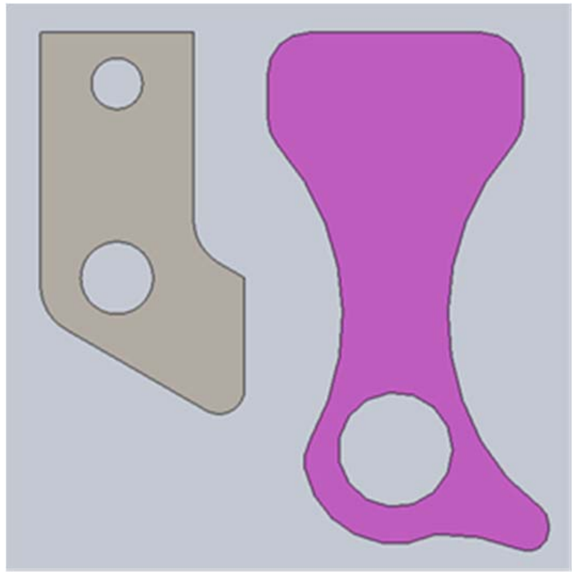

Figure 44 Comparison of the old hammer design (left) and the new hammer design (right).

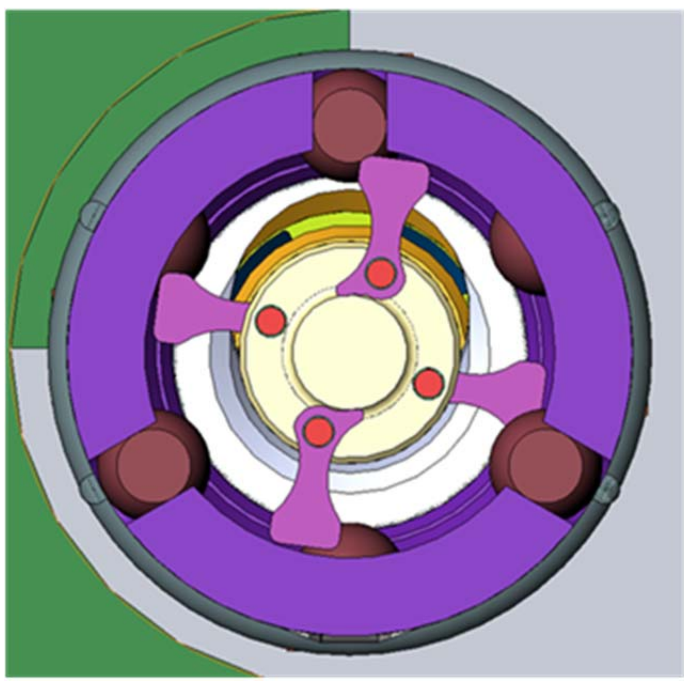

Figure 45 Cross section of the new hammer source design showing the hammer and anvil configurations.

Another possible issue with the prior noise source was that the frequency content of each impact might have been too low for proper algorithm operation. During Hertzian impact of two bodies, the frequency content of the resulting stress waves is dependent on the time the two bodies are in contact. The shorter the contact time, the higher the frequency content of the impulsive force imparted from the hammer to the anvil. The earlier design had springs pulling the hammers back up to striking position rather than relying on centrifugal force to restore the hammers. This may have had the unintended consequence of increasing the contact time, and so decreasing the impulse frequency content.

The current design is planned for dry use, without either water or drill mud. The bearings used in the source do not rely on fluid lubrication and fluid use is not recommended as it could impede the movement of the hammers and also dampen the sound. Interior head components are not made from stainless steel. Thus, rust could form inside the source which could also inhibit movement of the hammers.

The assembled hammer section is shown in Figure 46.

Figure 46 Photograph of the dry fit hammer assembly.

Figure 47 shows a close-up of the hammer assembly with an uninstalled anvil in place.

Figure 47 Close-up of the hammer and anvil assembly, showing how the hammers will strike the anvils in the actual source.

Figure 48 shows a detail view of the hammers (right) and anvil buttons (left).

Figure 48 Close-up of the anvil (left) and hammer (right) to be used in the enhanced acoustic source. A ball point pen is included for scale.

A smaller inner drive rod is used to rotate the hammer assembly. Figure 49 shows part of this coupling assembly that will be torqued to the inner drive rod of the horizontal directional drill.

Figure 49 Photograph of the coupling/drive assembly for the acoustic source. The inner drive rod of the dual rod system will be used to rotate the near fitting, resulting in the hammer rotation and impacts.

Figure 50 is a photograph of the outer shell of the source. After the holes for the anvils were cut, anvils were positioned to the proper depth and welded into place. Anvils are made up of approximately 1 inch long sections of 1 inch diameter heat treated rod.

Figure 50 Photograph of the hammer section of the acoustic source after the hardened anvils have been welded in place. Diameter of this section is 5.5 inches.

Figure **51** is a photograph of the assembled source, prior to installation on the drill. This is the uphole end of the source. Note the inner and outer rod assembly. As described, the inner rod rotates independently of the outer rod so that the hammers can strike the anvils.

For this head, the normal tri-cone bit used in rock drilling applications is replaced by a simple bullet head. Two views of this assembly are shown in Figure 52. While not optimal for steering, this head proved adequate for testing.

Figure 51 Photograph of the source showing the uphole rod-in-rod design. The inner rod turns the hammer assembly.

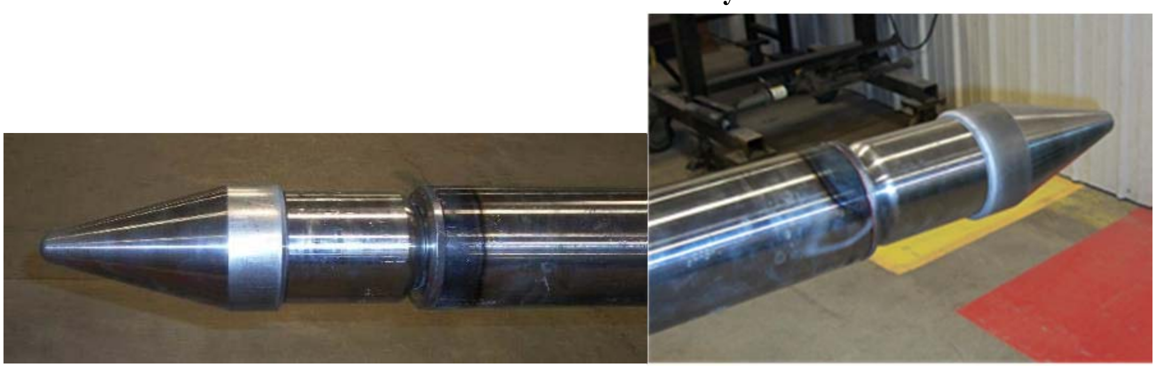

Figure 52 Photographs of the nose of the acoustic source. This nose piece rotates independently of the larger diameter outer rod seen to the rear of the nose.

Initial Source Tests

The first test conducted with this head consisted of attaching it to the 36x50 DR drill and ensuring that when spun up the hammers struck the anvils, creating sound without jamming or premature failure of the hammer assembly. This was completed by attaching the head to three sections of the dual rod on the surface. Figure 53 shows the head on the surface during this test. In this configuration, the hammers were rotated at a higher rate than the design called for, up to

270 rpm. Hammers could be heard striking the anvils, and no mechanical failures or jams occurred.

Figure 53 Photograph of the source during initial testing. During this test the hammers were rotated up to a maximum of 270 rpm with no failures or jams.

The acoustic source is intended to produce vibrational energy up to approximately 1.5 kHz. To test the energy spectrum produced by the source, an ultrasonic tester was rented. The accelerometers provided with this instrument are capable of recording up to 50 kHz, but were band limited to below 5 kHz.

Several local area tests were conducted with the acoustic source. These included:

1. A first set of data were collected with the source above ground. Vibrational data were collected with the accelerometer attached directly to the source housing, while the drill was off (background 1), with the drill on and at idle speed (background 2), and at operating speed with the hammers rotating.
2. The source was placed underground and data were collected with the drill off to obtain a background noise level.
3. With the drill running at low and high idle, data were collected to determine the noise level due to drill machine noise.
4. Finally, at several distances from the acoustic source vibrational data were collected with the source running at different rotation rates.

The drill for these local area tests was set approximately 30 feet back from the bore entrance pit, as shown in Figure 54. For source testing, the head was drilled an additional 30 feet in from the entrance pit. Therefore, the drill was approximately 60 feet from the head location where source testing was conducted.

For tests with the source running, data were collected with the hammers rotating at both 120 and 240 rpm. Not surprisingly, the 240 rpm data had significantly higher amplitude, and so will be the only data shown here. In addition, data were collected at offsets from the head of 0, 2, 4, and 6 feet. The purpose of these measurements was to obtain a feeling for the signal amplitude decay with distance from the source. For all tests, the head was at a depth of 4 feet.

Figure 54 shows the rig deployment along with the sensor location for 0 foot offset distance. The vibration measurements were made with an Olson Instruments Impact Echo Test System. For these tests, a 100 microsecond sampling rate was used along with a record length of 2048 points. This resulted in a total time series record of 0.2047 seconds, and a Nyquist frequency of 5000 Hz.

Accelerometers were mounted on the top surface of an aluminum cube fitted with a 3-inch long conical spike. The spike was fully pressed into the ground surface to provide coupling. The sensor mounting was moved to different distances from the head to collect distance versus amplitude data. There was considerable wind present during the tests and so sandbags were placed on top and to the sides of the sensors to dampen wind noise.

Figure 54 Data collection setup. Accelerometers mounted on aluminum cubes were placed at varying distances from the source as its hammer assembly was rotated at 120 and 240 rpm.

Figure 55 shows the vibrational time series and amplitude spectrum collected with the drill shut off and only ambient environmental noise present. The overall amplitude of the time series signal is very low and only a few spectral peaks exist, although the high end spectral energy is above 4000 Hz. Roughly speaking, the peak-to-peak amplitude is about 0.04 units.

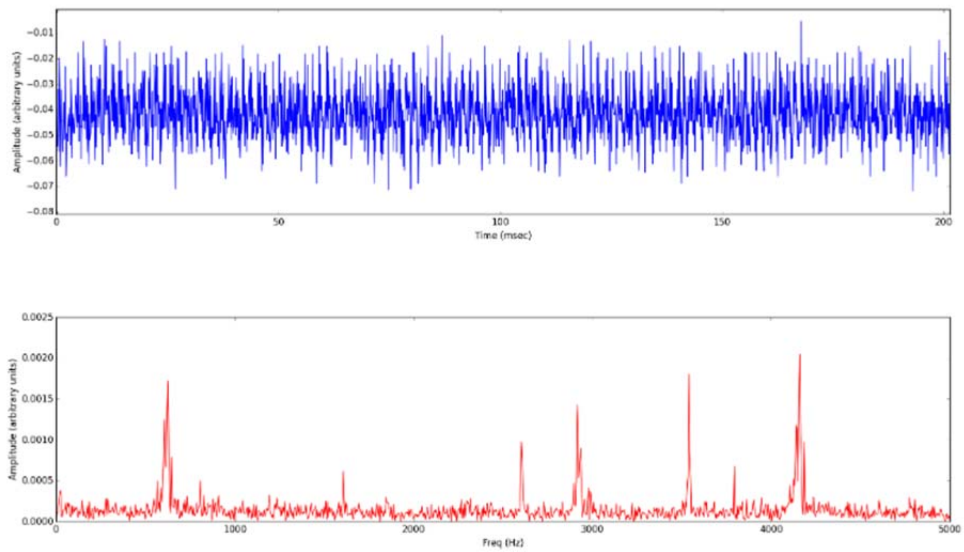

Figure 55 Time series and amplitude spectrum collected with the sensor directly above the source and the drill completely off. In general, the amplitude is low and frequencies greater than 4000 Hz are measured.

Figure 56 is a similar plot collected with the source off, but with the drill operating at a high idle speed. With the exception of two or three bursts, the overall amplitude is again 0.04 units. The spectral contect is also very similar. Thus, at a distance of 60 feet it does not appear that the drill engine vibrations contribute to the vibrations measured.

Figure 57 was collected with the zero offset sensor, with the drill on and the acoustic hammer source rotating at the drill top speed of 240 rpm. Peak-to-peak amplitude of this signal is about 0.4 units, an order of magnitude larger than the background noise measured in Figure 55 and Figure 56. The spectrum of the data has also shifted to lower frequencies, with the energy largely dying out by around 500 Hz, although minor energy exists at higher frequencies.

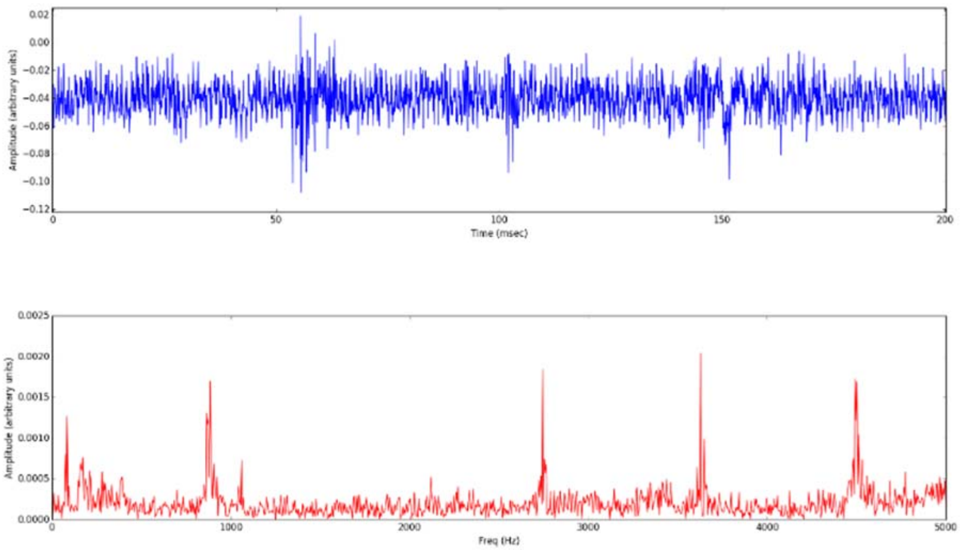

Figure 56 Vibrational data collected from a sensor placed directly over the source with the drill engine operating at high idle. No significant increase in signal amplitude can be seen over the data collected with the drill off in Figure 55.

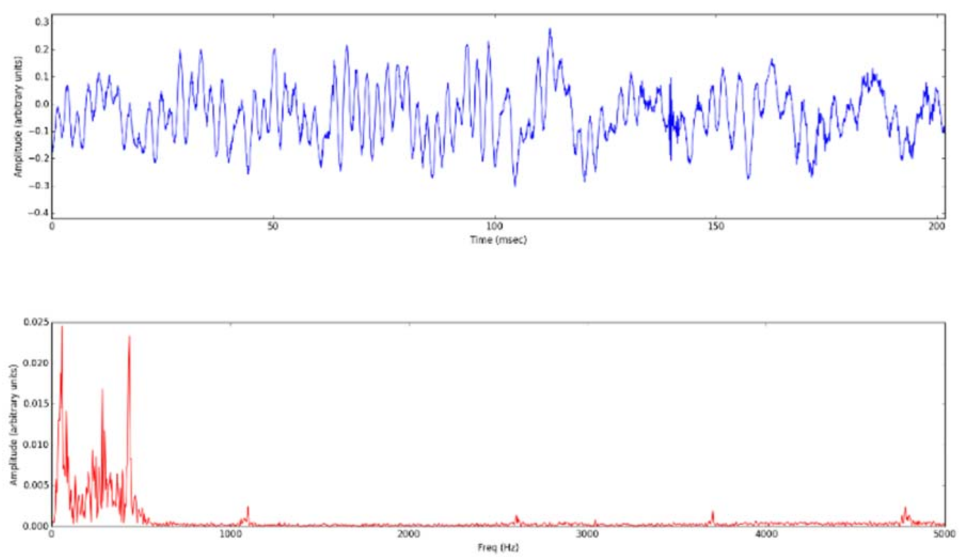

Figure 57 Vibration data collected with the hammer source rotating at 240 rpm and the sensor directly above the source. Signal amplitude is both lower in frequency and an order of magnitude larger in amplitude than that with the drill off or at idle.

At 4 feet offset from the source (and 4 foot depth) the measured vibrations are both lower in amplitude and lower in frequency content (Figure 58). Peak-to-peak amplitude is about 0.2 units and the energy is concentrated below around 300 Hz. This is qualitatively reasonable as amplitude should decrease with distance due to both geometric spreading and intrinsic attenuation. The lower frequency content is also reasonable as acoustic attenuation in soils tends to be frequency dependent with higher attenuation at higher frequencies. It should be noted that even though the vibration amplitude has decreased, it is still significantly larger than background.

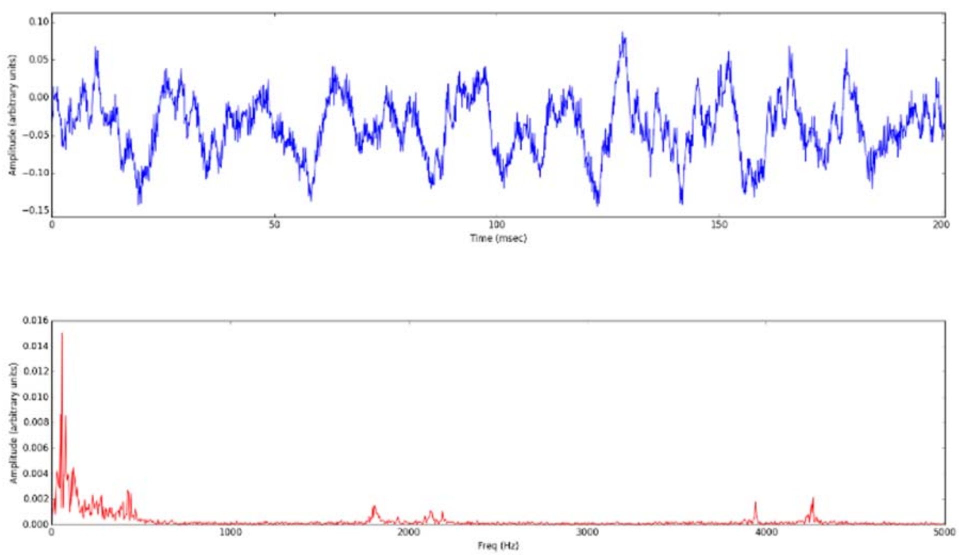

Figure 58 Vibration data collected with the sensor offset 4 feet from the source location (4 feet deep and 4 feet offset). Compared to the zero offset data, amplitude is lower and spectral energy is concentrated at lower frequencies.

Finally, a set of data were collected at an offset of 6 feet (4 feet depth and 6 feet offset). These data are shown in Figure 59. The peak-to-peak amplitude has again dropped (to 0.15 units) and the spectral energy is concentrated at slightly lower frequencies. Again, this is qualitatively reasonable with what would be expected. This range is approximately double that of the zero offset data (4 feet versus 7.2 feet). Even at 0.15 units, the amplitude of the signals is well over background indicating potentially useful energy exists at this distance range.

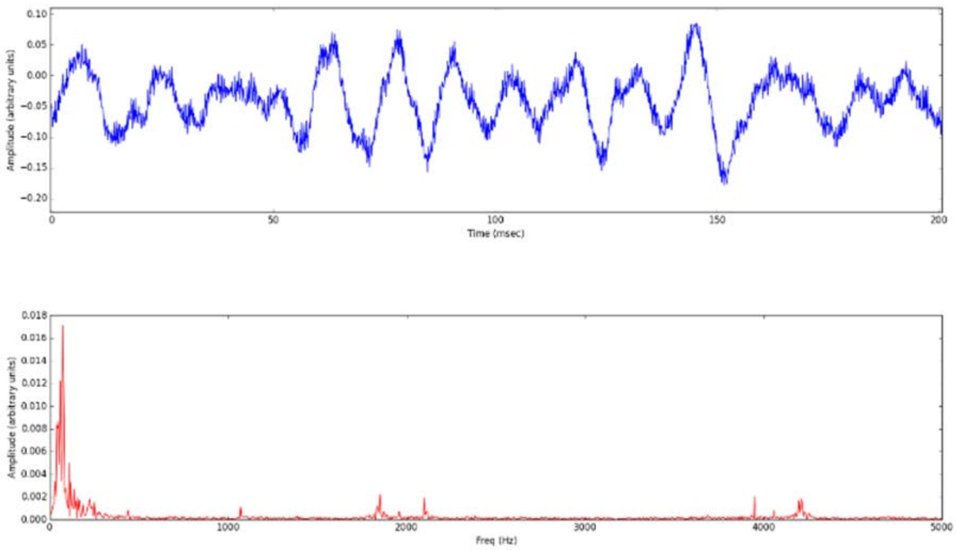

Figure 59 Vibration data collected at an offset of 6 feet from the source. Amplitude and frequency have dropped compared to smaller offset distances, but usable energy is still present.

Source Post Mortem – Initial Tests

After the initial source tests were completed, the source was disassembled and examined for wear and damage. Figure 60 and Figure 61 illustrate the damage observed. Several of the steel rods used to pin the hammers in place sheared and broke. In addition, several of the hammers exhibited fractures adjacent to the pin hole (Figure 60). The main shaft of the hammer assembly was also slightly bent.

Figure 60 Photograph of the damaged hammer assembly recovered after initial source testing. Both failed rods and hammers can be seen. Failures were most likely due to counter-rotation of the hammers against the anvils, as explained in the text.

Figure 61 View of the pieces of the hammers and rods recovered from the source after initial testing.

An analysis of the failure mode indicated that most of the damage was caused by the inner rod rotating clockwise relative to the outer shell (with the anvils). This resulted in the hammers locking against the dogs meant to prevent the hammers from over-rotating after each impact. The stress caused the fractures seen in the hammers and shearing of the rods.

This mis-rotation occurred due to a misunderstanding of the rod operation. If the inner rod is not rotated while the outer rod is rotating, there is a relative clockwise rotation between the two, even though the inner rod is not actively rotating. This situation occurred several times during the initial testing, and this is suspected of being the cause of the hammer failures.

To repair the source, the second hammer assembly was modified and installed. Procedures were modified to prevent any chance of counter-rotation between the inner and outer rods. Care was taken in both assembly and disassembly of the source to avoid and additional damage.

Source Post Mortem – After Local Area Tests

After local area tests with the obstacle detection sensor were completed in December 2015, the source was again disassembled to inspect for damage. There was essentially no wear on either the hammer or anvil (Figure 62) impact points. In contrast to the initial tests, the source after local area tests showed almost no damage. As shown in Figure 63, one hammer was cracked, and no rods were damaged.

The local area tests involved approximately 150 feet of drilling and slightly more than 3 hours of continuous source usage. Except for one short duration test at the beginning of field work, all tests were conducted with a rotation rate of 240 rpm.

Figure 62 View down the interior of the outer head casing showing anvils. This photo was taken after operating procedures were corrected and trials conducted. There is essentially no wear on the anvils resulting from testing.

Figure 63 View of the hammer assembly recovered after the completion of trials. Other than damage to one hammer, no wear or damage could be found on the source.

Acoustic Sensor Improvement

Observations from the previous local area tests have suggested that additional coupling weight for the sensor module during the system operation maybe needed to ensure robust coupling effect to the test ground. Several weighting mechanism designs were reviewed and evaluated. The preliminary study indicates that the add-on design maybe the most effective and the easiest to implement.

No major modification to the sensor array structure except an external, capped mechanism to each sensor module was considered during the design review. Initial bench test indicated that one to three pounds weight is required to provide enhanced ground coupling effect for various ground situations. Several weighting materials, mainly metals (like aluminum, steel, and copper with density ranges from 170 to 550 lb/ft^3), were evaluated based on the desired form factor to conform to the existing array (and sensor module) design.

Figure 64 shows the comparison between the current sensor module design and the new metallic cap configuration. The thickness of the weighting disk/cap is about one (1) inch which complies with the articulation limit specified in the existing sensor design specification and requirements.

Several pieces of metallic disks/caps were made and fitted to the existing sensor modules, see Figure 64c. These external weighting mechanisms were made of stainless steel with volume density of approximate 500 lb/ft^3. Each disk/cap weights about 2 pounds. When fully mounted to the existing sensor module, the sensing transducer will be loaded with approximately 3 pounds force when coupling to the ground. Based on the previous OTD/GTI project result, this weighting configuration is well within the optimal range of the sensor mounting arrangement.

From the finding of sensor evaluation in the bench tests and analysis of results, as well as the new weighting configuration, no major modification of the current damping mechanism design was necessary to provide any further coupling improvement.

Figure 65 shows the improved array structure with optimized coupling mechanism mounted to the sensor modules. The overall weight of the array has been increased about 12 additional pounds. This additional coupling weight provides a much more stable array deployment, especially in rough, uneven terrain.

Figure 66 shows the same improved array structure deployed and tested on the grassy field. The additional weight helped the sensor module more tightly couple to the ground. The array mobility, however, suffers some due to the overall weight increase.

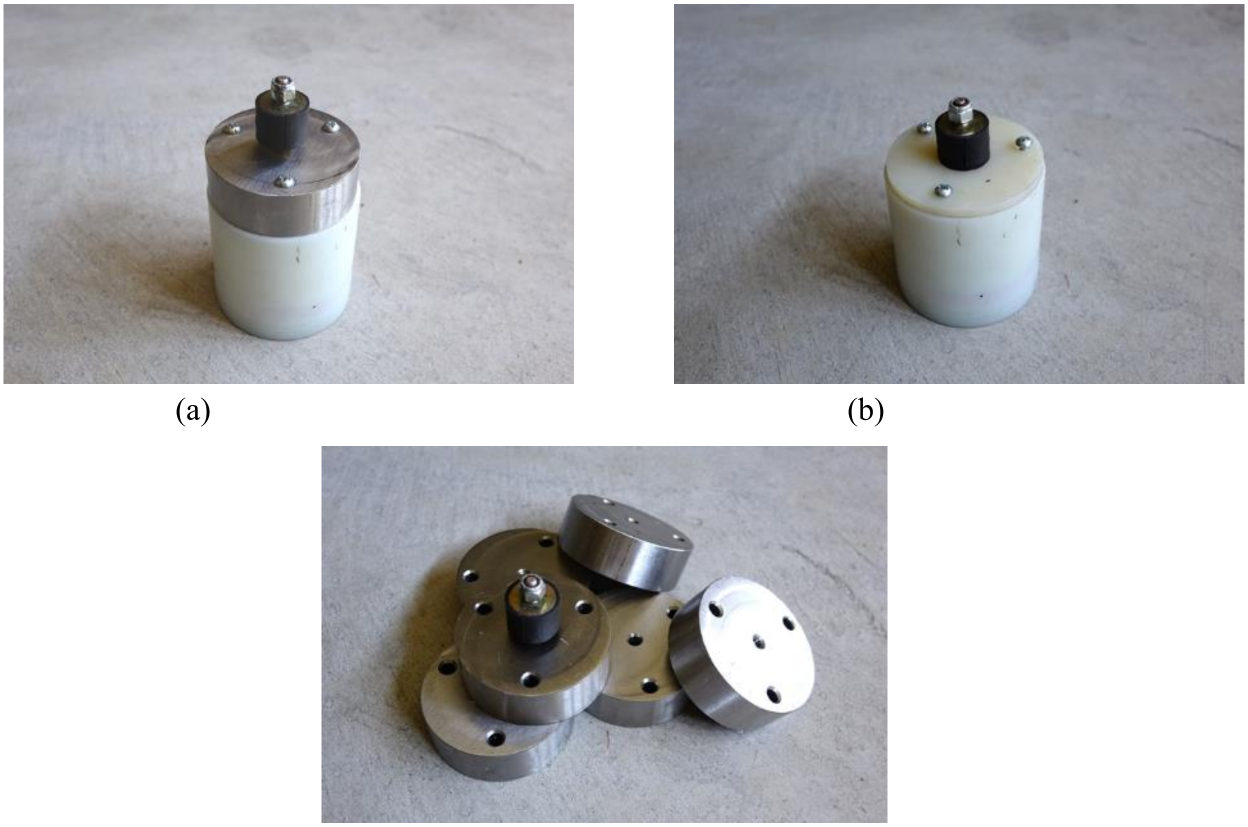

(a) (b)

(c)

Figure 64 Ground coupling enhancement of sensor module: (a) new external, metallic capping weight mounted on the existing sensor module vs. (b) the original plastic cap on the sensor module, and (c) metallic add-on disks/caps used to improve coupling mechanism of the existing sensor module – made of stainless steel material with about two (2) pounds of coupling weight.

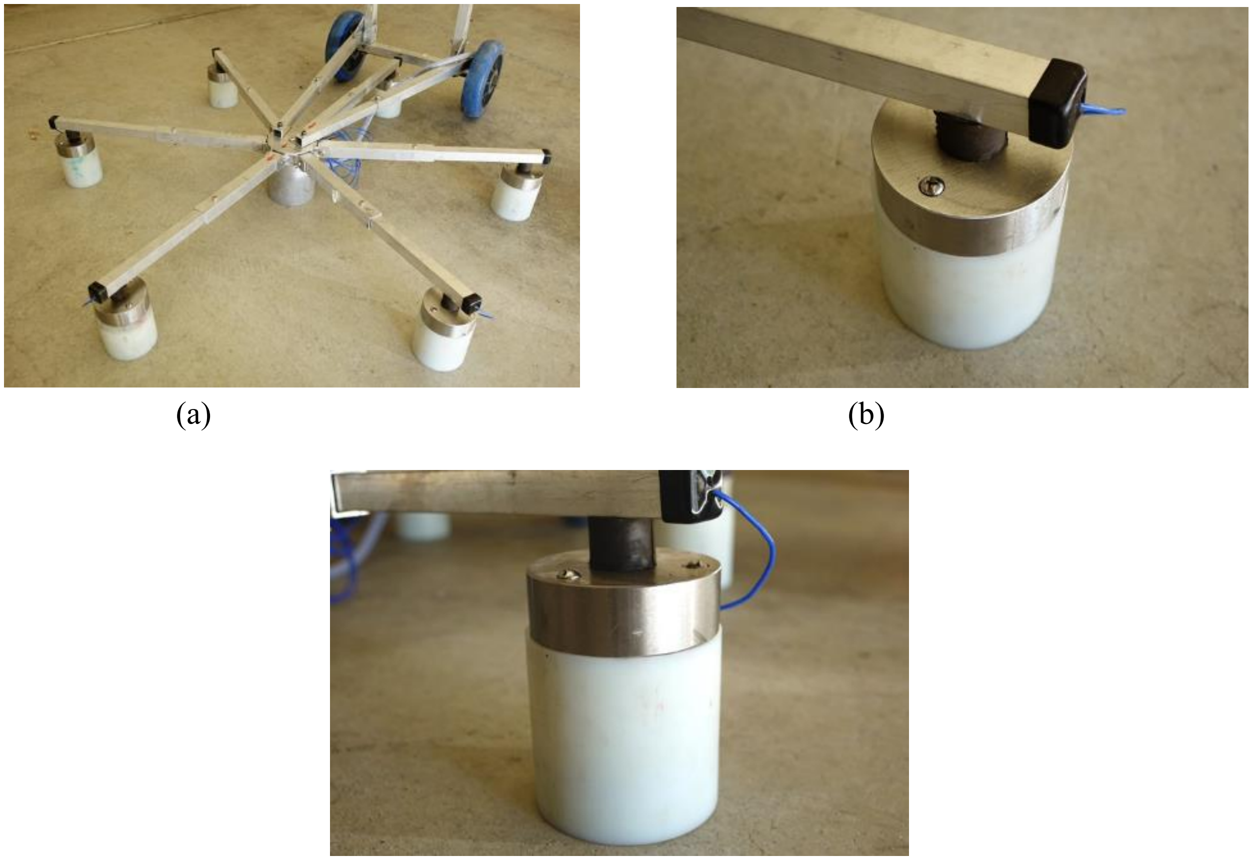

(a) (b)

(c)

Figure 65 The finalized array structure with newly optimized coupling mechanisms mounted: (a) improved array structure tested on the concrete surface, and (b - c) close-up views of the new metallic-capped sensor module.


(a)


(b)


(c)

Figure 66 Local area test of finalized array structure with newly optimized coupling mechanisms: (a) improved array structure tested on the grassy field, and (b - c) close-up views of the new metallic-capped sensor module when coupling to the ground.

Noise Source Analysis and Findings from the Seismic Detection System

Noise source analyses were performed after completion of the local area testing (December 2015 tests). Some performance variations in the noise source were observed and recorded throughout the tests. The most noticeable performance change of the source was noted during audible airborne noise tests conducted during last hole drilled during the December tests. A very distinctive noise level difference was noted between the start and end of the drilling test, while the after-test inspection of the noise source showed insignificant changes to the source's overall mechanical integrity. This particular set of observations were made when the source was in contact with mud in the launch pit, and then after the source was withdrawn from the pit and was totally in air. The observed sound variation could have been caused by soil and mud damping the airborne audible noise.

Table 7 shows the measured and calculated (equivalent) noise source performance before, during, and at the end of the local area test. Sample data from the performance analysis are illustrated from Figure 67 to Figure 70 (refer to APPENDIX B for the Test Group #). For the complexity of the local area test situation, several test references and parameters were considered in comparing and deriving the equivalent noise source's performance value:

- Noise source depth
- Spacing between array and noise source
- Measured signal strength and frequency response
- Calculated equivalent value based on simple form of soil attenuation

Table 7. Signal Strength of the Noise Source (raw rms value, all in millivolt)

	18" steel	10" PVC	Vertical 6" PVC (beginning)	Vertical 6" PVC (end)
Measured+	**4.2**	**5.6**	**8.4**	**19.5**
Calculated*			**2.7**	**5.4**

+ fixed sensor channel (closest and strongest), raw data reading in rms value.
* the estimated signal strength was based on the simplest attenuation law: $A=A_0 \cdot e^{-kfx}$, where k is the attenuation coefficient (dB/KHz•cm), f is frequency, and x is distance.

In addition to the above analysis, several noise source performance measurements were recorded (see Figure 71 to Figure 73) from various test situations and setups (e.g., 120 rpm/240 rpm tests, and Sledgehammer tests). These data sets were presented for noise source performance comparison; no analysis of detection/solution generation was intended.

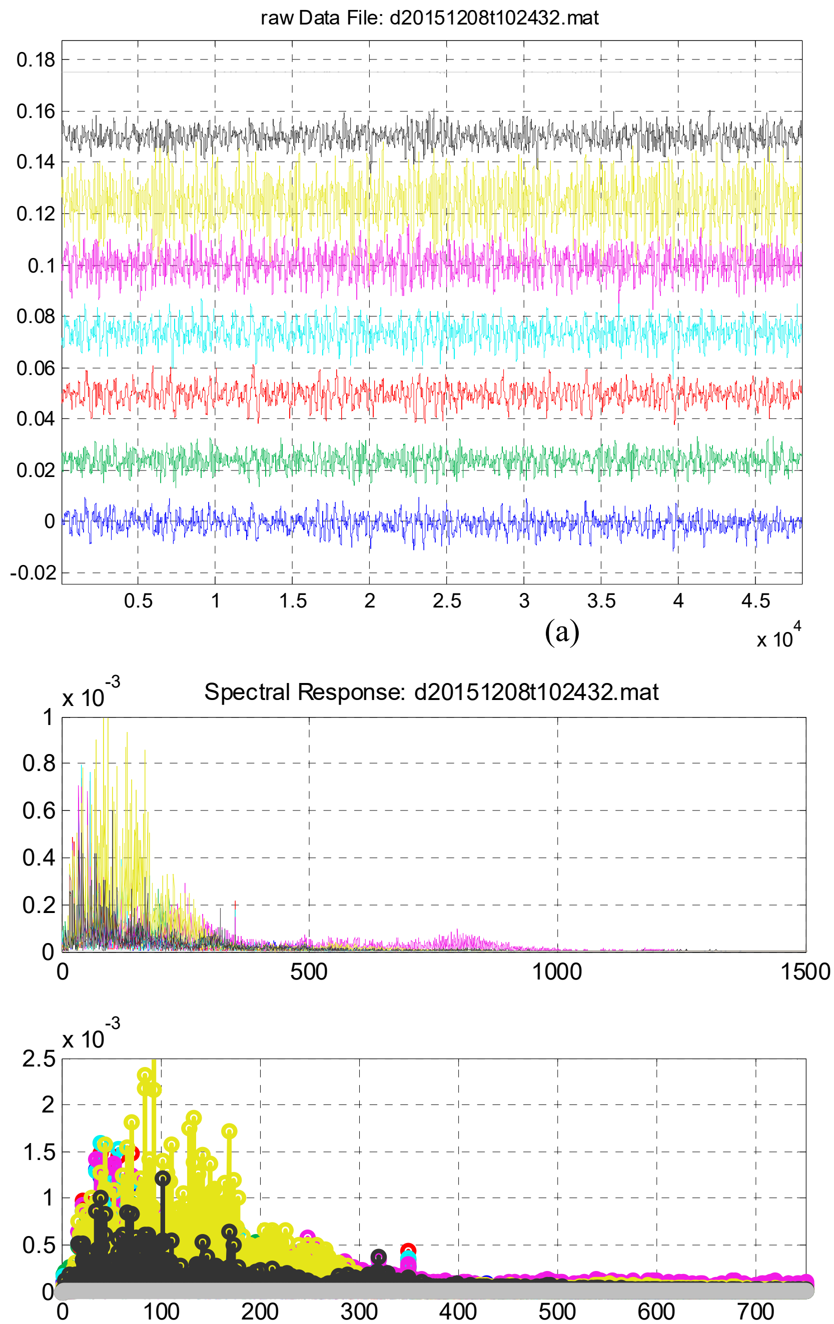

(b)

Figure 67 Test Group #8: 18" Steel Pipe, 4' deep, 2'5" away (4.72' actual distance between sensor array and noise source]; middle of test; 4.2mv [(a) sensitivity axes: vertical in mv, horizontal in (no. of) sample; (b) spectrum axes: vertical in arbitrary unit, horizontal in Hz]

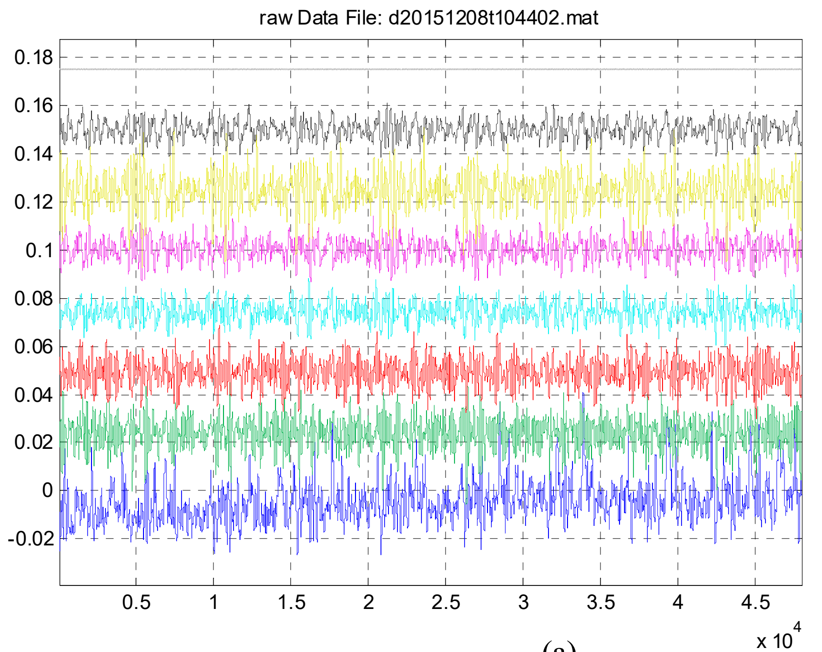

(a)

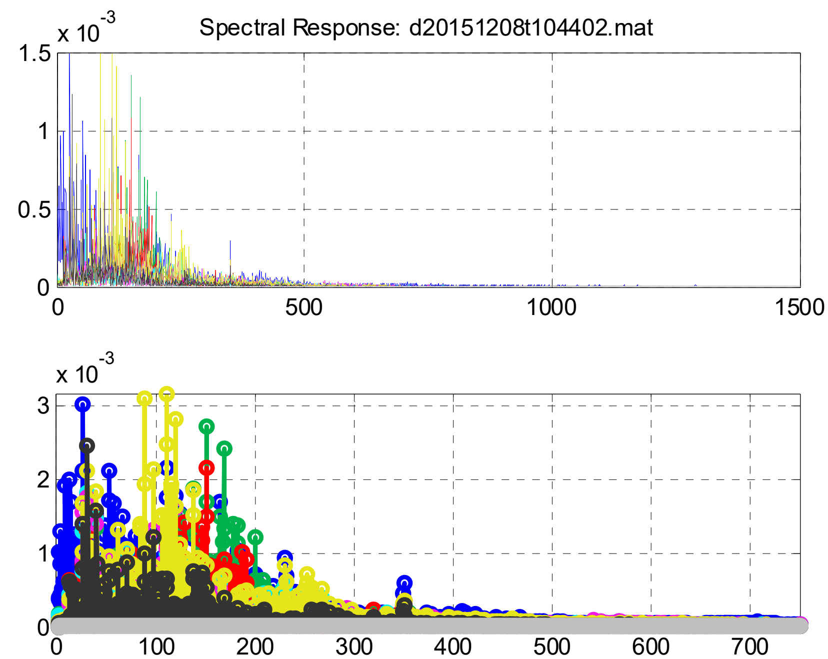

(b)

Figure 68 Test Group #10: 10" PVC Pipe, 4' deep, 2'5" away (4.72' actual distance between sensor array and noise source); beginning of test; 5.6 mv [(a) sensitivity axes: vertical in mv, horizontal in (no. of) sample; (b) spectrum axes: vertical in arbitrary unit, horizontal in Hz]

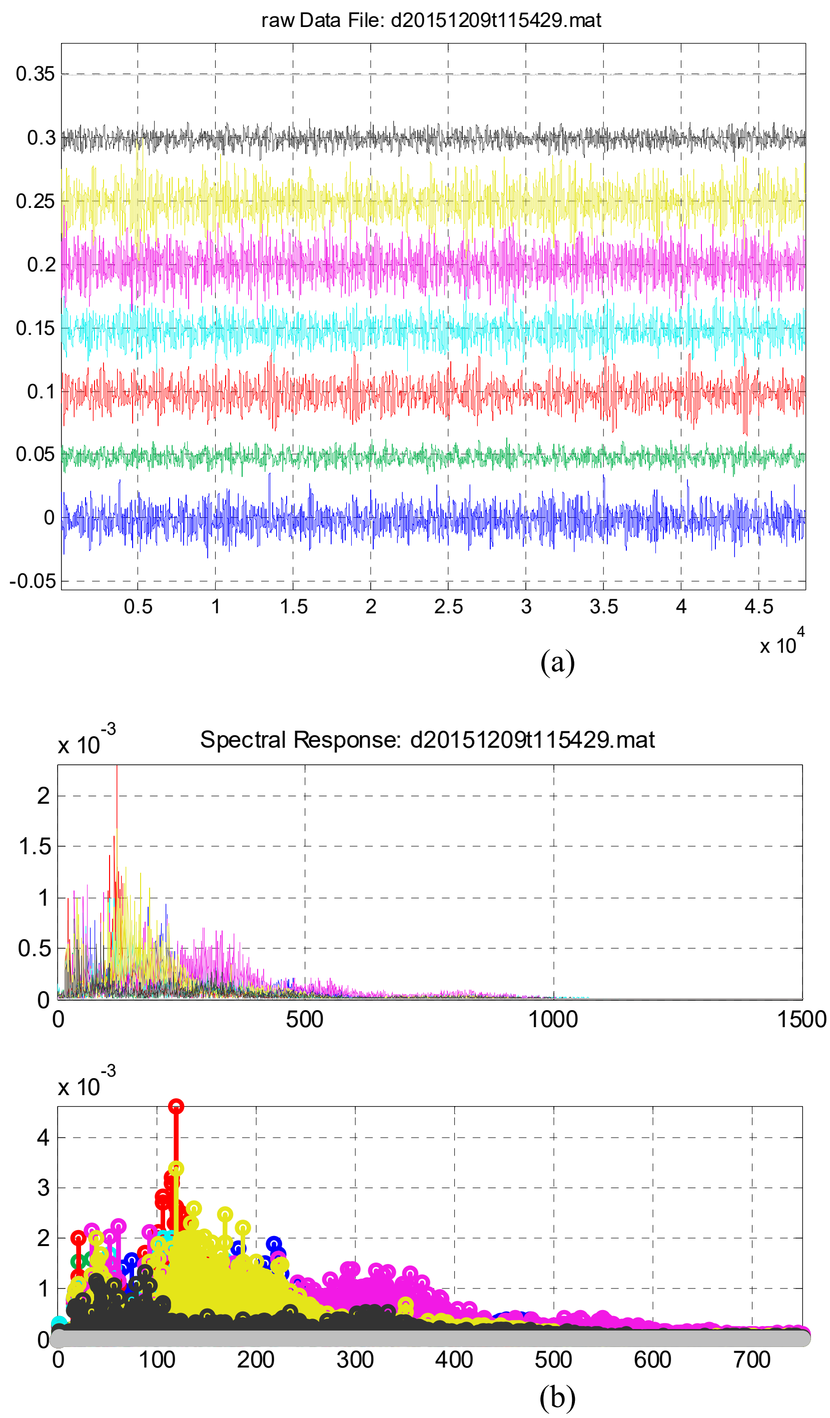

Figure 69 Test Group #36: Vertical Pipe, 2'10″ deep, 2'2″ away (3.57' actual distance between sensor array and noise source); beginning of test; 8.4 mv, due to soil attenuation ≈ 2.7 mv @ 4.72'; [(a) sensitivity axes: vertical in mv, horizontal in (no. of) sample; (b) spectrum axes: vertical in arbitrary unit, horizontal in Hz]

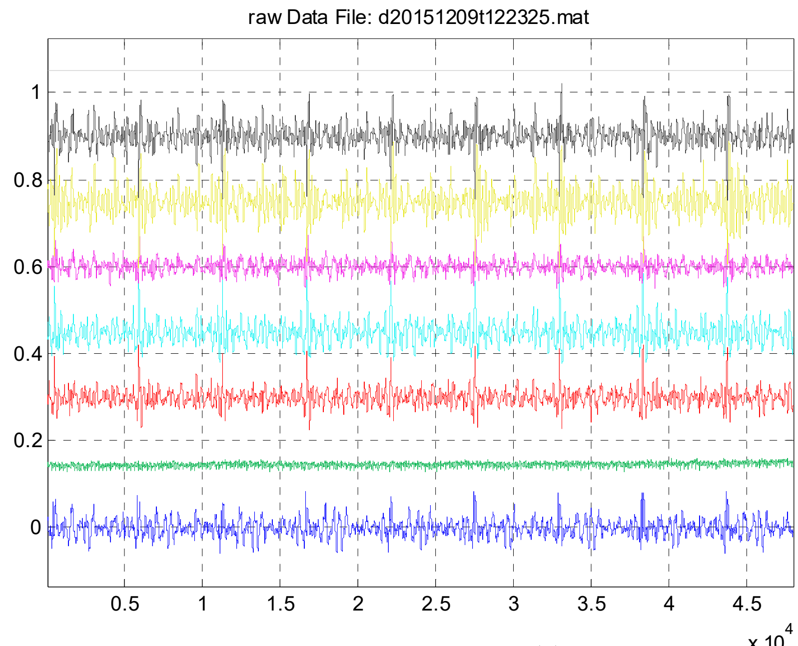

(a)

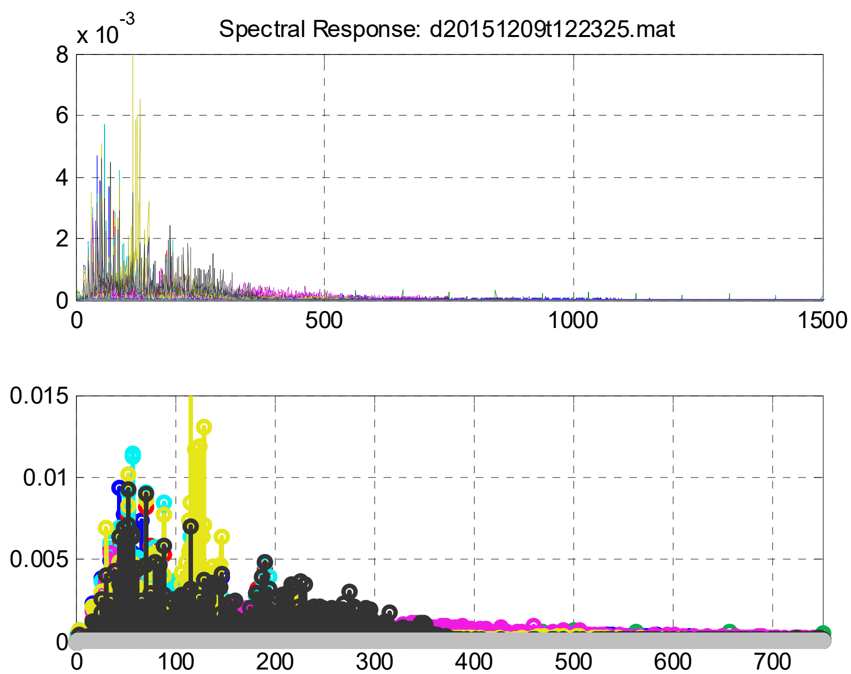

(b)

Figure 70 Test Group #42: Vertical Pipe, 2'8″ deep, 2' away (3.44' actual distance between sensor array and noise source); end of test; 19.5 mv, due soil attenuation ≈ 5.4 mv @ 4.72' [(a) sensitivity axes: vertical in mv, horizontal in (no. of) sample; (b) spectrum axes: vertical in arbitrary unit, horizontal in Hz]

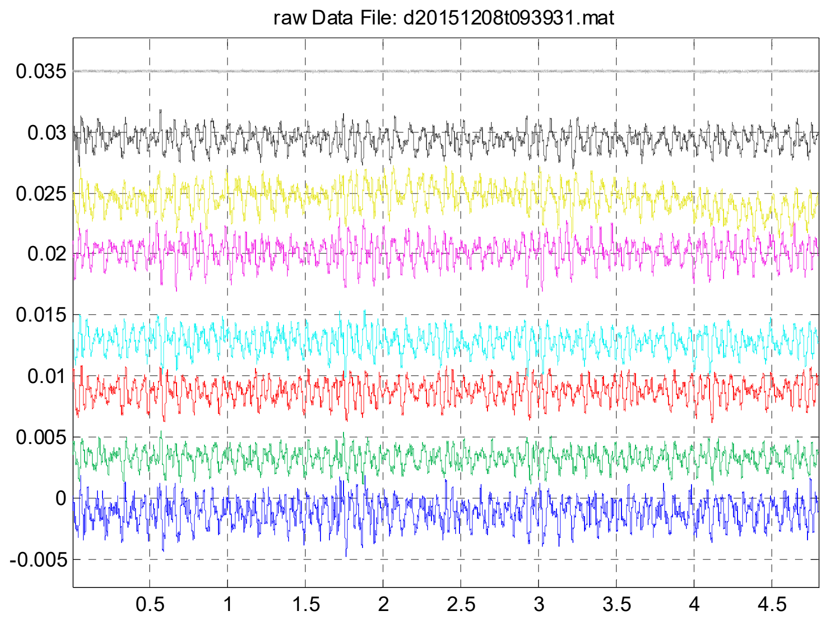

(a)

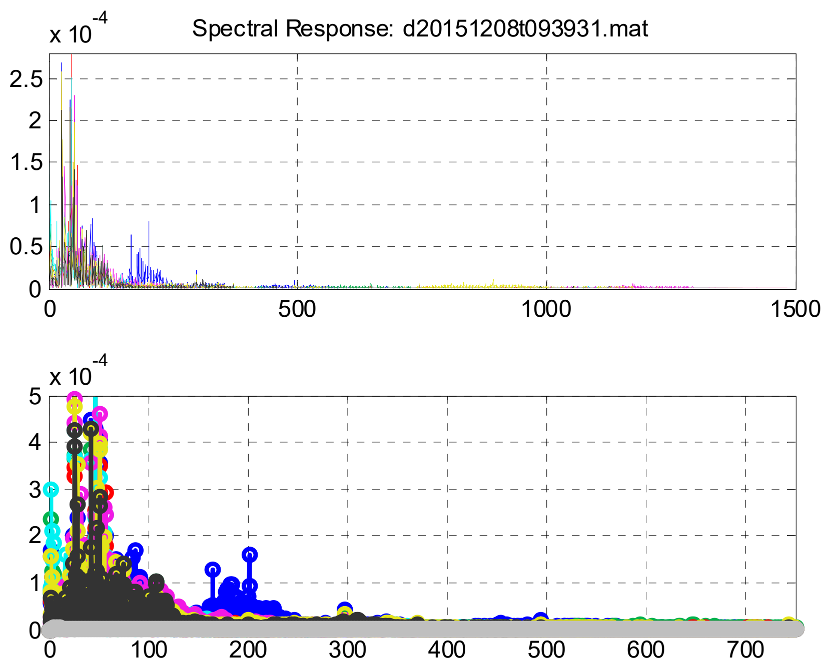

(b)

Figure 71 Pre-test run 120 rpm; >10' away, 3.5' deep; 0.9 mv [(a) sensitivity axes: vertical in mv, horizontal in (no. of) sample; (b) spectrum axes: vertical in arbitrary unit, horizontal in Hz].

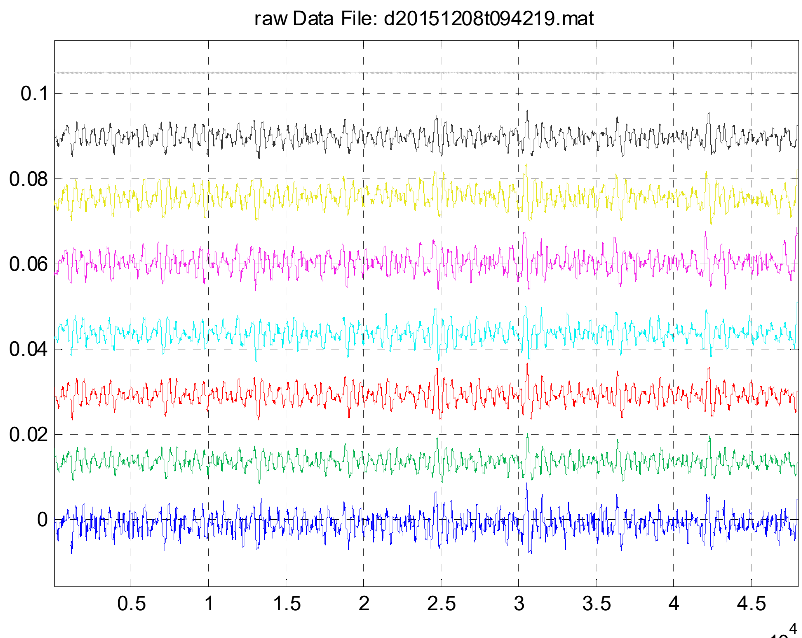

(a)

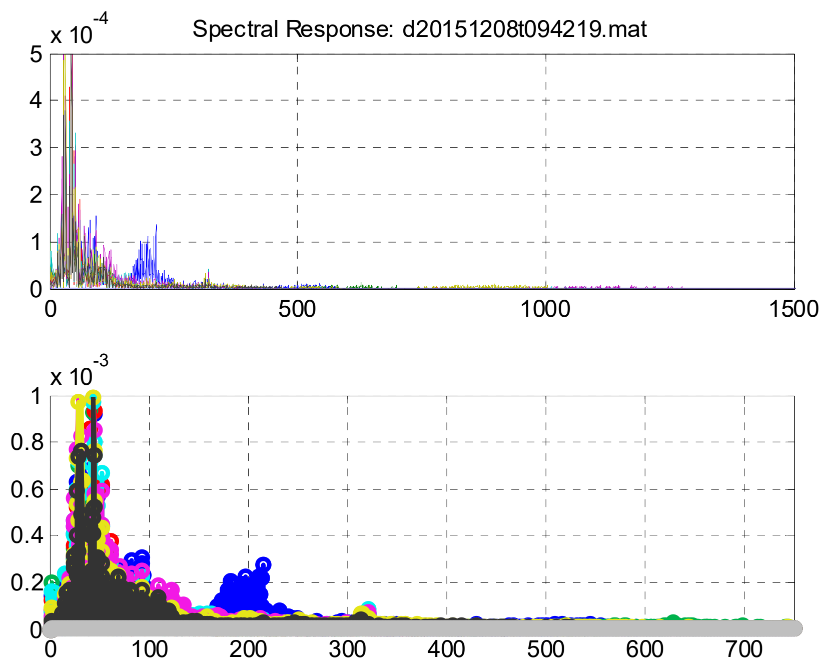

(b)

Figure 72 Pre-test run 240 rpm; >10' away, 3.5' deep; 2.0 mv [(a) sensitivity axes: vertical in mv, horizontal in (no. of) sample; (b) spectrum axes: vertical in arbitrary unit, horizontal in Hz].

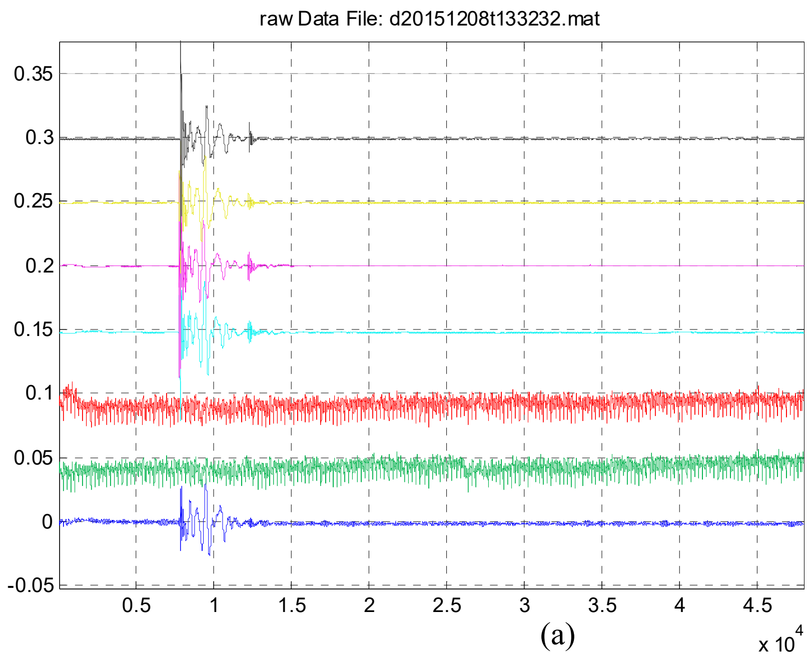

(a)

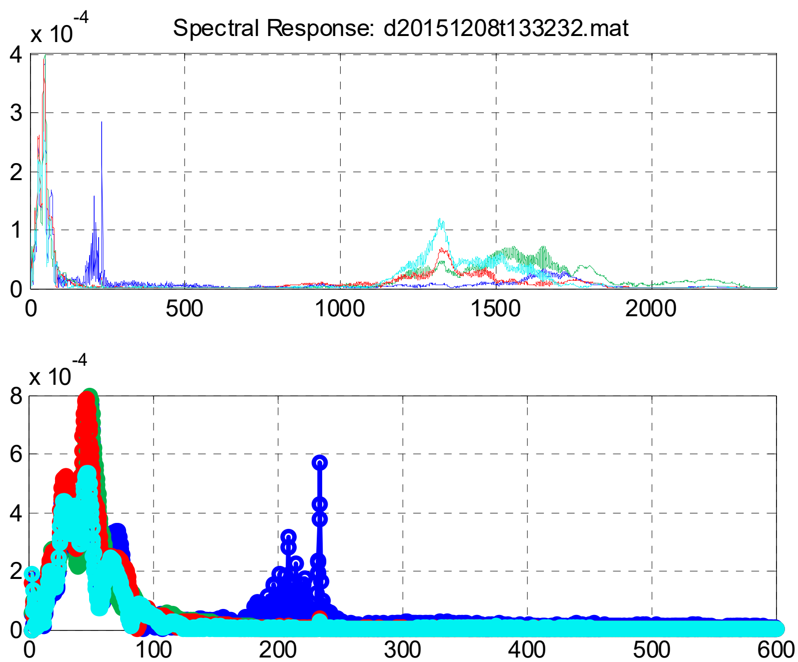

(b)

Figure 73 Test Group #17: Sledgehammer trial, 20' away, ground surface; chn#2 & #3 disconnected [(a) sensitivity axes: vertical in mv, horizontal in (no. of) sample; (b) spectrum axes: vertical in arbitrary unit, horizontal in Hz].

Local Area Tests in December 2015

The December 2015 trials were conducted in the same area as those performed in 2014. The two targets from the earlier test in November 2014 (18" steel culvert, 10" PVC pipe) were left undisturbed. Both these targets were at a depth of approximately 5-6 feet, buried horizontally, in approximately a north-south orientation. Trials were conducted by drilling a bore with the acoustic source toward a target. The sensor array was placed at various distances from the source and target, and target locations computed from the vibration data collected.

Test Procedure

As shown in Figure 74 and Figure 75, three bores were made from a single entrance pit. Two of the bores were used to detect the steel culvert and PVC pipe. The third was directed toward a vertical 4-inch diameter PVC pipe. The locations of all three targets are noted on Figure 75. The entrance pit was approximately 15 feet from the point where initial data were collected for each line, and the drill was 15 feet behind this. Thus, the drill was a minimum of 30 feet from the closest sensor location (Figure 74). Based on the source testing, this was sufficient to prevent any drill vibrations from contaminating the acoustic measurements.

Table 8 lists the source and receiver locations used for each line. Where source or receiver coordinates are repeated, the location was not moved for that data set. For example, on line 1 reference numbers 3 and 4, data were collected at source location 3, using sensor locations 1 and 4. A total of 39 distinct source/sensor location pairs were used. This does not include tests performed with a sledge hammer source, tests performed with the sensor array off-bore, or initial signal level tests.

Data were collected using only the downhole source. As with other tests performed, the test procedure followed was to place the sensor array on the surface and ensure that all sensors were adequately coupled and active. This sensor location was set to be within 10 feet of the source. Once the sensors were placed and the source drilled in to the desired location, the inner rod was spun at 240 rpm generating acoustic noise from the rotating hammers. During this rotation, the acoustic obstacle detection sensor was activated and the computed location of each data point visually read and recorded. The source was shut down, either the source or sensor array was moved, and the process repeated. Sensor positions were aligned with the drill bore path.

Figure 75 provides details of the bore path, source, and sensor locations.

During data collection only solutions ahead of the sensor array were retained. In all cases, the sensor array was ahead of the source. In some cases, the sensor was located directly over what was assumed to be the target location. During testing, location and depth of the source were determined via walkover locator. The locator was positioned 2.4 feet behind the center of the source, and the center of the source was 3.6 feet behind the tip of the drill head. Thus, the locator center was 6.0 feet behind the drill head tip. The average bore depths for the three lines were 4 feet, 3.85 feet, and 2.75 feet for lines 1, 2, and 3, respectively. Again, as with all previous testing, initial obstacle locations were generated in a local reference frame, with the center of the sensor array as the origin. During processing these locations were transformed into a global reference frame that included the target pipe, source, and sensor positions.

During the course of testing, 474 data points were logged in the field. During data collection, there were again a number of cases where the system was activated, but no solution could be calculated. The number of these 'No Solutions' cases for each set are shown in column 3 of Table 9. The final proportion of 'Good' solutions varied from a high of 100% to a low of 8%, with the percent of good solutions for all tests reaching 83.1%. Locations were recorded to the nearest 0.5 feet. It should be noted that these solutions did not include results from the sledgehammer tests, sensor off-bore tests, or initial noise tests. In addition, these results only include solutions logged in the field, real-time during testing. Post-acquisition processing results in a slightly different number of computed solutions.

Figure 74 is a photograph of the local area setup during collection of data for line 2. The sensor is placed, and the source located, as indicated by flags placed in the ground. The distance from the drill to the most distant sensor location was about 80 to 85 feet.

Figure 74 Photograph of the setup during December 2015 testing. Flags indicate the location of locator sonde positions, sensor, and source locations along the bore.

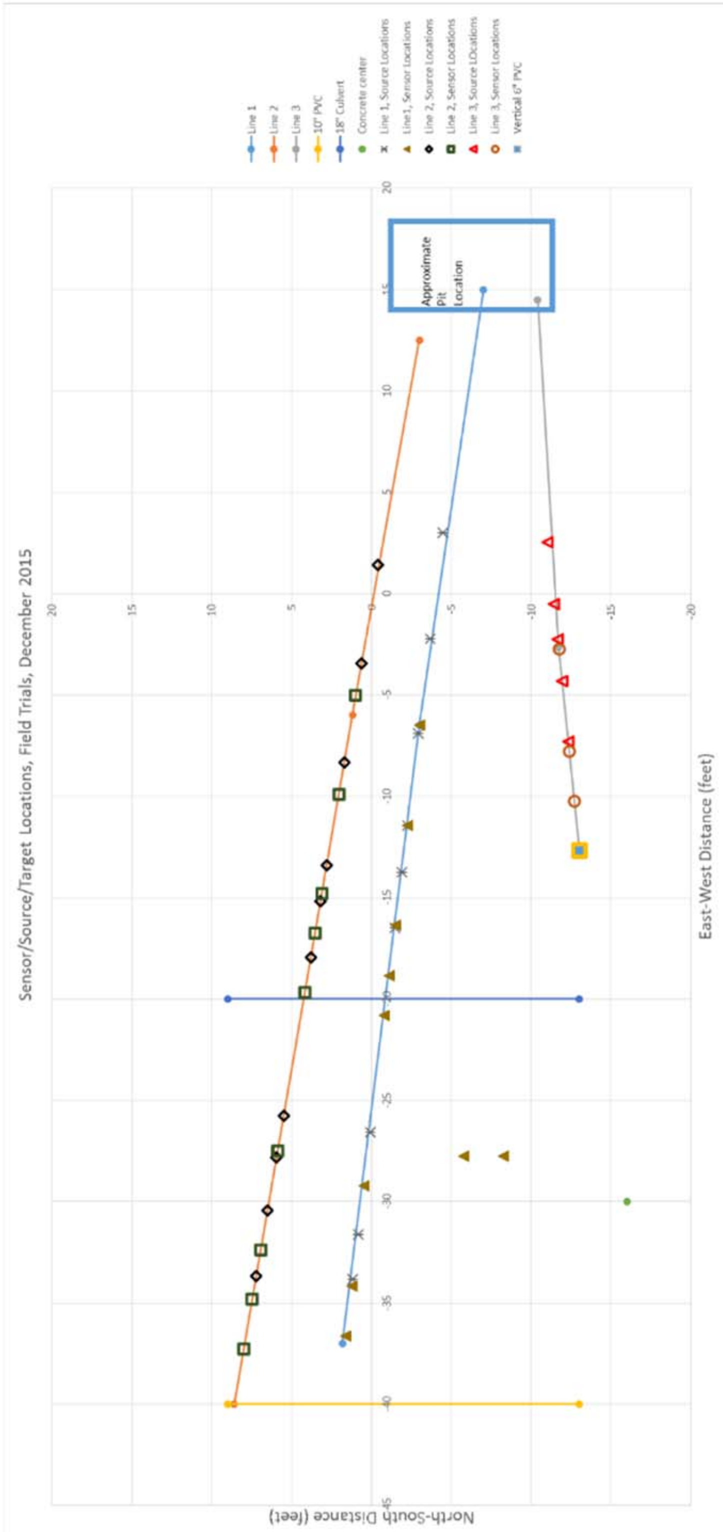

Figure 75 Plan view map of the bore path, sensor, source, and target locations during trials conducted during December 2015.

Table 8. Correlation of Sensor and Source Locations for December 2015 Local Area Trials

Source/ Sensor Ref. No.	Line No.	Sensor Location Number	Source Location Number	Sensor X (E-W) Location (ft)	Sensor Y (N-S) Location (ft)	Source X (E-W) Location (ft)	Source Y (N-S) Location (ft)
1	1	1	1	-6.50	-3.00	2.99	-4.45
2	1	1	2	-6.50	-3.00	-2.22	-3.65
3	1	1	3	-6.50	-3.00	-6.90	-2.94
4	1	4	3	-11.44	-2.24	-6.90	-2.94
5	1	4	5	-11.44	-2.24	-11.44	-2.24
6	1	6	5	-16.38	-1.49	-11.44	-2.24
7	1	6	7	-16.38	-1.49	-13.75	-1.89
8	1	8	7	-18.86	-1.11	-13.75	-1.89
9	1	8	9	-18.86	-1.11	-16.48	-1.47
10	1	10	9	-20.83	-0.81	-16.48	-1.47
11	1	11	11	-29.24	0.48	-26.60	0.08
12	1	12	11	-34.18	1.24	-26.60	0.08
13	1	12	13	-34.18	1.24	-31.63	0.85
14	1	14	13	-36.65	1.61	-31.63	0.85
15	1	15	15	-36.65	1.61	-33.85	1.19
16	2	1	1	-5.02	0.99	1.41	-0.41
17	2	1	2	-5.02	0.99	-3.46	0.65
18	2	3	2	-9.91	2.05	-3.46	0.65
19	2	3	4	-9.91	2.05	-8.35	1.71
20	2	5	4	-14.79	3.11	-8.35	1.71
21	2	5	6	-14.79	3.11	-13.41	2.81
22	2	7	6	-16.75	3.54	-13.41	2.81
23	2	8	6	-19.68	4.18	-13.41	2.81
24	2	8	9	-19.68	4.18	-15.20	3.20
25	2	8	10	-19.68	4.18	-17.97	3.80
26	2	11	11	-27.50	5.88	-25.79	5.50
27	2	12	11	-32.38	6.94	-25.79	5.50
28	2	12	13	-32.38	6.94	-27.82	5.95
29	2	14	13	-34.83	7.47	-27.82	5.95
30	2	14	15	-34.83	7.47	-30.43	6.51
31	2	16	15	-37.27	8.00	-30.43	6.51
32	2	16	17	-37.27	8.00	-33.69	7.22
33	3	1	1	-2.75	-11.71	2.54	-11.02
34	3	1	2	-2.75	-11.71	-0.52	-11.42
35	3	3	2	-7.79	-12.37	-0.52	-11.42
36	3	3	4	-7.79	-12.37	-2.26	-11.65
37	3	3	5	-7.79	-12.37	-4.32	-11.91
38	3	6	5	-10.27	-12.69	-4.32	-11.91

39	3	6	7	-10.27	-12.69	-7.30	-12.30

Table 9. Summary of Field Test Results

Source/ Sensor Ref. No.	Line No.	No Solution	Good Solution	Total	Percent Good Solutions
1	1	0	7	7	100.0%
2	1	0	5	5	100.0%
3	1	0	5	5	100.0%
4	1	1	7	8	87.5%
5	1	0	4	4	100.0%
6	1	0	8	8	100.0%
7	1	0	12	12	100.0%
8	1	2	8	10	80.0%
9	1	3	8	11	72.7%
10	1	10	7	17	41.2%
11	1	1	13	14	92.9%
12	1	5	8	12	66.7%
13	1	0	10	10	100.0%
14	1	6	6	12	50.0%
15	1	1	12	13	92.3%
16	2	4	3	7	42.9%
17	2	3	8	11	72.7%
18	2	7	3	10	30.0%
19	2	0	12	12	100.0%
20	2	1	10	11	90.9%
21	2	5	8	13	61.5%
22	2	0	11	11	100.0%
23	2	0	14	14	100.0%
24	2	1	14	15	93.3%
25	2	3	12	15	80.0%
26	2	0	15	15	100.0%
27	2	5	9	14	64.3%
28	2	0	17	17	100.0%
29	2	0	15	15	100.0%
30	2	2	12	14	85.7%
31	2	0	13	13	100.0%
32	2	1	19	20	95.0%
33	3	0	10	10	100.0%
34	3	0	12	12	100.0%
35	3	5	11	16	68.8%

36	3	2	12	14	85.7%
37	3	1	14	15	93.3%
38	3	11	1	12	8.3%
39	3	1	19	20	95.0%
Percent good solution	83.1%				
Percent no solution	17.1%				

Test Results from Recorded Data in Field

All data solutions for each line were converted from a local to global reference frame and plotted on a plan view map of the test area. The data for Lines 1, 2 and 3 are shown in Figure 76, Figure **77**, and Figure 78, respectively.

In all three lines there appears to be a weak clustering of solutions in the vicinity of the three targets. While the clusters of solutions over the targets (especially the culvert and 10” PVC) are scattered and spread over a large area, to the eye there appear to be more solutions in the vicinity of the targets. When results for all three lines are plotted on the same map (Figure 79), this apparent clustering remains.

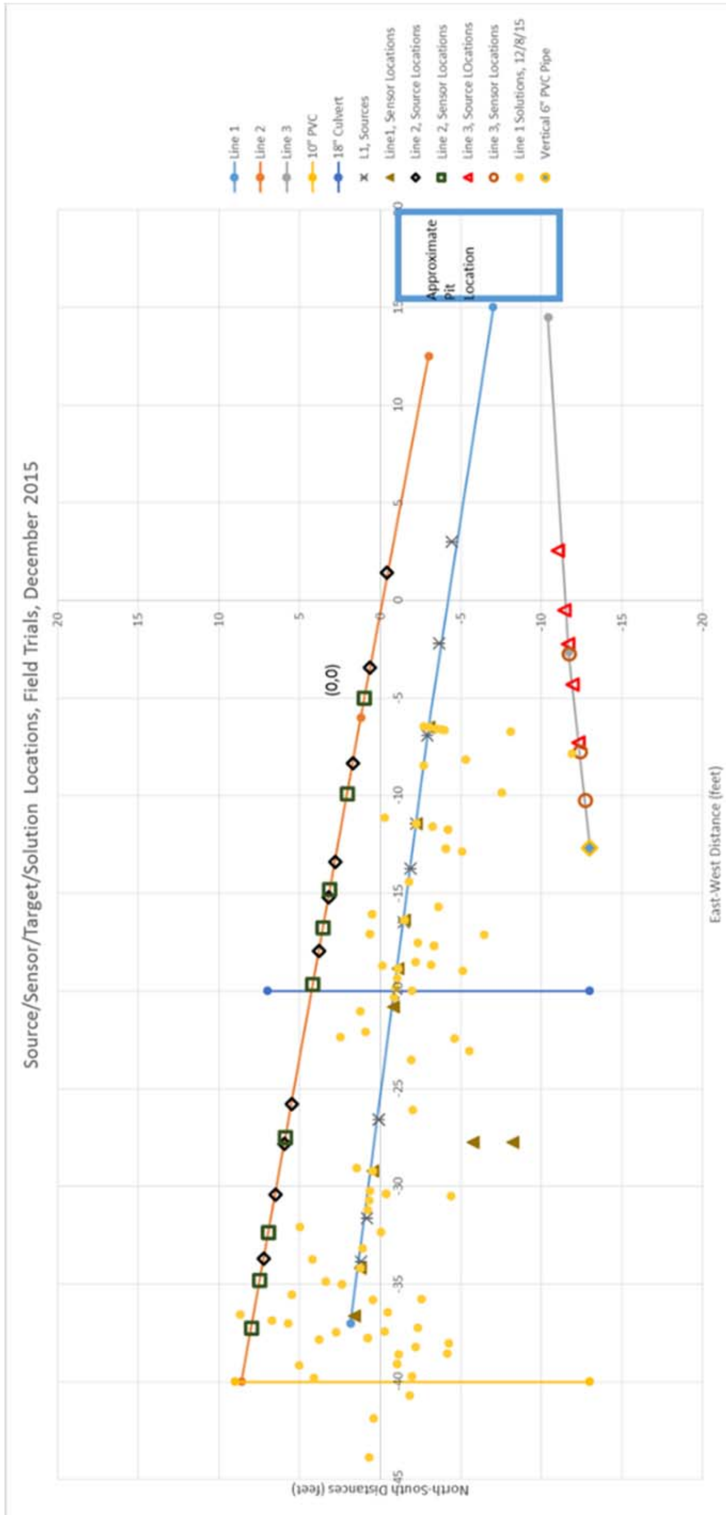

Figure 76 Plot of the data solutions generated for all sensor and source locations for line 1.

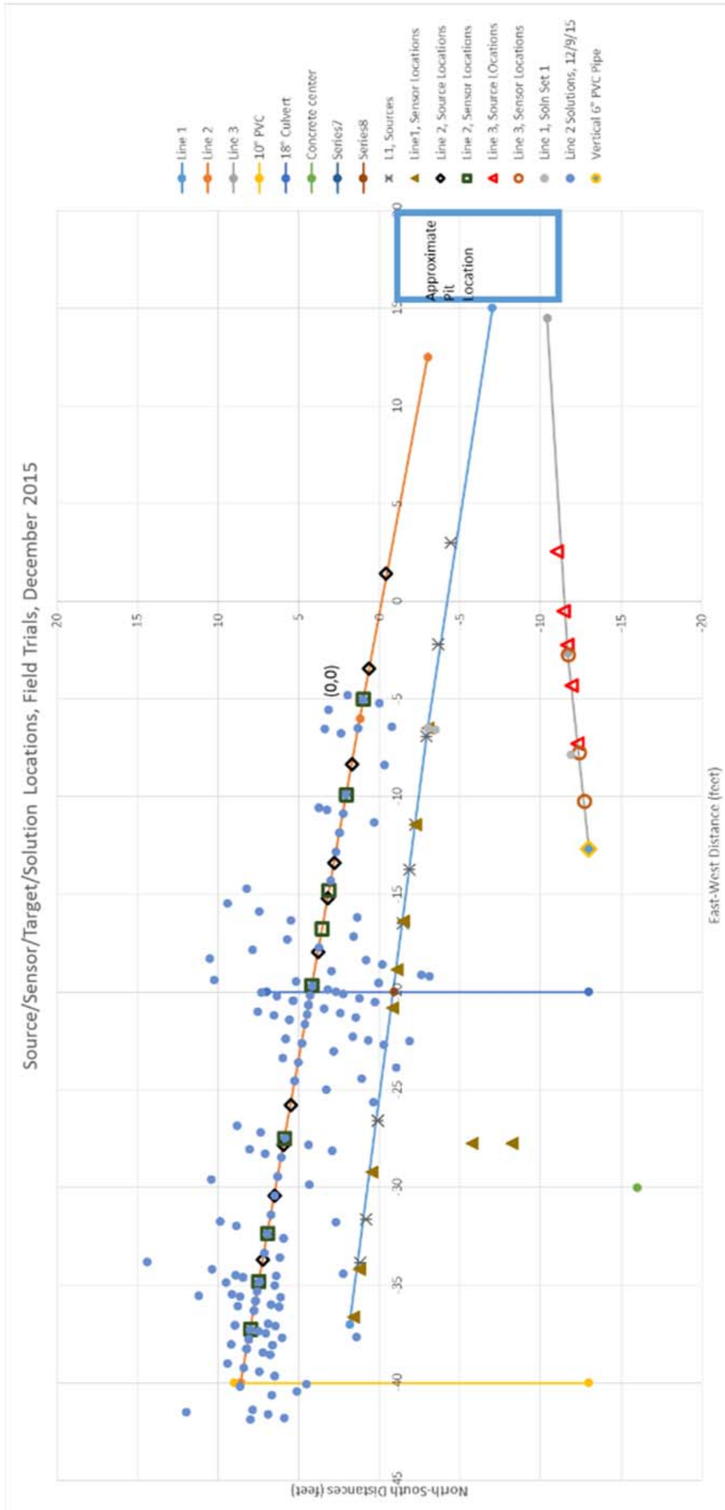

Figure 77 Plot of the data solutions generated for all sensor and source locations for line 2.

gti

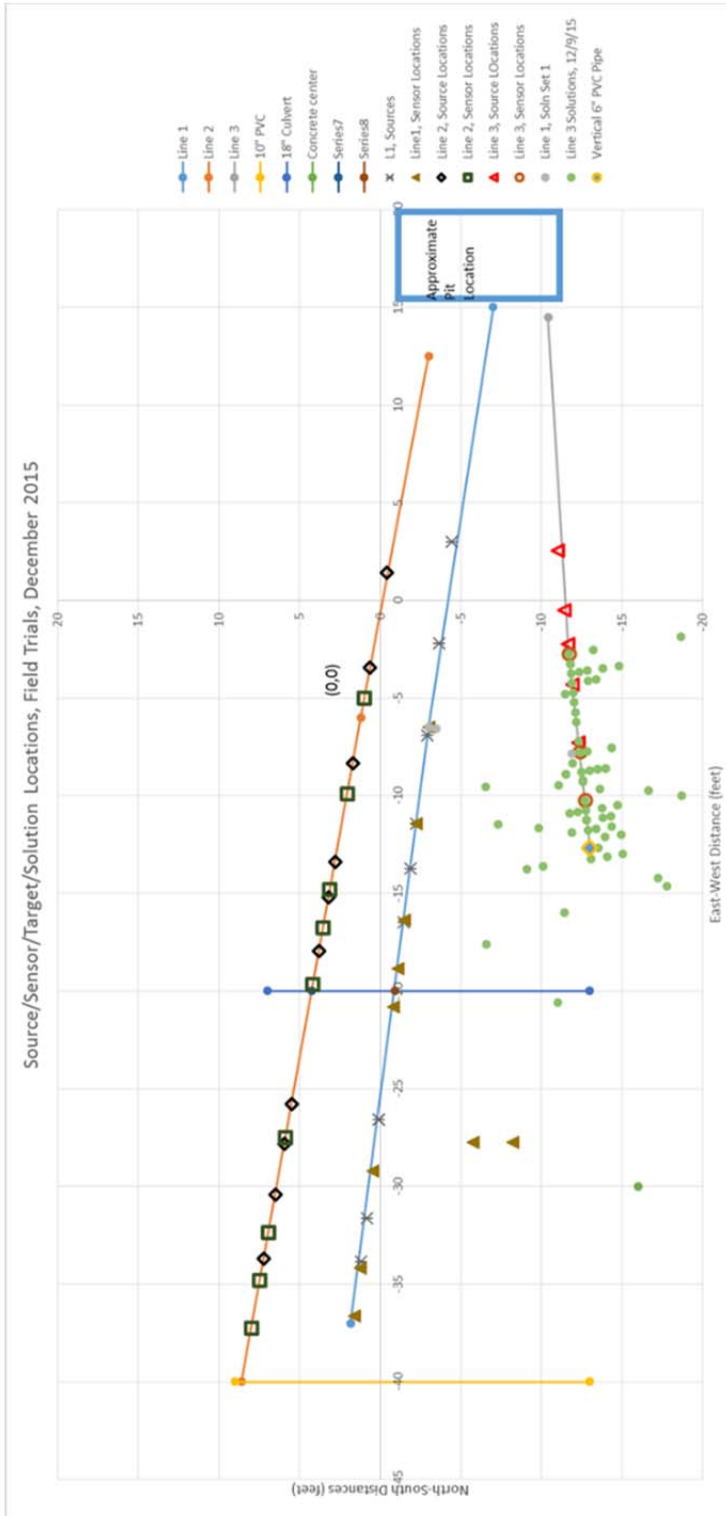

Figure 78 Plot of the data solutions generated for all sensor and source locations for line 3.

gti

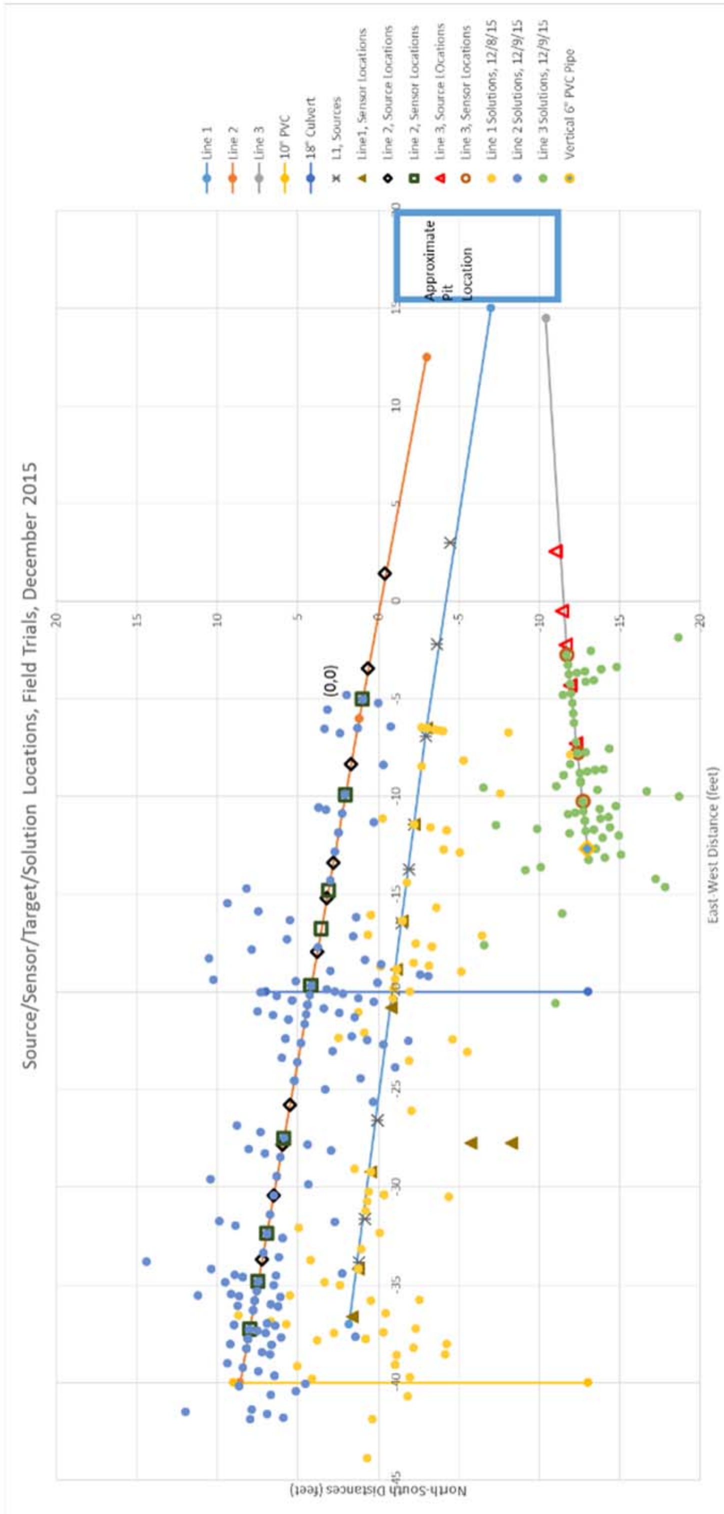

Figure 79 Plot of all solutions obtained from testing conducted in December 2015. To the eye, there appears to be a weak clustering of solutions around the three targets.

Test Results from the Acoustic Detection System

More than 489 data sets/test points were collected during the local area tests. The local area test summary was based on the validated 445 data sets recorded from the local area tests. These test results achieved better than 90% detection rate of objects (pipe or other object) during the trial. The performance evaluation of the acoustic detection system was based on the following test aspects/criteria:

1. Perceivable acoustic energy level (> background noise) generated from the noise source,
2. Frequency response above detectable range for the buried pipes/obstacles,
3. Verifiable (pipe installation information) and detected pipe location (red dot), and
4. Relative testing range/distance between acoustic array and the pipe(s) under test.

Due to the field of view limitation of the acoustic test program/software, the estimated drill-head position was based on the recorded local area test setup/situation – relative distances between noise source, array center, and the depth of the drill-head. No compensation of the distance offset (lateral "Y-axis") between drill-head and array center was applied in the final calculation and processing.

The test site is an open field with soil composed mostly of highly attenuative clay soil. The noise level generated by the new noise maker was improved over the previous iterations. However, the noise source, according to the field measurements, is still lacking needed energy strength and frequency range for the effective pipe detection.

Figure 80 and Figure 81 show some typical measurements of the noise signal generated by the new noise maker during the local area tests. It should be noted that no information on the previously drilled boreholes was available in the area and may have contaminated the final test results particularly for the "line#1". The detection effect of the space separation between "line#2" and "line#3" in the test setup was not specifically analyzed and could well be the "source" of contaminating the final test results due to its exiting drill hole/trench.

Occasionally, there were electrical disconnects between sensor module and the system processing unit; however, no apparent hardware malfunctions were observed throughout the entire local area tests. During the tests, the airborne sounding tests indicated, again unvalidated, that some operational or functional change(s) might have occurred to the noise source. Of course, factors like underground soil conditions and sensor coupling could also cause the measurement inconsistency. Nonetheless, the sensor array deployment was always carefully positioned to make sure the positioning of the sensor modules was adequate before collecting measurements. The performance changes of the noise source, so far, showed no conclusive after-effect to the overall performance of the detection system. Further data analysis may be needed to narrow down the exact cause and effect on the overall system performance during the local area tests.

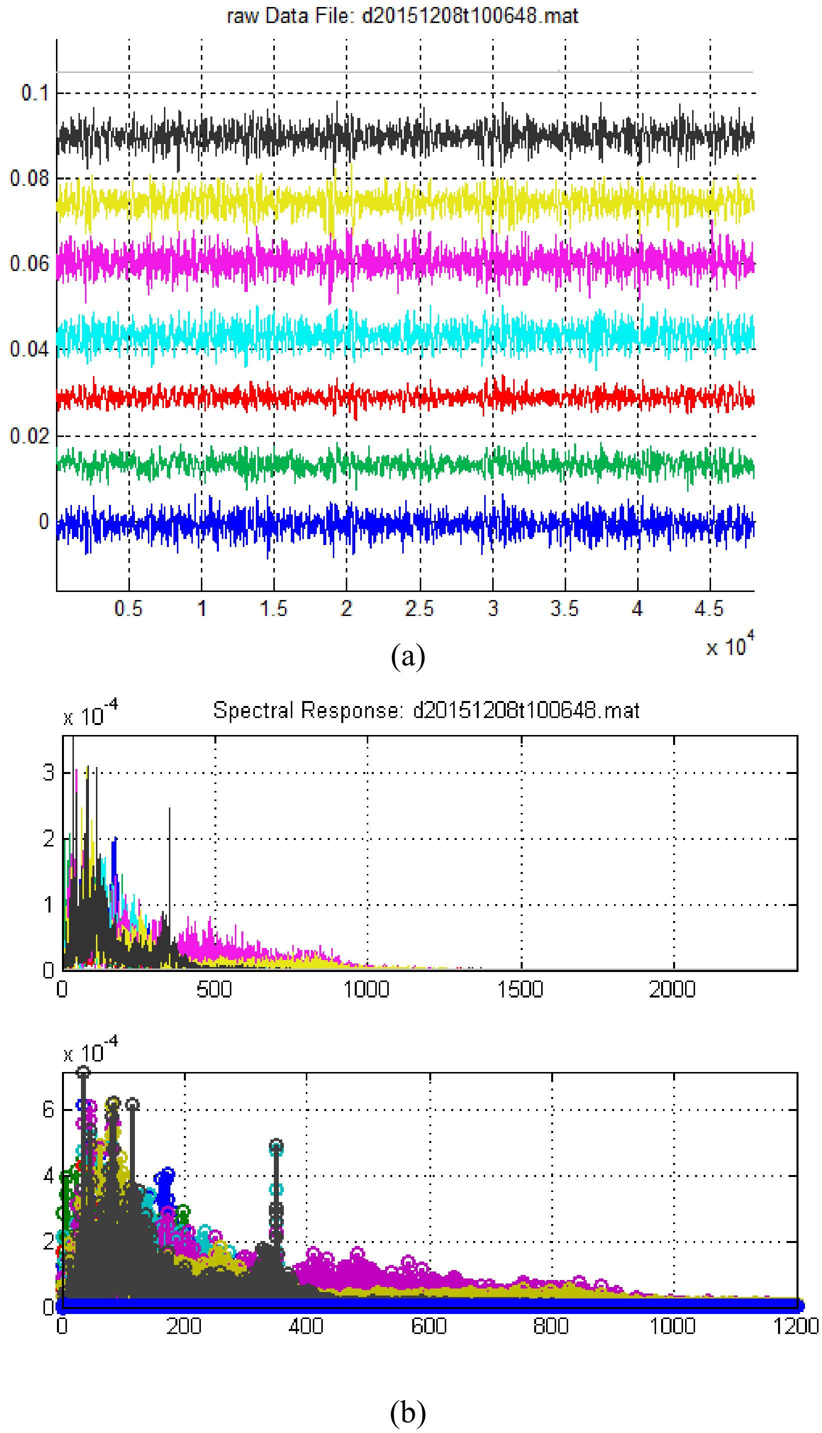

Figure 80 Typical ("line#1") noise source performance with consistent (with respect to sensor-to-source distance) sensitivity readings among receiving sensors [(a) sensitivity axes: vertical in mv, horizontal in (no. of) sample; (b) spectrum axes: vertical in arbitrary unit, horizontal in Hz].

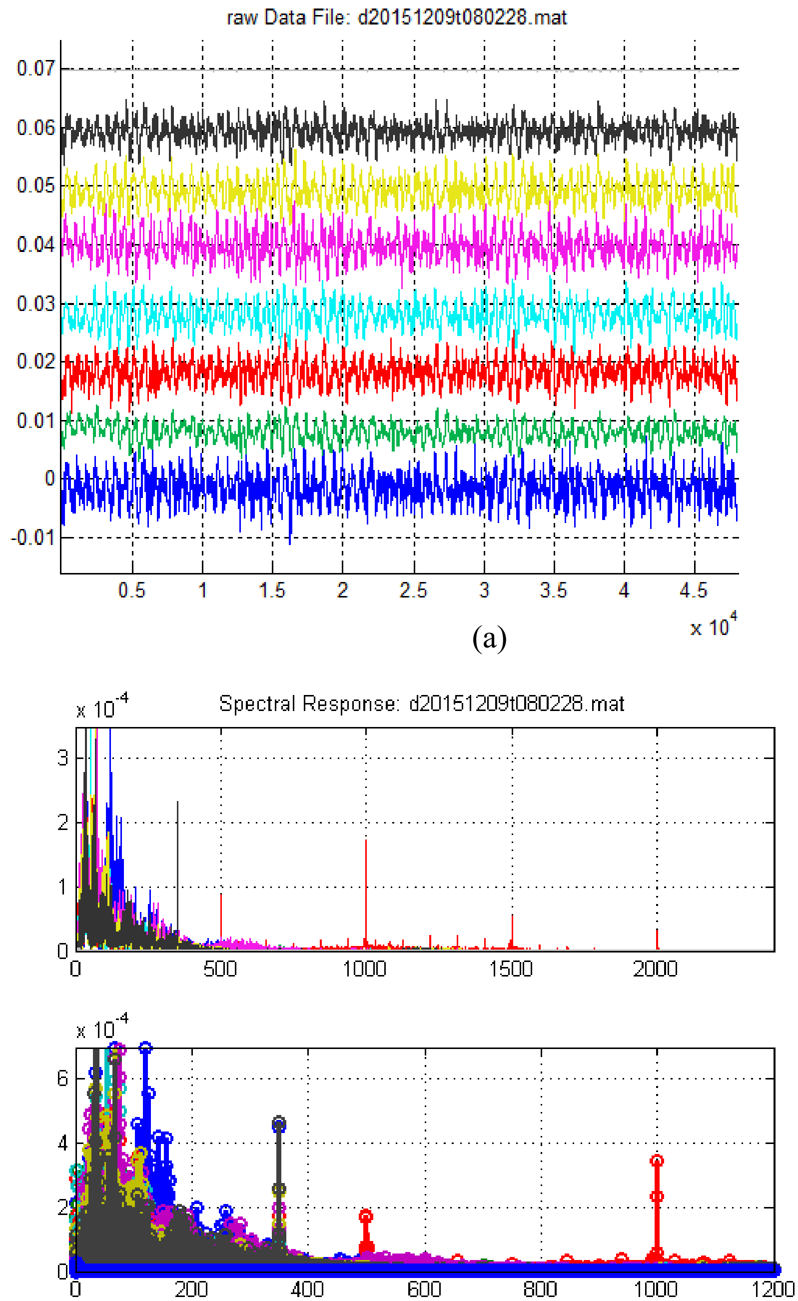

Figure 81 Typical ("line#2") noise maker performance with consistent (with respect to sensor-to-source distance) sensitivity readings among receiving sensors [(a) sensitivity axes: vertical in mv, horizontal in (no. of) sample; (b) spectrum axes: vertical in arbitrary unit, horizontal in Hz].

Overall, the acoustic pipe detection system was able to achieve with detection accuracy of ± 2' on average for a pipe-array separation on the order of 5 feet. For detection ranges greater than 10 feet, the detection accuracy goes down to 7.9' – 13.5', on average. The acoustic system worked well and achieved better than a 91% (445/489) solution generation rate for underground pipes or other obstacles. The detection of a pipe or object was not confirmed by exposure digs at the site.

Table 10 is a brief summary of the acoustic system performance with the improved hammer/anvil noise source design during the local area tests. A detailed test log with performance accuracy is listed in the Appendix C. In essence, due to range coverage of the acoustic system, limited noise source performance, and highly attenuative soil situation as tested, the acoustic system detection performance varied with specific test condition.

Table 10. Acoustic System Performance During the Third Local Area Test

Testing Range (Pipe-to-Array)*	~ 15ft (4 test groups†)	~ 10ft (10 test groups)	< 5ft (26 test groups)
Detection Accuracy (± ft)	**13.5'**	**7.9'**	**2.0'**
Overall (± ft)	**4.6'**		

* test condition – both static and dynamic procedures were included

† "test groups" are unique and validated local area tests under various test locations with specific test setup and procedure during the local area tests

Summary

Both design and manufacturing of a new downhole acoustic source were completed. The overall size of the source assembly (including sonde housing) is about 9 feet in length and weighs about 500 lbs. Several modifications were made to the design to increase both longevity and energy coupled to the ground.

Local area tests to examine the amplitude and spectral content of vibrations coupled from the source into the surrounding soil were conducted. For a point 4 feet directly above the drill, the vibration amplitudes were 10 times that of background noise with most energy at or below 500 Hz. As the distance between source and sensor was increased, both amplitude and spectral content decreased. At double the initial distance from the source, usable energy was still detectable. While quantitative data are not available for a comparison, these signal levels are significantly higher than those in prior tests. In addition, the source survived the test campaign with minimal wear and could be re-used. However, the target spectral content of up to 1.5 kHz was not observed in the field. This could have been due to not generating these frequencies, not coupling the energy into the soil, or intrinsic soil attenuation damping these higher frequencies before they reached monitoring sensors.

During December 2015, a series of local area trials of the acoustic sensor system were conducted. Targets were an 18-inch diameter steel culvert, 10-inch diameter PVC pipe (both buried horizontally at 5 to 6-foot depth), and a vertical 4-inch diameter PVC pipe. A total of 474 data points were collected in real-time, with 394 (83%) providing a calculated solution. When the data solutions (computed target locations) were plotted on a plan view map, the results appeared to have a degree of solution clustering in the vicinity of the buried targets. Since some degree of clustering could be seen with the eye, a series of statistical tests were performed in an attempt to confirm a correlation between the target locations and the computed solutions. However no statistical measure was found to support a correlation between the target/obstacles and solution locations.

The operation of the noise source was analyzed further after field tests were concluded. This analysis showed that the noise source is still lacking needed energy strength and improvement in the frequency range. The acoustic system performance based on validated data sets (445 out of 489, i.e. 90% success rate) showed that the system was able to achieve the average pipe detection accuracy of 4.6 feet with accuracy of 2 feet within a pipe to sensor separation distance of 5 feet. It should be noted that the acoustic system detected the obstacle/pipe as far as 15 feet from the system, although with higher scatter. In future, if this scatter can be reduced and it can be confirmed that the detection is related to the pipe or obstacle of interest, the information can assist the HDD operator to review the drilling plan and modify appropriately. It should be noted that the tests were at the site with soil conditions where other technology (e.g., ground penetrating radar) will not be able to detect buried pipes.

The observed local area test outcomes can be categorized into the following aspects:

- Range limitation of the acoustic system was affected by both noise source performance and the acoustic system sensing/receiving sensitivity
- Noise source performance, in both signal strength and frequency spectrum, limited suitable signal available to the sensing transducers of the acoustic system for processing
- Data interpretation and signal processing may need further refinement and performance review
- For prototype development, test conditions and test field arrangements need to be controlled and configurable to prevent unintentional obstacles or trenches from being detected and cluttering results from planted targets
- Other field situations – sandy soil, concrete/asphalt, top soil, etc., – were not tested at the facility and could be an important factor impacting the overall detection system's performance.

Recommendations

First, the use of a downhole source (either mechanical or due to drill noise in rocky ground) may not be adequate for consistent results. Downhole sources (be they rod-in-rod or mud motor driven) are cumbersome and may not meet with widespread commercial acceptance. In addition, the working range of the current noise source may be limited so that obstacle detection at long range in front of the drill may not be possible. This working range needs to be defined and the potential limitation clearly understood by users. Ultimately, the best controlled acoustic noise source may be one that is on the surface. This would make the sensor system independent of the drill. In this configuration, the source could be engineered to provide an optimal random waveform, and could be moved to illuminate ground well ahead of the drill. One disadvantage of this configuration is that it becomes unworkable if the surface is inaccessible.

Acoustic wave propagation is highly frequency dependent, and lower operating frequencies should provide greater range. Engineering a source that uses lower frequencies might enhance the system's operating range. However, this comes with longer wavelengths that may cause detection issues due to the limited size of the sensor array/aperture. Longer wavelengths also limit the smallest size obstacle that can theoretically be detected.

The overall processing used to generate solutions has been operational for some time, with some success. However, it may be valuable to revisit some of the processing steps, especially if lower frequencies and larger sensor apertures are used. The solution algorithm should be evaluated to see if the probability of detection can be increased and the false alarm rate reduced.

The current method of coupling sensors to the ground is very attractive in that it is rapid and easy to accomplish. However, further improvements to sensor coupling might reduce possible false alarms, increase repeatability, and increase operating range.

Finally, in directly addressing the results from the December 2015 trials, the condition of the two major buried targets needs to be considered. The two buried pipes have been in place for about one year, and most probably have filled with a water/mud mixture. It is possible that the acoustic impedance mismatch that is responsible for acoustic reflections has been reduced, resulting in weaker or non-existent reflected energy. This could, in turn, reduce the system operating range and degrade algorithm performance. It may be valuable to change the targets to a set that are known to be air-filled, providing the maximum possible impedance mismatch.

Outside of the hardware and software improvements, future system enhancements can be made by a defined operation guideline for the detection system and noise source deployment. Direct feed of drill-head position to the acoustic system is one of the operational improvements that can be applied to gain better detection results. Configurable local area tests, using well-defined field layouts, assorted soil compositions, and "pipe farm" installations all could be valuable for fine tuning system performance and field evaluation.

Appendix A

List of Local Area Test Setup (May 2014)

Test Group	Noise Source	Utility	Setup Spacing[0] P_A_N	Data Sets[1] (#)
1	Concrete Blocks	10” PVC / 3” Steel	4.5'_*_10'	11
2	Concrete Blocks	10” PVC / 3” Steel	4.5'_*_5'	4
3	Concrete Blocks	10” PVC / 3” Steel	4.5'_*_15'	10
4	Concrete Blocks	10” PVC / 3” Steel	0'_*_15'	11
5	Concrete Blocks	10” PVC / 3” Steel	0'_*_10'	12
6	Concrete Blocks	10” PVC / 3” Steel	0'_*_5'	15
7	Concrete Blocks	10” PVC / 3” Steel	-4.5'_*_10'[2]	9
8	Axial E. Motor	3” Steel	10'_*_12.5'	6
9	Axial E. Motor	3” Steel	10'_*←12.5'	-
10	Axial E. Motor	3” Steel	5'_*_7.5'	9
11	Axial E. Motor	3” Steel	5'_*←7.5'	-
12	Axial E. Motor	3” Steel	0'_*_7.5'	6
13	Axial E. Motor	3” Steel	0'_*←7.5'	-
14	Rotary E. Motor	3” Steel / 10” PVC	12'_*_17.5'	13
15	Rotary E. Motor	3” Steel / 10” PVC	12'_*←17.5'	-
16	Rotary E. Motor	3” Steel / 10” PVC	7'_*_12.5'	14
17	Rotary E. Motor	3” Steel / 10” PVC	7'_*←12.5'	-
18	Rotary E. Motor	3” Steel / 10” PVC	2'_*_7.5'	21
19	Rotary E. Motor	3” Steel / 10” PVC	2'_*←7.5'	-
20	Pneumatic Mole	3” Steel	5'_*_15'	1
21	Pneumatic Mole	10” PVC	5'_*_40'	14
22	Tactile Transducer	10” PVC	5'_*_5'	3
			Total	159

[0] Test setup: Spacing between pipe, array(*), and noise source in feet
← Indicates moving drill head
[1] Number of the validated test data sets
[2] Opposite side of the pipe

Appendix B

List of Local Area Test Setup (November 2014)

Test Group	Noise Source	Utility	Setup Spacing[0] P_A_N	Data Sets[1] (#)
1	Concrete Block	18" metal culvert	15'_*_5'	4
2	Concrete Block	18" metal culvert	15'_*_5'	8
3	Concrete Block	18" metal culvert	10'_*_5'	1_[2]
4	Concrete Block	18" metal culvert	5'_*_15'	8
5	Concrete Block	18" metal culvert	15'_*_5'	11
6	Concrete Block	18" metal culvert	15'_*_5'	8
7	Concrete Block	18" metal culvert	15'_*_5'	1_[2]
8	Rotary E. Motor	18" metal culvert	10'_*_5'	10
9	Rotary E. Motor	18" metal culvert	10'_*_5'	9
10	Rotary E. Motor	18" metal culvert	10'_*←5'	18
11	Rotary E. Motor	18" metal culvert	5'_*_5'	12
12	Rotary E. Motor	18" metal culvert	5'_*←5'	11
13	Rotary E. Motor	18" metal culvert	5'_*_0'	14
14	Rotary E. Motor	10" PVC	15'_*_5'	10
15	Rotary E. Motor	10" PVC	15'_*←5'	14
16	Rotary E. Motor	10" PVC	15'_*←5'	10
17	Rotary E. Motor	10" PVC	10'_*←5'	13
18	Rotary E. Motor	10" PVC	10'_*_5'	2_[2]
19	Rotary E. Motor	10" PVC	10'_*←5'	9
20	Rotary E. Motor	10" PVC	10'_*←5'	9
21	Rotary E. Motor	10" PVC	5'_*_5'	12
22	Rotary E. Motor	10" PVC	5'_*←5'	9
23	Rotary E. Motor	18" metal culvert	10'_*_5'	11
24	Rotary E. Motor	18" metal culvert	5'_*_5'	8
25	Rotary E. Motor	18" metal culvert	5'_*_5'	8
26	Rotary E. Motor	18" metal culvert	5'_*←5'	10
	(23 setups)		total	240

[0] Test setup: spacing (ft) between **P**ipe, **A**rray(*), and **N**oise source; '←' indicates moving drill head

[1] Number of the validated test data sets with detected obstacle/pipe

[2] Test data were not used in the individual statistic calculation due to insufficient sample(s)

Appendix C

List of Local Area Test Setup (December 2015)

Test Group	Noise Source	Utility	Setup Spacing[0] P_A_N	Accuracy (ft)	Data Sets[1] (#)
1	Hammer/anvil	18" steel culvert	15'_*_4'	13.4	4
2	Hammer/anvil	18" steel culvert	15'_*_0'	14.4	5
3	Hammer/anvil	18" steel culvert	10'_*_5'	7.4	7
4	Hammer/anvil	18" steel culvert	10'_*_0'	9.8	4
5	Hammer/anvil	18" steel culvert	5'_*_5'	3.6	8
6	Hammer/anvil	18" steel culvert	5'_*_3'	3.7	12
7	Hammer/anvil	18" steel culvert	3'_*_5'	2.3	11
8	Hammer/anvil	18" steel culvert	3'_*_3'	2.3	6
9	Hammer/anvil	18" steel culvert	0'_*_4'	5	11
10	Hammer/anvil	10" PVC	10'_*_3'	8.8	13
11	Hammer/anvil	10" PVC	5'_*_8'	3	11
12	Hammer/anvil	10" PVC	5'_*_3'	4.3	10
13	Hammer/anvil	10" PVC	3'_*_5'	0	6
14	Hammer/anvil	10" PVC	3'_*_3'	0	13
15	Hammer/anvil	Concrete block	10'_*_6'	6.1	16
16	Hammer/anvil	Concrete block	8'_*_9'	6.1	14
17	Hammer/anvil	Sledge hammer	10'_*_v'	x	2[2]
18	Hammer/anvil	18" steel culvert	15'_*_7'	12.3	4
19	Hammer/anvil	18" steel culvert	15'_*_2'	14	6
20	Hammer/anvil	18" steel culvert	10'_*_7'	7.5	5
21	Hammer/anvil	18" steel culvert	10'_*_2'	8.8	12
22	Hammer/anvil	18" steel culvert	5'_*_7'	2.1	10
23	Hammer/anvil	18" steel culvert	5'_*_2'	0.5	10
24	Hammer/anvil	18" steel culvert	3'_*_4'	1.8	11
25	Hammer/anvil	18" steel culvert	0'_*_7'	3	14
26	Hammer/anvil	18" steel culvert	0'_*_5'	1.3	15
27	Hammer/anvil	18" steel culvert	0'_*_2'	1.2	13
28	Hammer/anvil	18" steel culvert	10'_*_2'	8.3	15
29	Hammer/anvil	18" steel culvert	5'_*_7'	0.8	10
30	Hammer/anvil	18" steel culvert	5'_*_5'	3.6	17
31	Hammer/anvil	18" steel culvert	3'_*_7'	1.3	15
32	Hammer/anvil	18" steel culvert	3'_*_5'	1.7	12
33	Hammer/anvil	18" steel culvert	0'_*_7'	2.3	13
34	Hammer/anvil	18" steel culvert	0'_*_4'	0.8	20

35	Hammer/anvil	6” PVC, vertical	10'_*_5'	8.4	10
36	Hammer/anvil	6” PVC, vertical	10'_*_2'	7.3	12
37	Hammer/anvil	6” PVC, vertical	5'_*_7'	0.4	15
38	Hammer/anvil	6” PVC, vertical	5'_*_6'	1.8	12
39	Hammer/anvil	6” PVC, vertical	5'_*_4'	3.7	14
40	Hammer/anvil	6” PVC, vertical	3'_*_6'	x	0[2]
41	Hammer/anvil	6” PVC, vertical	3'_*_3'	0.3	20
42	Hammer/anvil	6” PVC, vertical	3'_*_2'	0.4	9
	(40 validated test groups)		total		445

[0] Test setup: spacing (ft, round-off to nearest distance) between **P**ipe, **A**rray (*), and **N**oise source

[1] Number of the validated test data sets with detected obstacle/pipe

[2] Test data were not used in the individual statistic calculation due to insufficient statistical sample(s)

End of Report